PUBLICATIONS OF
THE UNIVERSITY OF EASTERN FINLAND

Dissertations in Forestry and Natural Sciences

UNIVERSITY OF
EASTERN FINLAND

ANDREI BELIAEV

EFFICIENT PUSH-PULL FLUOROPHORES UTILIZING PHOSPHORUS ELECTRON ACCEPTOR UNITS

Andrei Beliaev

EFFICIENT PUSH-PULL FLUOROPHORES UTILIZING PHOSPHORUS ELECTRON ACCEPTOR UNITS

Publications of the University of Eastern Finland
Dissertations in Forestry and Natural Sciences
No 366

University of Eastern Finland
Joensuu
2020

Academic dissertation
To be presented by permission of the Faculty of Science and Forestry for public examination in the Auditorium F100 in the Futura Building at the University of Eastern Finland, Joensuu, on January 31, 2020, at 12 o'clock noon

Grano Oy
Jyväskylä, 2020
Editors: Pertti Pasanen, Raine Kortet,
Jukka Tuomela, Matti Tedre, Niina Hakulinen
Distribution: University of Eastern Finland / Sales of publications
www.uef.fi/kirjasto
ISBN: 978-952-61-3284-6 (print)
ISBN: 978-952-61-3285-3 (PDF)
ISSNL: 1798-5668
ISSN: 1798-5668
ISSN: 1798-5676 (PDF)

Author's address: Andrei Beliaev
University of Eastern Finland
Department of Chemistry
P.O. Box 111
80101 JOENSUU, FINLAND
email: andreib@uef.fi

Supervisors: Professor Igor O. Koshevoy, Ph.D.
University of Eastern Finland
Department of Chemistry
P.O. Box 111
80101 JOENSUU, FINLAND
email: igor.koshevoy@uef.fi

Reviewers: Professor Kari Rissanen, Ph.D
University of Jyväskylä
Department of Chemistry
P.O. Box 35
40014 JYVÄSKYLÄ, FINLAND
email: kari.t.rissanen@jyu.fi

Professor Rudolf Pietschnig, Ph.D
University of Kassel
Institute of Chemistry
34132 KASSEL, GERMANY
email: pietschnig@uni-kassel.de

Opponent: Directeur de Recherche Christophe Lescop, Ph.D
Institut des Sciences Chimiques de Rennes
35708 RENNES, FRANCE
email: christophe.lescop@insa-rennes.fr

Beliaev Andrei
Efficient push-pull fluorophores utilizing phosphorus electron acceptor units
Joensuu: University of Eastern Finland, 2020
Publications of the University of Eastern Finland
Dissertations in Forestry and Natural Sciences 2020; 366
ISBN: 978-952-61-3284-6 (print)
ISSNL: 1798-5668
ISSN: 1798-5668
ISBN: 978-952-61-3285-3 (PDF)
ISSN: 1798-5676 (PDF)

ABSTRACT

Nowadays, the research related to the development of efficient light generating molecular materials (luminophores), based on the rational design at the molecular level, is of primary importance. The worldwide academic and industrial interest in the large family of chemical entities exhibiting this optical phenomenon is determined by their extremely broad range of applications in advanced technologies, which, in particular, cover the fields of biomedical visualization/diagnostics/therapy, light-emitting devices, new sensing techniques, photoswitches/smart responsive materials, and photovoltaic cells. To meet the constantly raising requirements of the related areas, many elegant and practical strategies have been successfully applied for the construction of organic chromophores with the desired physical properties. Among them, one popular approach relies on the use of phosphorus to form a diversity of acyclic/cyclic scaffolds (*i.e.*, phospholes, phosphinines, phosphine oxides, and metal-organic phosphine complexes) capable of emitting light. One major beneficial feature of organophosphorus blocks is their ability to significantly impact the electronic properties of dyes. A relatively easy chemical modification of a trivalent phosphorus center (*i.e.*, oxidation, complexation, and alkylation) is a typical way to convert it into an electron acceptor (*A*) and therefore, to tune the optical characteristics of the entire organophosphorus motif. Simultaneously, the electron-deficient nature of the P-containing units (*A*: $R_3P{=}E$, E=O, S; R_4P^+, *etc.*), combined with the electron donor moieties (*D*) in one molecule, can give raise to intramolecular charge transfer (ICT), thereby resulting in the dramatic modulation of the physical behavior. In view of these advantages, versatile phosphorus motifs have been utilized as powerful tuning tools in molecular design and chemical engineering.

The research presented in this thesis highlights the great potential and importance of the electron-accepting phosphorus center for the development of new chromophores of a general donor–acceptor (*D*–*A*) architecture, with the aim to attain high tunability and adaptivity of the optical characteristics. Particularly, three

different approaches, which utilize electron deficient phosphonium (R_2P^+</ R_3P^+–) and gold(I)-phosphine (–Ph_2P–Au^I–) motifs, were explored for the construction of *D*–*A* dyes. Their photophysical properties were controlled by adjusting the optical band gap, primarily achieved *via* systematic alteration of the π-conjugated organic core of the chromophores. The incorporation of the phosphonium unit into the polyaromatic scaffolds by facile intramolecular copper(II)-mediated phospha-annulation reaction allowed the elaboration of a series of very efficient P-heterocyclic fluorophores with emission colors spanning from deep blue to near-infrared (420–780 nm) in solution and quantum efficiencies up to unity. The ionic nature of these polycyclic dyes provided decent water solubility that made them suitable for bioimaging application. In turn, tailoring the pendant phosphonium group (R_3P^+–) to the emissive fragments *D*–π– delivered topologically simple linear *D*–π–A^+ cationic luminophores with a plethora of colors ranging from sky blue to deep red (487–709 nm). Unexpectedly, certain dyes within this series demonstrated anomalous dual emission, resulting from the photoinduced ICT and an unconventional counterion migration that occurred in the non-dissociated ion pairs. Ultimately, merging the donor–acceptor phosphine–gold fluorophores with europium (red emitter) afforded Au–Eu dyads, which exhibited a wide variation of luminescence colors, including white light emission, and illustrated a convenient strategy for the development of panchromatic luminophores with dynamic photophysical behavior.

University Decimal Classification: 535.371, 535.373.1, 546.18, 628.9.03, 661.143

CAB Thesaurus: organophosphorus, solvatochromism, donor-acceptor, intramolecular charge transfer, phospha-dyes, chromophores, fluorescence, metal-organic complexes

ACKNOWLEDGEMENTS

This work was carried out at the Department of Chemistry, University of Eastern Finland between January 2016 and January 2020. The financial support provided by the Faculty of Science and Forestry of the University of Eastern Finland (SCITECO fellowship) and the Academy of Finland (grant no. 317903) is gratefully acknowledged.

First of all, I would like to express my deepest gratitude to my supervisor Prof. Igor Koshevoy. It was a great pleasure to work with such a superior chemist, a boss and a friend. After every discussion with you, I had thoughts and research ideas in my head that I always wanted to realize.

I am also thankful to my first teachers from Saint-Petersburg State University: Dr. Dmitry Krupenya, Dr. Ilya Kritchenkov and Prof. Sergey Tunik for your tremendous contribution that had an impact on my desire to be a synthetic chemist.

In addition, I would like to thank all collaborators who were involved into these studies. Particularly Prof. Pi-Tai Chou, Dr. Carlos Romero-Nieto, Prof. Antti Kartunen, Prof. Janne Jänis, Dr. Elena Grachova, MSc. Igor Solovyev and Dr. Yi-Ting Chen. Special thanks I address to MSc. Zong-Ying Liu, who on the other side of the world has been always ready to help with photophysical measurements.

Furthermore, I appreciate Prof. Kari Rissanen and Prof. Rudolf Pietschnig for their carefull reading and scrupulously detailed review of this piece of work.

I would like to extend my thanks to Prof. Mika Suvanto, Dr. Sari Suvanto, Prof. Tapani Pakkanen, Prof. Tuula Pakkanen, Dr. Janne Hirvi, Ms. Leila Alvila, Dr. Nina Hakulinen, Dr. Pipsa Hirva, Ms. Mari Heiskanen, Ms. Taina Nivajärvi, Mr. Urpo Ratinen, Mr. Martti Lappalainen, Ms. Päivi Inkinen, Ms. Tarja Virrantalo, and all administrative personnel, teachers and technical staff of the Department of Chemistry, for their smiles, help and support throughout the years.

I sincerely thank my dear colleagues: Dr. Kristina Kisel, Dr. Vasily Sivchik, Dr. Sergey Malykhin, Dr. Igor Reduto, MSc. Marina Fetisova, MSc. Kirill Kulish, MSc. Nastya Solomatina, Dr. Yulia Shakirova, MSc. Ilya Kondrasenko, Dr. Gomathy Chakkaradhari, MSc. Diana Temerova, MSc. Filipp Temerov, MSc. Iida Partanen and Dr. Dau Thuy Minh for fruitful discussions, assistance on any occasion, and joint time we spent together in Joensuu or Saint-Petersburg.

I also thank all my close friends and relatives for making good atmosphere outside the laboratory.

Finally, I would like to express my boundless love and gratitude to my wonderful and incredibly patient wife Mariia. Your warm attitude, priceless help and support give me the motivation and aspiration to become better every day.

Joensuu, 18th December 2019 Andrei Beliaev

LIST OF ABBREVIATIONS

(PH)OLED	(Phosphorescent) organic light-emitting diode
HOMO/LUMO	Highest occupied/lowest unoccupied molecular orbitals
ΔE_{ST}	Energy band gap
TADF	Thermally activated delayed fluorescence
SOC	Spin-orbit coupling
ISC/RISC	Intersystem crossing/reverse intersystem crossing
ICT	Intramolecular charge transfer
CT	Charge transfer
OPV	Organic photovoltaics
MO	Molecular orbital
CIE	Commission Internationale de l'Eclairage
EQE	External quantum efficiency
PO	Phosphine oxide
D/A	Donor/acceptor
NICS	Nucleus-independent chemical shift
TD-DFT	Time-dependent density functional theory
PAH	Polyaromatic hydrocarbons
HE/LE	High/low energy
SET	Single electron transfer
NIR	Near-infrared
UV/vis	Ultraviolet/visible
GM	Goeppert-Mayer
TPA	Two-photon absorption
ESI^+ MS	Electrospray ionization mass spectra
FTIR	Fourier-transform infrared spectroscopy
NMR	Nuclear magnetic resonance
ESI	Electronic support information
DCM	Dichloromethane
MeOH	Methanol
DMSO	Dimethylsulfoxide
PBS	Phosphate-buffered saline
DCE	1,2-Dichloroethane
MeCN	Acetonitrile
BARF	Tetrakis[3,5-bis(trifluoromethyl)phenyl]borate
μ	Dipole moment
epbpy	5-(4-Ethynylphenyl)-2,2′-bipyridine
tta	3-Thenoyltrifluoroacetonate
ET	Energy transfer
rt	Room temperature

LIST OF ORIGINAL PUBLICATION

This thesis is based on data presented in the following articles, referred to by the Roman Numerals I-IV.

I Belyaev A, Chen Y.-T, Su S.-H, Tseng Y.-J, Karttunen A. J, Tunik S. P, Chou P.-T, Koshevoy I. O. Copper-mediated phospha-annulation to attain water-soluble polycyclic luminophores. *Chemical Communications 53: 10954-10957, 2017.*

II Belyaev A, Chen Y.-T, Liu Z.-Y, Hindenberg P, Wu C.-H, Chou P.-T, Romero-Nieto C, Koshevoy I. O. Intramolecular phosphacyclization: polyaromatic phosphonium P-heterocycles with wide-tuning optical properties. *Chemistry – A European Journal 25: 6332-6341, 2019.*

III Belyaev A, Cheng Y.-H, Liu Z.-Y, Karttunen A. J, Chou P.-T, Koshevoy I. O. A facile molecular machine: optically triggered counterion migration via charge transfer of linear *D*–π–*A* phosphonium fluorophores. *Angewandte Chemie International Edition 58: 13456-13465, 2019.*

IV Belyaev A, Slavova S. O, Solovyev I. V, Sizov V, Jänis J, Grachova E. V, Koshevoy I. O. Solvatochromic dual luminescence of Eu-Au dyads decorated with chromophore phosphines. *Inorganic Chemistry Frontiers 7: 140-149, 2020.*

The publications were adapted with the permission of the copyright owners.

AUTHOR'S CONTRIBUTION

The author performed all the syntheses and characterization analyses (*i.e.*, NMR, IR, TGA, and X-ray diffraction experiments), except for the ESI^+ MS and elemental analyses of the materials in the related publications I–IV. The author also carried out a significant part of the photophysical investigations for publications II–IV. The additional photophysical data and all the theoretical studies were performed by collaborating groups and the author took part in the interpretation of the obtained data. Finally, the author actively contributed to the project planning, molecular design, and writing of the manuscripts in collaboration with the supervisor and other co-authors.

Other related publications by the author during the study not included in this thesis:

(i). Belyaev A, Krupenya D. V, Grachova E.V, Gurzhiy V. V, Melnikov A. S, Serdobintsev P. Y, Sinitsyna E. S, Vlakh E. G, Tennikova T. B, Tunik S. P. Supramolecular Au^{I}–Cu^{I} complexes as new luminescent labels for covalent bioconjugation. *Bioconjugate Chemistry 27: 143-150, 2016.*

(ii). Belyaev A, Dau T. M, Jänis J, Grachova E. V, Tunik S. P, Koshevoy I. O. Low-nuclearity alkynyl d^{10} clusters supported by chelating multidentate phosphines. *Organometallics 35: 3763-3774, 2016.*

(iii). Dau T. M, Asamoah B. D, Belyaev A, Chakkaradhari G, Hirva P, Jänis J, Grachova E. V, Tunik S. P, Koshevoy I. O. Adjustable coordination of a hybrid phosphine–phosphine oxide ligand in luminescent Cu, Ag and Au complexes. *Dalton Transactions 45: 14160-14173, 2016.*

(iv). Belyaev A, Eskelinen T, Dau T. M, Ershova Y. Y, Tunik S. P, Melnikov A. S, Hirva P, Koshevoy I. O. Cyanide-assembled d^{10} coordination polymers and cycles: excited state metallophilic modulation of solid-state luminescence. *Chemistry - A European Journal 24: 1404-1415, 2018.*

(v). Glebko N, Dau T. M, Melnikov A. S, Grachova E. V, Solovyev I. V, Belyaev A, Karttunen A. J, Koshevoy I. O. Luminescence Thermochromism of Gold(I) Phosphane-Iodide Complexes: A Rule or an Exception? *Chemistry - A European Journal 24: 3021-3029, 2018.*

(vi). Temerov F, Belyaev A, Ankudze B, Pakkanen T. T. Preparation and photoluminescence properties of graphene quantum dots by decomposition of graphene-encapsulated metal nanoparticles derived from Kraft lignin and transition metal salts. *Journal of Luminescence 206: 403-411, 2019.*

(vii). Chakkaradhari G, Eskelinen T, Degbe C, Belyaev A, Melnikov A. S, Grachova E. V, Tunik S. P, Hirva P, Koshevoy I. O. Oligophosphine-thiocyanate Copper(I) and Silver(I) Complexes and Their Borane Derivatives Showing Delayed Fluorescence. *Inorganic Chemistry 58: 3646-3660, 2019.*

(viii). Belyaev A, Kolesnikov I, Melnikov A. S, Gurzhiy V. V, Tunik S. P, Koshevoy I. O. Solution versus solid-state dual emission of the Au(i)-alkynyl diphosphine complexes via modification of polyaromatic spacers. *New Journal of Chemistry 43: 13741-13750, 2019.*

CONTENTS

1 INTRODUCTION

In a passionate aspiration to attain the elixir of life and the "philosopher's stone" after hundreds of various unfortunate experiments, in 1669, the famous German alchemist and pharmacist Henning Brandt identified a new element, which he named phosphorus.[1] The white crystalline powder, obtained during the sublimation of urine sludge, readily ignited in air and glowed in the dark after exposure to oxygen (Figure 1). Brandt defined the new element by the Latin words "*phosphorus mirabilis*," which literally means miraculous light bearer. Eventually, the scientist did not magically turn the obtained "light and fire" into gold or any of the other noble metals; however, as a result of his contribution, after almost four hundred years since its discovery, phosphorus chemistry today constitutes a vital part of chemical science and everyday life.

Figure 1. Discovery of the phosphorus element by Henning Brandt, painted by Joseph Wright in 1771.

The widespread presence of phosphorus in bound form (there are $>10^6$ known phosphorus-containing compounds) arises from the particular electronic configuration of the family of elements known as pnictogens, which form Group VA(15) of the periodic table. Phosphorus (symbol P) is a non-metallic p-block element with the atomic number 15 and weight 30.974 g/mol, which is defined as the second most important and abundant pnictogen after nitrogen. Owing to its $[Ne]3s^23p^3$ electronic shell, phosphorus favors the valences three and five and generally appears in linear, tri-, tetra-, and hexa-coordinated compounds to form covalent, ionic, and even metallic bonds. Compared to nitrogen, phosphorus demonstrates high chemical reactivity and is unavailable in the earth's crust and atmosphere in its free form; however, it is often found as a main component in many inorganic phosphate rocks and minerals.

Phosphorus is essential for all known forms of life: phosphates (PO_4^{3-}) are major structural blocks of the nucleic acids (DNA and RNA), energy carriers (ATP and ADP), nutrition proteins, and phospholipids and are located in the skeleton, muscles, and nervous tissue.

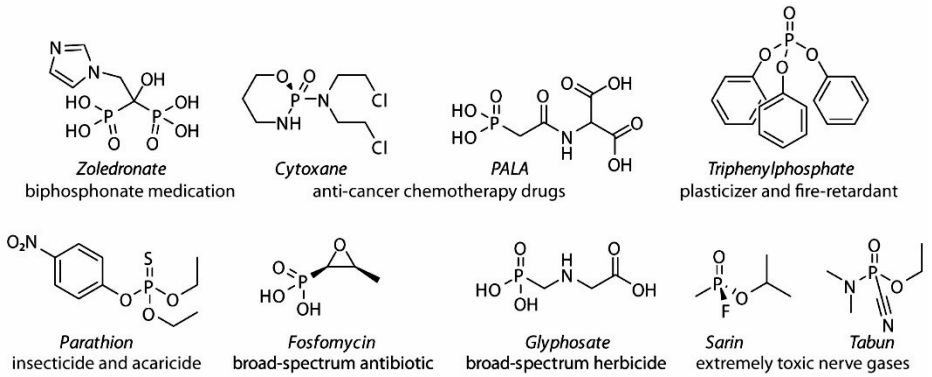

Figure 2. Selected organophosphorus derivatives and their uses.

Since the nineteenth century, the use of phosphorus compounds in industry and low-tech fields (*e.g.* as fertilizers, pesticides, detergents, and flameproof agents) has increased greatly (Figure 2).[2] Later, starting from the middle of the twentieth century, in virtue of the progress in organophosphorus chemistry, the significant role of this element has been maintained in the newest high-technology areas. These include nano-engineering, new electronic and optical materials,[3,4] anti-cancer chemotherapy drugs[5,6] in medicine, and vectors in gene therapy[7]. Distinctly standing out is their utilization as chemical warfare, *e.g.*, the colorless and odorless organophosphates *VX*, *Sarin,* and *Tabun* are extremely toxic substances in minuscule doses and are 26 times deadlier than cyanides.[8,9]

Organophosphorus chemistry now represents an eminent segment of chemical science. The pioneering research breakthroughs are associated with the seminal works of August Michaelis and Aleksandr Arbuzov on the synthesis of various phosphonates, phosphinates, and phosphine oxides. Further development of the field has led to the disclosure of phosphorus yilides and imides, phosphonium salts, and phospholes for P–X and C–X bond formation, where X can be almost any main group element.[2,10] The scientific community has highly appreciated the importance of these early contributors, many of which were immortalized by naming the corresponding organophosphorus reactions after them (*e.g.*, Michaelis–Arbuzov, Wittig, Horner–Wadsworth–Emmons, Abramov, Appel, Staudinger, *etc.*) and awarding the Nobel Prize for the most prominent advances (1957/L. Todd; 1979/H. C. Brown and G. Wittig). On the other hand, organophosphorus derivatives serve as a diverse functional toolbox for coordination and organometallic chemistry to produce numerous metal complexes, supramolecular assemblies, and clusters. In

addition to their fundamental role in the preparation of metal compounds, it is difficult to underestimate the impact of phosphines as spectator ligands on modern organic syntheses. This area has displayed a dramatic progress as a result of the abundant metal-catalyzed organic transformations, spanning from fine enantioselective catalysis[11–13] to large-scale industrial processes (hydrogenation and formylation, poly- and oligomerization, *etc*.).[14]

Finally, with reference to the etymological origin of the name of the element ("light bearer"), the phenomenon of photoluminescence, *i.e.*, the re-emission of light after illumination, is one of the key features of many (metal)-organophosphorus compounds that has been actively studied over the last decades. The continuous growth in research interest in the development of new light-emitting phosphorus-based materials is stimulated by their successful applications in biology and medicine as dye vectors for screening and tracking, photovoltaics and organic light-emitting diodes (OLEDs) as emitting and charge injecting/transporting layers, sensing and detecting devices as stimuli-responsive species, *etc*.[15–22] The raising demands of these practically important fields require the judicious design of new chemical entities with the high tunability and tailorability of optical characteristics.

1.1 GENERAL OVERVIEW AND OPTICAL FEATURES OF ORGANOPHOSPHORUS COMPOUNDS

For a long time, organic optoelectronic materials were predominantly constructed of light second-row atoms (carbon, nitrogen, and oxygen).[23] In the search for novel physical properties, diversification of the molecular design relied on the addition of heavier hetero-elements such a sulfur,[23–26] selenium,[23,27,28] silicon,[23,29] boron,[23,29–32] and particularly phosphorus to the π-conjugated carboskeleton. The utilization of the latter element has offered unique reactivity through the facile transformation of the trivalent P-center into tetra- and pentavalent derivatives, owing to its appreciable nucleophilicity and coordination ability. This change in the oxidation state substantially affects the energy of the highest occupied and lowest unoccupied molecular orbitals (HOMO/LUMO), which primarily regulate the processes of light absorption and emission. Moreover, phosphorus is considered as a "*carbon copy*" or *"photocopy,"* owing to the comparable element electronegativities (2.2 for phosphorous *versus* 2.5 for carbon), chemical analogy and ionization energies of the P=C (P=P) and C=C bonds, and isolobality of the tertial configuration PR_3 to C-sp^3 fragments.[33–35] The aforementioned arguments indicate a possible avenue for the rational design of new photofunctional compounds, which might allow an accessible modulation of their optoelectronic properties by careful consideration of suitable phosphorus synthons to tune the HOMO/LUMO gap.

The nomenclature to describe the phosphorus center was accepted after the discovery of low- and hyper-coordinate species (*e.g.* diphosphenes and phosphoranes), which currently uses the two-symbol notation $\lambda^X\sigma^X$. The first index

λ^X represents the *valence number*, which is equal to the number of bonds in which the phosphorus atom is involved. The second term σ^X is defined as the *coordination number* and corresponds to the number of atoms that are directly bonded to the phosphorus center.[2]

The organophosphorus compounds with the $\lambda^3\sigma^3$ configuration of the P-atom bear three alkyl/aryl substituents connected by P–C bonds. Among them, phosphines, phospholes, and phospholanes (Figure 3A) are found to be versatile building blocks for the construction of more sophisticated derivatives *via* the modification of the phosphorus center. This reactivity originates from the electronic structure of the $\lambda^3\sigma^3$ center, which can donate a lone pair (Lewis σ-base) and accept external electron density into the σ*(P–C) molecular orbitals (Lewis π-acid). Typically, such compounds demonstrate negligible luminescence, owing to the effective non-radiative relaxation of the excited state as a result of photoinduced electron transfer.[36–40] To date, few highly emissive phosphines have been reported in the literature.[41–43] Consequently, the deactivation of the electron pair by forming covalent bonds with chalcogens (O, S, and Se), metals, organic groups (alkyl/aryl), and Lewis acids (BR_3), by means of oxidation, quaternization, and coordination reactions, leads to diverse photophysical behavior of the $\lambda^5\sigma^4$- and $\lambda^4\sigma^4$-P successors (Figure 3A).[16,41,44] The rare examples of photoluminescent compounds with other phospha-centers (not listed in Figure 3), *e.g.*, $\lambda^3\sigma^2$ phosphinines and $\lambda^5\sigma^4$ diphosphenes, will be considered below (Chapter 1.3.3).

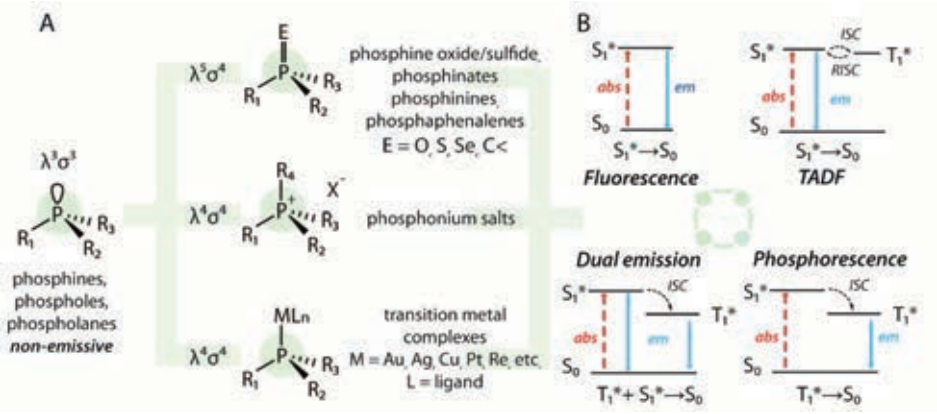

Figure 3. A: Diversity of organophosphorus fragments and B: Typical emission behavior of (metal)-organophosphorus emitters.

Following light absorption, most luminescent organophosphorus species display prompt *fluorescence* – a spin-allowed radiative relaxation ($S_1^* \rightarrow S_0$) characterized by the short excited state lifetimes (τ ~ps and ns; Figure 3B). Alternatively, molecules with a high degree of spin-orbit coupling (SOC) may change their spin multiplicity and undergo a non-radiative transition from the singlet excited state (S_1^*) to a lower

energy triplet state (T_1^*) via intersystem crossing (ISC). The probability of this process depends of the degree of SOC, which is proportional, among other factors, to the mass of the atom(s) attached to the chromophore motif. Therefore, a "forbidden" room-temperature *phosphorescence* relaxation ($T_1^* \rightarrow S_0$) might operate for complexes containing heavy metals (*i.e.*, $Au^{I/III}$, Ag^{I}, Cu^{I}, Pt^{II}, Re^{I}, Ir^{III}, *etc.*).[45,46] Because of their different multiplicity, the $T_1^* \rightarrow S_0$ transitions are relatively slow and occur in a milli- or microsecond timescale.

Notably, the excited state relaxation cannot be always solely classified as *fluorescence* or *phosphorescence* and might occur through a more sophisticated path-way. For instance, *thermally activated delayed fluorescence* (TADF; Figure 3B), appears if the excited states S_1^* and T_1^* are close in energies (*i.e.,* near-zero singlet–triplet energy splitting, ΔE_{ST} <1000 cm^{-1} or 0.3 eV), and the reverse ISC process (RISC) takes place under ambient conditions because of thermal activation. In this case, the excited molecule decays back *via* the radiative transition $S_1^* \rightarrow S_0$ in a timescale between those of *fluorescence* and *phosphorescence*. The aforementioned concept of TADF theoretically allows for approaching the 100% internal efficiency of the OLED.[47] Alternatively, *dual* or *multiple emission* behavior can be realized *via* different physical phenomena, *e.g.*, simultaneous radiative relaxation ($S_1^* + T_1^*) \rightarrow S_0$ (Figure 3B),[48,49] a combination of monomer-excimer emissions, conformational or chemical changes producing different excited species, and the binding of two or more individual emitters in one molecular entity. This unique behavior is beneficial for applications comprising ratiometric sensing[50] and white-light generation.[51]

Evidently, the key to the successful tuning of the photophysical properties of organoelement molecular materials and the perspectives of their further applications lie around the origin of the HOMO/LUMO. The optical gap can be controlled according to the following general strategies: (*i*) modification of the size and stereochemistry of the hydrocarbon π-conjugated chromophore; (*ii*) utilization of the lateral substituents with electronically contrasting characteristics (*i.e.,* construction of donor-acceptor systems); and (*iii*) incorporation of the heteroatomic motifs into the polyaromatic hydrocarbon frameworks and their further chemical modification.

In this view, the number of established synthetic ways to form quite stable P–C bonds and the selection of organophosphorus units with P-$\lambda^3\sigma^3$, $\lambda^5\sigma^4$, and $\lambda^4\sigma^4$ configurations offer very attractive opportunities for the design of new chromophores. By means of feasible electronic modifications, which are not always accessible for conventional organic blocks, phosphorus can significantly expand the range of di- and multi-polar compounds with new physical and chemical functionalities.

1.2 ACYCLIC ORGANOPHOSPHORUS CHROMOPHORES

The widely utilized and readily available tertial $\lambda^3\sigma^3$ aryl phosphines are probably the main source of engineered acyclic phosphorus-containing chromophores of several architectures (Figure 4). Three classical approaches are currently used for the production of various phosphines (Scheme 1).[52] First, a relatively soft two-step procedure ***I*** implies the preparation of a pre-designed organometallic aryl or alkyl precursor (lithium or Grignard species), which is further treated with a chlorophosphine derivative (*i.e.*, PCl_3, $PhPCl_2$, and Ph_2PCl). The second path ***II*** is based on the reaction between organophosphides ($KPPh_2$ and $LiPPh_2$) and arylhalides, where a halide is typically the fluoride or chloride. The third method ***III*** is the catalytic P–C bond formation using the halo- or triflate arene substrates, diphenylphosphine (Ph_2PH), and Pd as the catalyst.

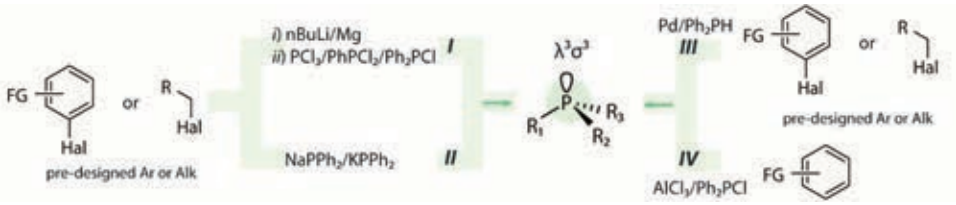

Scheme 1. General synthetic approaches to achieve $\lambda^3\sigma^3$ phosphines.

In addition, the Friedel-Crafts acylation reaction ***IV*** and the reduction of the $\lambda^5\sigma^4$ phospha-derivatives by strong-reducing agents (*i.e.*, silanes) are still employed. The nucleophilic nature of the $\lambda^3\sigma^3$ phosphines determines their possible post-modification (oxidation, coordination, and quaternization). The pronounced reactivity of these phosphines towards molecular oxygen, hydrogen peroxide, elemental sulfur, and selenium has attracted great attention in materials syntheses.

1.2.1 Pendant phospha-chalcogen groups P=E (E = O, S, and Se)

The strong electron-withdrawing ability together with the thermal stability and chemical resistance of the phosphorus-chalcogen (O, S, and Se) bond and entire $\lambda^5\sigma^4$ P-group make this bond a particularly important electronic modifier (Figure 4). In the case of the highly polar phosphoryl group, the strong P=O double bond character (E_{diss} = 575 kJ/mol) can be expressed by a simple ionic resonance structure P=O ↔ P^+–O^-. A significant shortening of the P=O distance (~1.5 Å) compared to those of its sulfur and selenium analogues (~1.9 and 2.1 Å, respectively) may be ascribed to the different bond order [≥2 for P=O, <2 for P=S(Se)], higher electronegativity of oxygen *vs* those of the other chalcogens, and the degree of effective negative conjugation. The latter model considers intramolecular interaction of the antibonding

orbitals of the Ar_3P motif with a filled 2p orbital of the oxygen atom that stabilizes and strengthens the P=O bond, thus increasing its order.

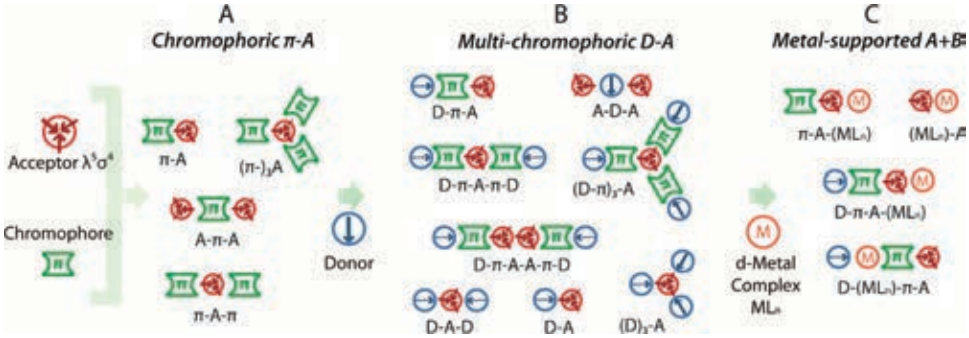

Figure 4. Versatile arrangements of the acyclic organophosphorus chromophores decorated with or built around a $\lambda^5\sigma^4$ P-group (Ar_3P=E, E=O, S, and Se).

The simplest representative of this class is the non-luminescent triphenylphosphine oxide (Ph_3PO). Substitution of the phenyl rings for the π-chromophore units leads to versatile phospha-emitters $(\pi)_x$–$(A)_y$, which display numerous geometry variations resulting from the ability of one P-center to accommodate up to three π-fragments (Figure 4A). For instance, binding of the Ph_3PO-group to pyrene (**1** and **2**; Figure 5) enhances the fluorescence intensity and slightly red-shifts the emission maximum of the $\lambda^5\sigma^4$ (Ph_2PO)-pyrene derivatives (**1**: Φ_{em} = 91%, λ_{em} = 380 nm, $CHCl_3$ and **2**: Φ_{em} = 76%, λ_{em} = 386 nm, CH_2Cl_2) compared to those of the parent pyrene (Φ_{em} = 28%, λ_{em} = 374 nm, CH_2Cl_2).[53,54] The impact of the number of chromophore substituents around the P atom has been studied in a series of air-stable pyrene-based triarylphosphine oxides [**1** π–*A*, **3** $(\pi)_2$–*A*, and **4** $(\pi)_3$–*A*; Figure 5A].[55] Despite the symmetric ground state, the substituent-dependent emissions for **3** and **4** in solution arise from the locally excited and intramolecular charge transfer (ICT) states. While an intense low-energy ICT band was observed in **4** at room temperature, it was completely absent in **1**. The emission of **4** visibly varied from cyan to deep blue in the temperature range -50 to 100 °C as a result of the large alteration in the intensities of the locally excited and ICT bands, potentially making this fluorophore a molecular thermometer (Figure 5B).

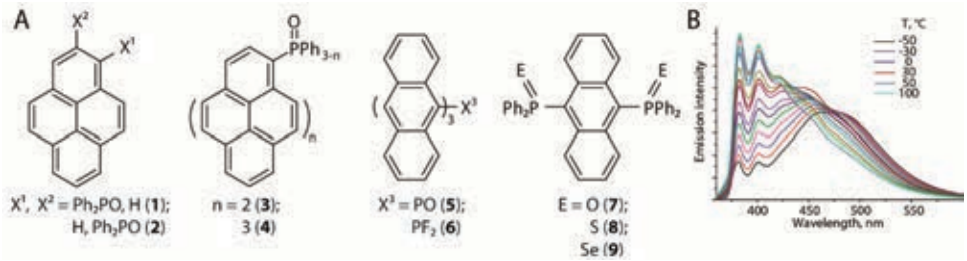

Figure 5. A: Chromophoric π–*A*-type $\lambda^5\sigma^4$ (**1–5** and **7–9**) and $\lambda^5\sigma^5$ (**6**) phospha-emitters and B: The emission spectra of **4** in methoxyethyl ether recorded in the range -50 to 100 °C.[55]

These findings are in sharp contrast with the work of Yamaguchi *et al*., in which the trianthrylphosphorus framework (**5**) with $\lambda^5\sigma^4$-P tetrahedral geometry displayed very weak fluorescence (Φ_{em} <1%) *vs* the highly emissive phosphorane **6** (Φ_{em} = 0.28) with a hypervalent $\lambda^5\sigma^5$ trigonal-bipyramidal arrangement (two fluorine atoms occupy axial positions).[38] Among the bis(chalcogenide)anthracene derivatives **7–9**, only the oxide decorated **7** exhibited blue emission in solution (λ_{em} = 450 nm). On the other hand, the intense solid-state emission of **8** (λ_{em} = 508 nm) was detected for its toluene solvate, owing to the specific C–H···π-ring intermolecular interactions of the solvent molecules with the emitter; *i.e.*, **8** acts as a chemosensor for small aromatic hydrocarbons.[56]

Recently, Butckevich *et al*., reported a comprehensive study of a family of organophosphorus dyes, the rational design of which allowed for the fine-tuning of their photophysical characteristics.[57] The presented strategy for the HOMO/LUMO variation relied on the modification of the well-known electrophilic cores (coumarine, pyronin, acridinium salt, *etc*.) through the direct tailoring of the $\lambda^3\sigma^3$-nucleophilic soft bases (phosphinites, phosphonites, and phosphoramidites) and their subsequent oxidation. These $\lambda^5\sigma^4$-phosphonylated dyes, exemplified by **10–12** (Figure 6), demonstrated lower fluorescence quantum yields and absorbed and emitted at longer wavelengths with increased Stokes shifts (≤7000 cm^{-1}) compared to those of the parent organic dyes. In general, the inclusion of a strong acceptor, particularly into the polarizable chromophore moieties, facilitates the ICT responsible for a decrease in the optical gap.

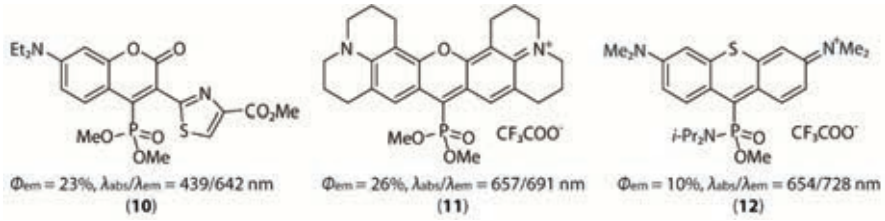

Figure 6. Phosphonylated dyes **10–12** and their photophysical characteristics in solution.[57]

Although not all the phosphine oxides with aromatic backbones display intense luminescence (*e.g.*, **13–15**; Figure 7), they can be applied as materials to improve the electron injection/transporting ability in multilayer OLEDs and organic photovoltaic (OPV) cells.[20,21,58–60]

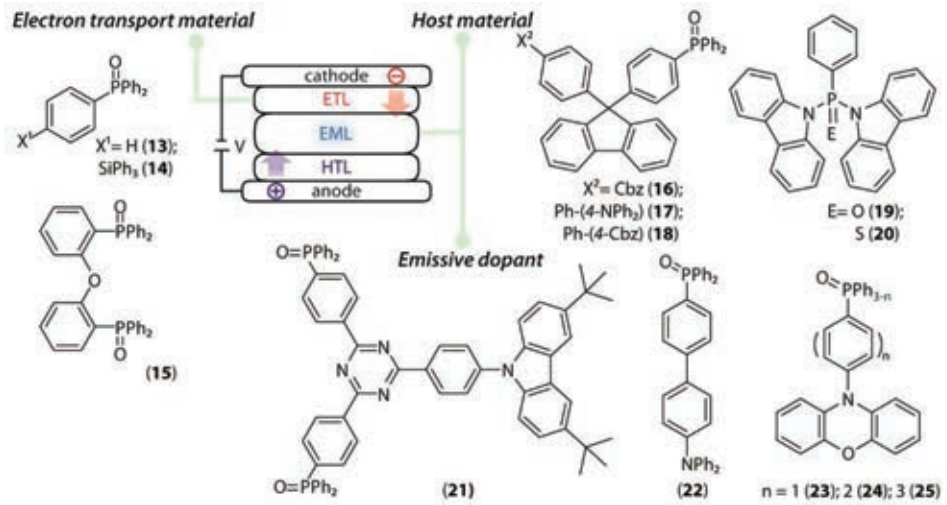

Figure 7. Simplified representation of a multilayer OLED structure (ETL/HTL = electron/hole transport layers, EML = emissive layer) and examples of utilized phospa-derivatives (Cbz = carbazole).

The relatively easy synthesis of P-chalcogenide derivatives and the electron accepting properties of the $-PR_2E$ groups define their popularity in the design of di- and multipolar "push-pull" (*D*–*A*) organophosphorus chromophores, which have been extensively studied (Figure 4B). The fundamental outcome of connecting an electron-rich group (*D*) with an electron-deficient P-$\lambda^5\sigma^4$ center (*A*) through a π-conjugated spacer is a distinct charge separation in the polarized *D*–π–*A* species; *i.e.*, the HOMO and LUMO are predominantly localized on the *D* and *A* moieties, respectively. The excitation of such molecules induces an ICT, which causes unique photoluminescence properties such as solvatochromism (*i.e.*, response on the polarity/viscosity of the solvent), thermochromism, dual emission, multi-photon absorption, and TADF.[61]

Ambipolar *D*–*A* compounds[62–68] meet the requirements for OLED host materials, including (*i*) balanced transport of the electrons and holes; (*ii*) a high triplet energy level; (*iii*) suppressed excimer/exciplex formation due to the amorphous morphology of the material, ensured by the tetrahedral arrangement of the P-center; and (*iv*) thermal/electrochemical stability and a high glass transition temperature.[20,69,70] The concept of indirect linkage was demonstrated by Ma *et al.*, for the series **16–18** (Figure 7).[65] In these asymmetric bipolar structures, the hole-transporting functions (diphenylamine/carbazole) did not influence the

contribution of the electron transporting group (diphenylphosphine oxide) and fluorene moiety to frontier the molecular orbitals, which is advantageous for reaching the relatively high triplet energy ~3.0 eV and small singlet-triplet energy gap ΔE_{ST} <0.5 eV. These characteristics of **16**–**18** with unusual spiro *D*–*A* separation allowed them to be employed as efficient hosts and achieve high EQEs, ≤14.4%, for a blue high-performance phosphorescent OLED (PHOLED) with bis[2-(4,6-difluorophenyl)pyridinato-C2,N](picolinato)iridium(III) (FIrpic) as the emitter. The blue emissive dicarbazolylphosphine oxide **19** and sulfide **20** (Figure 7) are illustrative examples of efficient semiconductors based on *D*–*A* architecture with greatly enhanced carrier transport properties, assigned to the resonance forms N–P=E ↔ N^{+}=P–E^{-} (E = O, S).[71,72] The latter form dominates in sulfur derivative **20**, where enantiotropic resonance is more favorable (ΔE ~0.13 eV) compared to that of **19** (ΔE ~0.28 eV); this is in accordance with the significant change in the bond order (P=O >2 and P=S <2). However, both host materials employed in the sky blue FIrpic-doped PHOLED devices produced high external quantum efficiencies (EQEs) of 16.5% (**19**) and 21.7% (**20**). It has been shown that the connecting unit between the donor and acceptor parts crucially influences the carrier conductivity.[63,67,70]

In 2014 Liu *et al.*, communicated on a simple multifunctional phosphine-oxide **22** with intense fluorescence (λ_{em} = 433 nm, Φ_{em} = 80% in ethyl acetate).[73] This compound was employed as a host for a green PhOLED reaching 18.1% of the EQE as well as a pure deep blue emitter for a non-doped device with 5.4% of the maximum EQE and the Commission Internationale de l'Eclairage (CIE 1931) coordinates (0.15, 0.06). Notwithstanding the seemingly moderate efficiency, the latter OLED produced a pure deep blue color that met the current standards of high-definition television HDTV (CIE 0.15, 0.06), which remains a technological problem. To date, the best performance achieved for deep blue OLEDs at practical luminance values (100–1000 cd/m^2) does not exceed 8.7% of the EQE.[74,75]

Materials exhibiting TADF, including *D*–*A* phosphine oxides, have been considered as breakthrough emitters that realize highly efficient blue diodes.[68,76–78] Organic TADF emitters provide several advantages over fluorophores and phosphors, such as (*i*) ≤100% exciton utilization upon electrostimulation that enhances the overall efficiency and (*ii*) prompt and delayed singlet excited state relaxations that result in a higher electroluminescence energy; therefore, deep blue emission color can be achieved. Several parameters, such as the π-spacer conjugation length, geometry and steric effects, and strength of both the acceptor and donor units should be considered for a delicate TADF design. Owing to this variability, there has been no general approach to develop simple and highly efficient deep blue TADF emitters to date.[79]

For example, a recently reported blue emitter **21** (Figure 7) consisted of the electron deficient 1,3,5-triazine spacer connected with a phenylcarbazole donor and two secondary accepting triphenylphosphine oxide groups. Emission maximized at 492 nm with the quantum yield approaching unity and ~98% RISC efficiency was

achieved in a film.[76] This "secondary acceptor" strategy allowed the fabrication of a sky blue OLED (0.18, 0.42), which displayed 28.9% of the maximum EQE. Evidently, a significant bathochromic shift occurs in the case of an extended conjugation system that is detrimental to attaining a true blue color. To eliminate this problem, a pyramidal $\lambda^5\sigma^4$-phospha center can be used as a conjugation-insulating joint.[78,80] The decoration of an $Ar_3P{=}O$ acceptor with up to three donor "phenoxazine arms" afforded the $(D{-}\pi)_n{-}A$ TADF molecules **23–25** (Figure 7). Along with the increasing number of phenoxazines (n = 1–3), the photoluminescence yield (Φ_{em}) improved from 45 to 65% due to the accelerated RISC process, with negligible emission red-shift (**23**, 448 nm → **24**, 460 nm → **25**, 464 nm). The OLED device with the CIE coordinates (0.17, 0.20) based on emitter **25** delivered the maximum EQE of 15.3%.

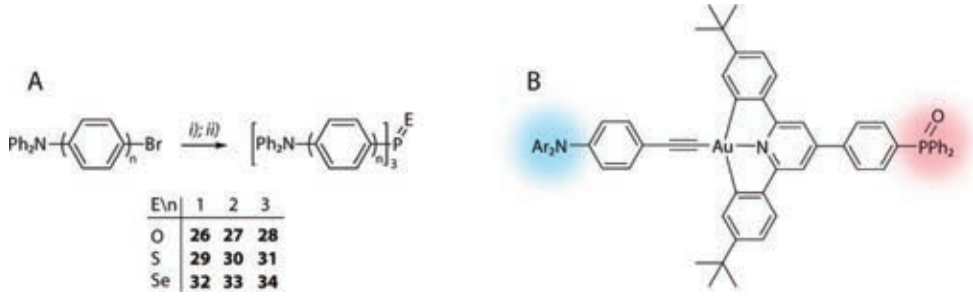

E\n	1	2	3
O	**26**	**27**	**28**
S	**29**	**30**	**31**
Se	**32**	**33**	**34**

Figure 8. A: Synthesis of the $(D{-}\pi)_3{-}A$ blue emitters **26–34** [*i*: n-BuLi, -78 °C, THF, PCl_3; *ii*: H_2O_2 (**26–28**), S_8 (**29–31**), and KSeCN (**32–34**), DCM][80] and B: Chemical structure of the phosphine oxide-containing bipolar alkynylgold(III) complexes.[81]

Concurrently, the properties of the C_{3v} symmetrical $(D{-}\pi)_3{-}A$ molecules have been studied by Koshevoy *et al*., wherein blue emission was finely tuned *via* the systematic variation of the $D{-}\pi$ spacer length and electron accepting effect of different chalcogenide P-$\lambda^5\sigma^4$ fragments.[80] The nature of the $Ar_3P{=}E$ (E = O, S, and Se) acceptor displayed a small influence on the emission wavelength; however, for the Se-derivatives (**32** and **33**), a dramatic drop in the emission intensity was observed. Selected compounds **27**, **28**, and **30** were used for the construction of doped and non-doped OLEDs with true blue CIE (0.15, 0.06) and the maximum EQE 6.5%, proposed to originate from singlet energy repopulation *via* a triplet-triplet annihilation mechanism.

Binding the heavy metal atoms (*e.g*., Ir^{III} and Au^{III}) to $\pi{-}A$ and $D{-}\pi{-}A$ phosphine oxide moieties often ensures phosphorescence character of the emission (Figure 4C). For instance, a cyclometalating ligand (*e.g.,* phenylpyridine) can be modified by attaching the electron-withdrawing phosphine oxide (PO). Its further coordination to the trivalent iridium ion yielded phosphorescent complexes with enhanced color tuning and improved charge carrier injection/transport.[82–86] The PO substituent in the pyridine ring causes a significant reduction (*i.e.,* stabilization) in

the LUMO for Ir complexes, accompanied by a phosphorescence bathochromic shift. In another approach described by Yam *et al.*, (Figure 8B), the heavy Au^{III} ion was used as a joint mediator between the dendrimeric diphenylamine/carbazole acetylene (*D*) and the cyclometalating phosphoryl-doped ligand (*A*).[81] The incorporation of the phosphine oxide moiety doubled the electroluminescence efficiency compared to the structural analogues, affording a green OLED (max. EQE 15.3%) with an extremely small roll-off (<1% at 500 cd/m^2).

According to the hard and soft Lewis acids and bases (HSAB) concept, phosphine oxides are classified as hard Lewis bases (HB). Because of their semi-ionic bond character (P=O ↔ P^+–O^-) these compounds readily act as ligands and display good affinity to produce stable covalent M–O bonds with lanthanide(III),[87] manganese(II),[88–91] and iridium(III),[92,93] ions. The emission in the case of lanthanides(III) dominantly occurs by means of metal-centered f→f transitions (*e.g.*, Eu^{3+} $^5D_0 \rightarrow {}^7F_n$, Tb^{3+} $^5D_4 \rightarrow {}^7F_j$), which are characterized by sharp emission bands, long excited lifetimes, and large Stokes shifts. Because the f→f transitions are parity-forbidden, the excited states of the f-metal ions can be populated *via* the antenna effect using the triplet state of the ligands (*e.g.*, phosphine oxide; Figure 9A). An incomplete energy transfer from the phosphine-oxide chromophore to the lanthanide ion resulted in multiple emissions.[94]

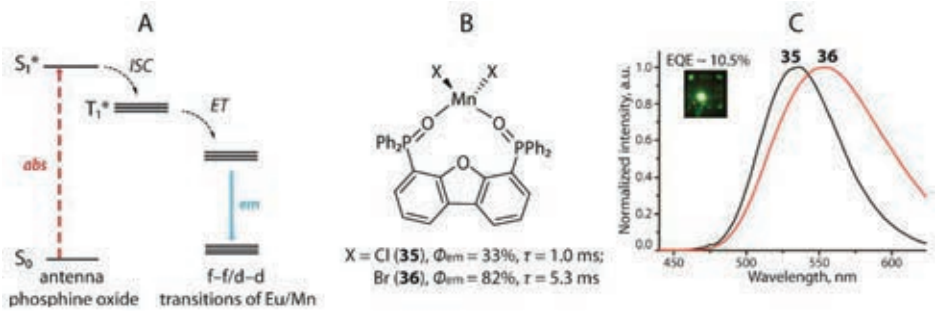

Figure 9. A: Schematic representation of the ligand-induced antenna effect (ET = energy transfer); B: Tetrahedral Mn^{II} highly emissive PO complexes **35**, **36**[88]; and C: Emission spectra in the solid state for **35**, **36**; inset depicts a green OLED constructed from **36** .

A similar behavior has been observed for the low-cost Mn^{II} complexes, whereby the metal-centered d–d ($^4T_1(G) \rightarrow {}^6A_1$) radiative transitions are sensitized by the energy transfer from the triplet excited state of the PO ligand (Figure 9A). Luminescence of Mn^{II} strongly depended on the crystal field, whereby the emission in the green (~520 nm)[89] and orange red (580–620 nm)[90] regions was associated with tetra- and penta-/octahedral geometries, respectively. Thus, modulation of the phosphorescence color can be rationally controlled by the geometry and rigidity of the PO ligand, the transition metal-to-PO ratio, or an external stimulus (*i.e.*, vapor of the solvent).[91] The rigidity of complexes **35** and **36** (Figure 9B) has been improved

by selecting dibenzofuran-phosphine oxide. Preventing nonradiative relaxation increased the quantum efficiency to values ≤82% with long τ values of ~5.3 ms at 530–560 nm in the solid state. Complex **36** is the first example of employing the manganese material as a dopant in a highly efficient (EQE ~10.5%) vacuum-deposited green OLED (Figure 9C).[88]

Despite the fact that the coordination chemistry of luminescent phosphine oxide complexes is interesting, it is not diverse because of the limited selection of such ligands reported to date. However, the reduction of the oxide group and direct usage of $\lambda^3\sigma^3$ tertiary phosphines as building blocks have been very well studied.

1.2.2 Phosphines as active components in light-emitting metal complexes

Nowadays, tertiary phosphines serve as a unique and powerful tool in coordination chemistry for the construction of metal-based luminophores.[95] Tunable electronic and steric properties of the three organic substituents together with the σ-donating and π-accepting abilities of their phosphorus centers makes them excellent supporting/acting ligands.[96] The affinity of the neutral tertiary phosphines to soft d^6–d^{10} transition metal ions (*i.e.*, Au^I, Ag^I, Cu^I, Pt^{II}, Re^I, *etc.*) combined with X-type ligands (*e.g.*, acetylenes, thiols, halides, and pseudohalides) has led to the formation of numerous homo-/heterometallic luminescent aggregates, cycles/cages and polymers, and simple mono- and binuclear complexes.[95,97–101] Diverse photophysical properties have arisen from various electronic transitions and their combinations, which include metal- and ligand-centered transitions (MC/LC) and ligand-to-ligand, metal-to-ligand, and ligand-to-metal charge transfers (LLCT, MLCT, and LMCT, respectively). The luminescence characteristics of these molecules can be tuned in many ways: controlling the nuclearity of the metal frameworks, modulating the metallophilic and other non-covalent interactions, and altering the stereochemistry, rigidity, and electronic features of the ligands. In recent years, research on metal compounds containing phosphorus ligands was stimulated by the design of highly effective Cu^I/Ag^I TADF[102–104] complexes, in which phosphines play an active role as stabilizing chelates and charge transfer (CT) acceptors that contribute to the emissive excited state.

A series of "superphenylphosphines" $P\{HBC(t\text{-}Bu)_5\}_nPh_{3-n}$ (n = 1–3) bearing one to three hexa-*peri*-hexabenzocoronene (HBC) substituents formed the palladium emissive species $PdCl_2L_2$ and $Pd_2Cl_4L_2$.[105] The Pd-complexes mimic the HBC characteristics, demonstrating extremely high optical absorptions ($\varepsilon \leq 6.5 \cdot 10^5$ M^{-1} cm^{-1}) and an intensive green emission (λ_{em} = 469 nm) assigned to LC ππ* transitions.

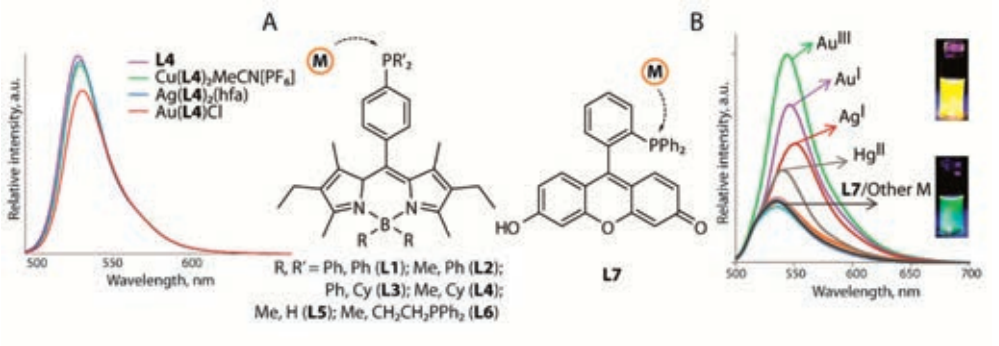

Figure 10. Phosphine-decorated chromophores and their metal complexes based on A: boron dipyrromethene (Bodipy; **L1–L6**)[106,107] and B: Fluorescein (**L7**) and their emission profiles in solution; Ph = phenyl, Me = methyl, Cy = cyclohexyl, and hfa = hexafluoroacetylacetonate.[43]

The phosphine-decorated chromophores, *e.g.*, boron dipyrromethene (Bodipy)[106,107] (**L1–L6**; Figure 10A) and fluorescein[43] (**L7**; Figure 10B) distinctly stand out as a new class of photoactive ligands. The coordination ability of the fluorescent phenyl-Bodipy skeleton functionalized with a P-$\lambda^3\sigma^3$ diphenylphosphine group (**L1–L6**) has been studied by Higham *et al*.[106,107] The boron and phosphorus atoms bearing aliphatic substituents (methyl and cyclohexyl) in **L4** presented higher quantum yields (**L1** Φ_{em} = 4% < **L3** Φ_{em} = 7% and **L2** Φ_{em} = 29% < **L4** Φ_{em} = 44%). Upon coordination of the highly emissive ligand **L4** to d^{10} metal ions, the fluorescence of the $\lambda^4\sigma^4$ derivatives remained nearly unaffected (Figure 10A; λ_{em} = 527 nm), thereby indicating negligible contribution of the phosphorus-metal character in the lowest excited state. In a continuation of this study, the tridentate pincer ligand **L6** was synthesized by the convenient hydrophosphination reaction of **L5** with two equivalents of vinyldiphenylphosphine. The complexation of **L6** with rhenium(I) chloro carbonyl produced Re(**L6**)Cl$(CO)_2$, the photophysical behavior of which is comparable to that of its parent **L6** (λ_{abs} = 513 nm, λ_{em} = 527 nm, Φ_{em} = 24%). This complex was successfully applied to imaging studies of prostate carcinoma cells, whereas the $[^{99m}Tc(\mathbf{L6})(CO)_3]^+$ analogue was a suitable multi-modality imaging probe (*i.e.*, fluorescent and radio) for *in vivo* and *in vitro* medicinal investigations.[108] Coordination-based chemosensing was exemplified by the P-$\lambda^3\sigma^3$ phosphinofluorescein **L7** (Figure 10B).[43] A moderate emission of water-soluble phosphine was visibly perturbed by the heavy metal atom ($Au^{I/III}$, Ag^{I}, and Hg^{II}), with the highest 3.8-fold intensity raise and incremental red-shift of 10 nm in response to the Au^{III} ion.

Notably, although the intraligand fluorescence of coordinated phosphines has been observed for numerous complexes, the induction of ICT in phosphines with "push-pull" architecture, upon their coordination to the metal ion, has been virtually overlooked in the design of photofunctional metal complexes.

1.2.3 Phosphonium cation as a terminal group in emissive materials

While many examples of P-$\lambda^5\sigma^4$/$\lambda^4\sigma^4$ derivatives with terminal P=E/P−M motifs (E = O, S; M = Au^I, Ag^I, and Cu^I) have been explored, the number of luminescent compounds bearing a quaternized pendant phosphonium group (P^+R_4), is still quite limited.

The synthetic approaches to $\lambda^4\sigma^4$ alkyltriaryl- and tetraarylphosphonium salts are summarized in Scheme 2.

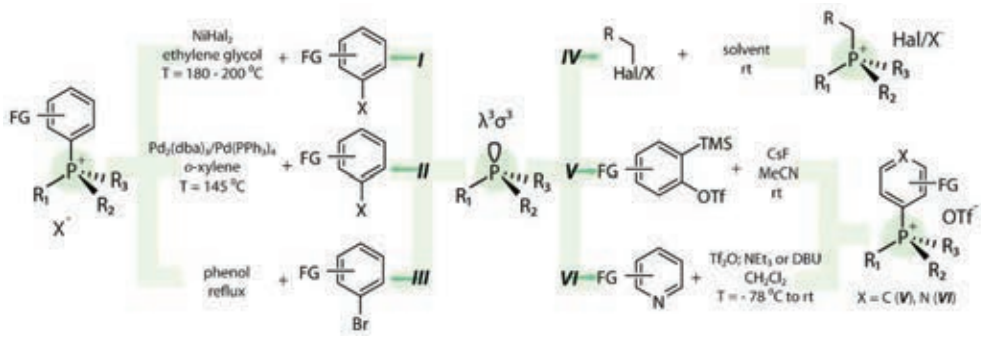

Scheme 2. Common synthetic pathways to quaternized phosphonium salts.

Ni- and Pd-catalyzed P–C bond formation processes (methods ***I*** and ***II***, Scheme 2) were originally introduced by Horner and Heck[109] and later, the reaction conditions (catalyst loading, concentration, and solvent) were optimized by Charette.[110,111] The general mechanism in both cases includes the oxidative addition of aryl halides/triflates to the Ni^+ and Pd^0 metal center, followed by the reductive elimination of the desired phosphonium salt. Despite the relatively high temperature, active functional groups such as alcohols, ketones, and aldehydes tolerated the reaction. An appealing metal-free coupling of triphenylphosphine with a variety of arylbromides in refluxing phenol (method ***III***) has been recently introduced by Huang *et al*.[112] A key feature of this procedure is the high degree of accessible functionalization under the readily accessible conditions. A well-known and commonly used pathway (method ***IV***) relies on the alkylation of the $\lambda^3\sigma^3$ phosphines by alkyl halides/triflates (*i.e.*, benzyl-, naphthyl-, anthryl bromides, and methyl iodide/triflate) under soft conditions. The main disadvantage of alkyl-triaryl phosphonium salts is the lack of stability toward basic conditions and nucleophilic attack, owing to phosphonium ylide formation. Nevertheless, this method is suitable for the simple construction of aliphatic phosphonium mechanochromic solid fluorophores.[113,114] Other mild syntheses of quaternary salts, *e.g.*, arylation *via* aryne intermediates ***V***,[115] synthesis of pyridine phosphonium salts ***VI***[116], and radical photoredox-mediated phosphine arylation by $[Ar^1\text{-}I^+\text{-}Ar^2]X$[117,118] have also been developed.

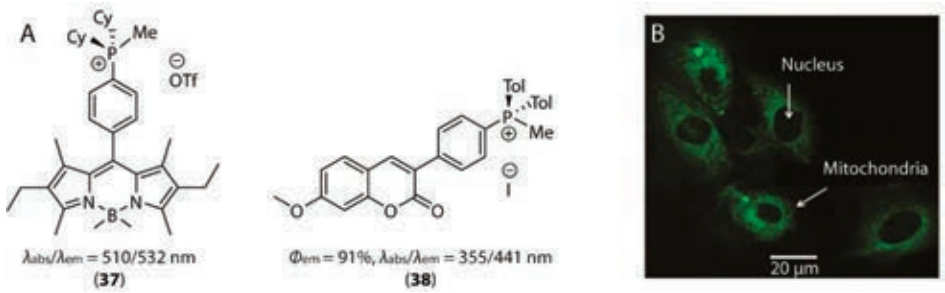

Figure 11. A: Phosphonium-modified chromophores **37** and **38** and B: Confocal microscopy photo of the H9c2 cell line stained with **37**.[119]

Modification of the chromophore-based phosphines was carried out by method ***IV*** to afford Bodipy-(**37**)[119] and coumarine-phosphonium salts (**38**)[120] (Figure 11A). A particular feature of lipophilic phosphonium dyes is their selective mitochondrion localization (illustrated by **37**; Figure 11B), which has been actively utilized in bioimaging applications.[121]

The nonlinear absorption (NLA) properties together with the negative solvato- (*i.e.*, hypsochromic shift of the absorption band upon increasing the polarity medium) and halo-(*i.e.,* reversible color changes upon treatment with the alkali metal cations) chromism of the dipolar linear $\lambda^4\sigma^4$ phosphonioarylamino dyes (Figure 12) have been discovered by Lambert *et al.*,[122] and Allen *et al*.[123,124] One-, two-, and three-dimensional dibutylaminoazobenzenephosphonium salts **39–41** illustrate the additive intensity growth of the ICT absorption band and substantial negative solvatochromism upon increasing the polarity of the medium ($CHCl_3$ → MeCN). The NLA of octupolar compound **41** is about threefold larger than that of dipolar congener **39**.

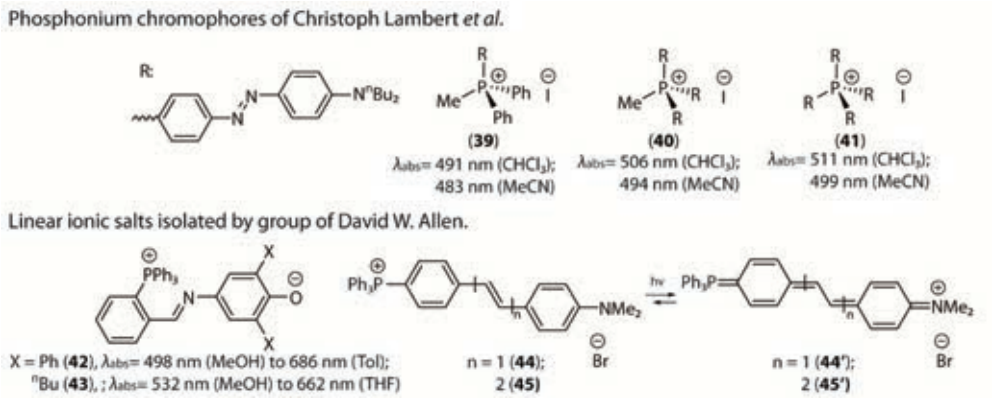

Figure 12. Selected $(D–\pi)_n–A$ linear phosphonium chromophores **39–45** studied by C. Lambert (top)[122] and D. W. Allen (bottom).[123,124]

More drastic absorption changes were observed for betaine dyes **42** and **43** as a result of a larger charge separation.[123] Thus, **42** appeared green in toluene (λ_{abs} = 686 nm), purple in dichloromethane (DCM; λ_{abs} = 596 nm), violet in acetonitrile (MeCN; λ_{abs} = 562 nm), and red in methanol (λ_{abs} = 498 nm), producing a maximum hypsochromic shift of the ICT absorption band of ~188 nm (~5500 cm^{-1}). As predicted, the presence of the electron deficient phosphonium cations in **44** (λ_{abs} = 406 nm, MeOH; 422 nm, DCM) and **45** (λ_{abs} = 422 nm, MeOH; 442 nm, DCM) induced distinct ICT and thus, upon photoexcitation charge migration is possible (**44** → **44′**).[124]

The combination of the $\lambda^4\sigma^4$-phosphonium motif with triarylboranes is perfectly suited for selective fluoride/cyanide anion optical detection by fluori- and colorimetric responses.[125–128]

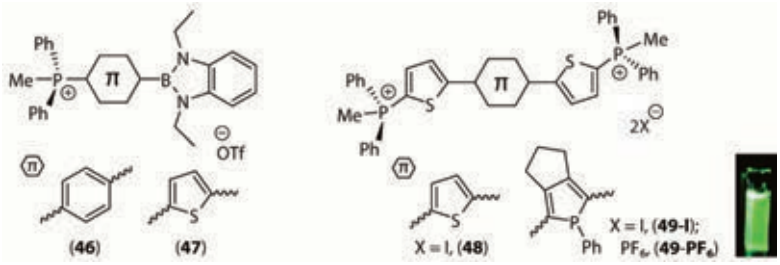

Figure 13. Schematic structures of the *D*–π–*A* **46**, **47** (left)[129] and *A*–π–*A* **48**, **49** (right) linear $\lambda^4\sigma^4$ phosphonium chromophores; inset photo displays the emission color of the **49-PF$_6$** solution.[130]

Compared to the frequently used electron defficient dimesityl boron group, the utilization of 1,3,2-benzodiazaborole as a weak donor in the push-pull linear salts **46** and **47** (Figure 13) enhances the emission. A key feature of the $-P^+Ph_2Me$ group *vs* $-PPh_2(X)$ (X = O, S, and AuCl) is the lower lying LUMO; thus, a more pronounced red-shift of the absorption and fluorescence bands accompanied with larger Stokes shifts ≤11150 cm^{-1} was achieved for the structurally analogous species.[129] The α,α'-terthiophene linked diphosphonium salt **48**[130] demonstrated NLA and blue emission in solution (λ_{abs} = 387 nm, λ_{em} = 475 nm, DCM) assigned to the $\pi\pi^*$ transitions based on theoretical calculations.

The emitting ability of **49** significantly depended on the counter ion nature and concentration: in the moderately polar DCM, the green emission of the diiodide salt **49-I** only reached Φ_{em} = 7% at high concentration with multiexponential decay [τ = 0.04 (76%), 0.51 (8%), 2.7 (16%) ns] whereas under the same conditions, the $\Phi_{em\ value}$ of **49-PF$_6$** was 86% with a single lifetime τ of 2.8 ns.[42] Additionally, the fluorescence intensity upon titration of a DCM solution of **49-I** by $^nBu_4NX$ was 4.9- (X = Cl) and 2.4 (X = Br) times larger than the initial value. Such an effect can be rationalized by the presence of the equilibrium contact ion pair ⇄ solvent-separated ion pair and therefore, effective quenching by the heavy iodine counterion takes place.

1.3 CONJUGATED PHOSPHACYCLIC CHROMOPHORES

The merging the organophosphorus blocks with carbon-rich π-conjugated scaffolds has become a useful tool for the construction and rational tuning of a diversity of chromophores. This type of modification leads to the controllable lowering of the LUMO, which is typically difficult to perform for pure carbon-based materials over a wide range. Partial involvement of the phosphorus lone pair into the conjugated system decreases the nucleophilicity of the P-donor and lowers the reactivity of the merged $\lambda^3\sigma^3$- phospha center compared to those of the pendant–PPh_2 groups. Nevertheless, all the chemical post-modifications of P-heterocycles (*i.e.*, alkylation, oxidation, and coordination) remain accessible analogously to acyclic phosphines. A substantial amount of publications since the 2000s have reported five-membered phosphole-type compounds. Conversely, other four-(phosphetes), six-(*e.g.*, phosphinines and phosphaphenalenes) and seven-(*e.g.*, phosphepines) membered homologues have been poorly explored.[22,131–134]

1.3.1 Five-membered luminescent phosphacycles

The widespread occurrence of phospholes is associated with their prominent feature known as the phenomenon of hyperconjugation. The effective interaction between the exocyclic σ*(P-R) and π* (butadiene) orbitals together with the pyramidal configuration of the phosphorus atom make phospholes less aromatic compared to their close congeners (thiophene, furan, and pyrrole) according to the nucleus-independent chemical shift (NICS, negative and positive values indicate aromaticity and antiaromaticity, respectively; Figure 14), with significantly lower LUMO orbitals and optical band gap.[22,135,136] The electron-accepting properties and chemical and thermal stabilities of phospholes can be additionally improved by converting the $\lambda^3\sigma^3$ P-center into the $\lambda^5\sigma^4/\lambda^4\sigma^4$ species. Taking advantage of these molecules, phosphole-based materials have been actively applied in the areas of organic- and bioelectronics.[16,22,59,131,132,137]

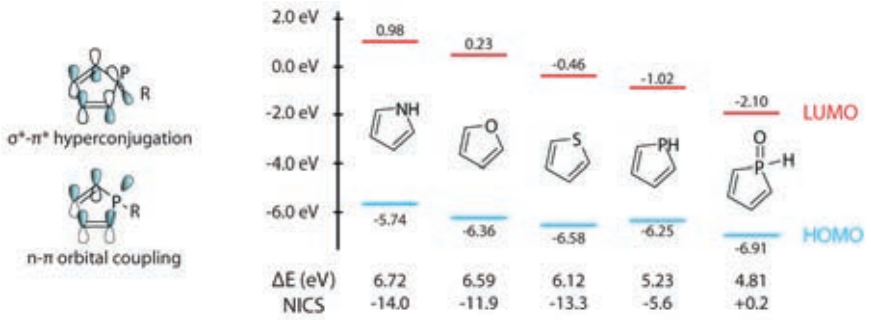

Figure 14. Phosphole orbital coupling (left) and aromaticity (NICS values) and HOMO-LUMO distribution of the pyrrole, furan, thiophene, and phospholes (right).

Several routes have been described for the preparation of substituted and annulated phospholes (Scheme 3). The first 5-phenyl-5*H*-dibenzophosphole was introduced by Wittig and Geissler[138] in 1953. It was obtained from the *ortho*-dihaloaromatics through a metalated intermediate (*e.g.*, lithiated) and further treated with dihaloarylphosphine (route ***I***^{a}). Alternatively, the direct addition of a dimetalphosphide (K or Na) to a haloaromatic (mainly a fluoroaromatic) has also been studied.[131,139] Similarly, modified method ***I***^{b} was based on the reaction of tin phosphide with a dihaloorganic precursor *via* refluxing with trifluorotoluene. Since then, a large variety of (hetero-)polyaromatic hydrocarbons (PAHs), including the simplest diarylenes,[139–141] mono and bipyridines,[142–144] dithienes,[145–147] and even porphyrins[148] have been merged with a phosphole moiety.

Scheme 3. General methods for the preparation of phosphole derivatives; procedure details: ***I***^{a} *i*) $^{n/t}$BuLi, TMEDA, THF/Et_2O, -78 °C and *ii*) $PhPCl_2$, -78 °C to rt; ***I***^{b} $PhP(SnMe_3)_2$ or ^{n}octylP$(SnMe_3)_2$, V-40, $PhCF_3$, 125 °C, 48 h; ***II*** $PhPBr_2/PhPCl_2$, THF, -78 °C to rt; ***III*** Ag^{I}, Mn^{III}, Cu^{II}/peroxide or Tf_2O/base, solvent, heating; ***IV***^{a} PBr_3/PCl_3, rt or reflux; and ***IV***^{b} *hv*, CH_2Cl_2, 1 h.

Route ***II***, which resembled route ***I***, relied on the intermediate zirconium and titanium metallacycles generated from suitable acetylenes and diynes, which undergo metal to phosphorus exchange when treated with $PhPBr_2/PhPCl_2$. Both these methods are popular in the construction of heteropolyaromatics[41,149,150] as well as phospholes suitable for further backbone post-modification and decoration by functional groups.[151,152] The unsymmetrical benzophosphole derivatives can be easily obtained through phosphinyl-radical metal-mediated[153,154] and phosphenium-cation metal-free[155–157] [3+2] intermolecular cycloaddition (method ***III*** in Scheme 3), which, however, exhibits poor selectivity towards unsymmetrical alkynes. The last method, ***IV***, comprises intramolecular cyclization. Introduced by Yamaguchi, selective *trans*-halophosphanylation route ***IV***^{a} successfully produced a family of environmentally sensitive *D*–π–*A* molecules.[158–160] The nucleophilic cascade marriage of phosphanyl/boryl-substituted diphenylacetylenes (Scheme 3, ***IV***^{b}), as a peculiar case of ***IV***, produces phosphonium/borate zwitterionic stilbene-like

luminophores.[30,161] Apart from the highlighted synthetic pathways, other methods are available and can be found in the detailed review published by Bałczewski.[139]
The multitude of factors that influence the photophysical properties of phosphole-containing luminophores have been systematically studied. Structural variations for the tuning of optical characteristics considered the following concepts: (*i*) variation of PAH systems linked to annulated/non-annulated phospholes,[162–164] (*ii*) utilization of additional heteroatoms (P, B, N, Si, S, *etc.*) attached to the phosphole core,[148,165,166] (*iii*) functionalization with donor substituents to decrease the band gap and facilitate CT,[158,167,168] and (*iv*) alteration of the valence/coordination environment and accepting properties of the $\lambda^3\sigma^3/\lambda^5\sigma^4/\lambda^4\sigma^4$ merged fragment.[41]

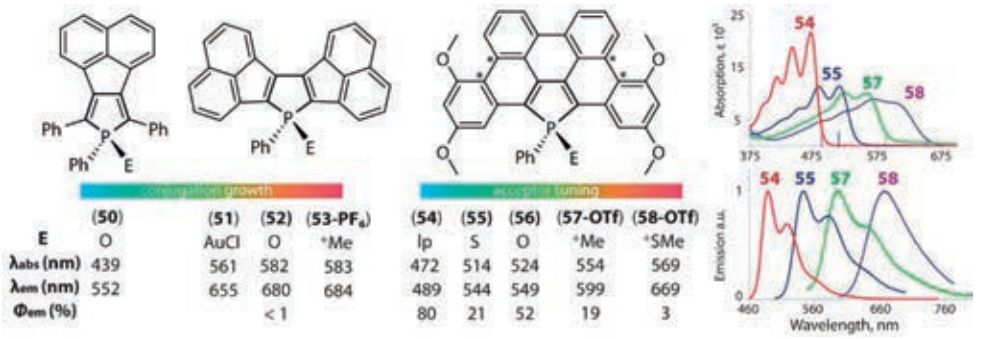

Figure 15. Schematic structures and photophysical behavior of mono- and diacenaphthophospholes **50**–**53**[141] and dibenzophosphapentaphenes **54**–**58**[41] (lp = lone pair), *absence of a carbon–carbon bond in phosphole **59**.

For example, acene-annulated phosphole systems **50**–**53** differ by the position connectivity and number of their naphthalene units (Figure 15).[141] Thus, mono-naphthalene dye **50** emitted at 552 nm in DCM, whereas the fluorescence band of **52** with two PAH units was significantly red-shifted to 128 nm. The congener species, gold(I) chloride **51**, oxide **52**, and phospholium salt **53**$^+$**,** revealed bathochromically shifted absorption ($\Delta\lambda_{abs}$ ~22 nm) and emission maxima ($\Delta\lambda_{abs}/\Delta\lambda_{em}$ 1–22/25û29 nm) with Φ_{em} <1%. An extended family of neutral (**54**–**56**) and ionic (**57**$^+$ and **58**$^+$) planarized dibenzophosphapentaphenes has been designed by Hissler and Réau (Figure 15).[41] Surprisingly, the larger PAH backbone compared to those of **50**–**53** resulted in higher absorption and emission energies, with a drastically more efficient ππ* fluorescence (Φ_{em} ≤80%). The modification of the $\lambda^3\sigma^3$ phosphorus center in **54** led to negative hyperconjugation of the PAH system with σ* P–R MOs and a considerable red-shift of the emission; however, this was accompanied by a drop in intensity because of the growing non-radiative rates. Interestingly, the predecessor of **54**–**58**, without the extended planar framework (**59**; *i.e.*, no carbon–carbon bond between C_7–C_8 and C_{17}–C_{18}; marked by * in Figure 14) did not display appreciable luminescence.[41,150]

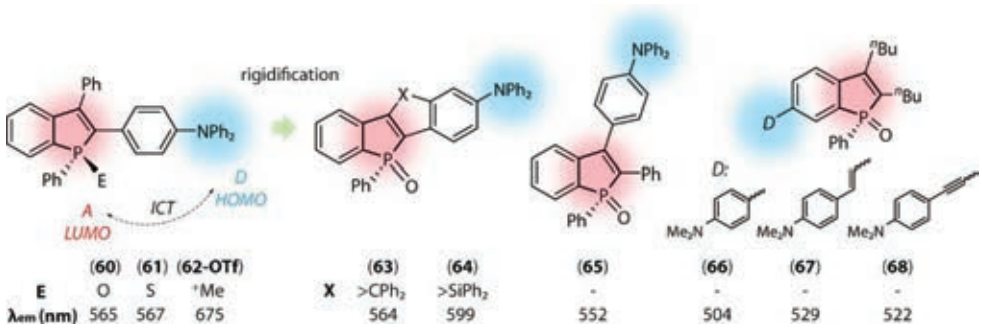

Figure 16. Schematic structures of the *D-A* molecules **60–68** based on benzo[b]phospholes and their emission maxima in dichloromethane solutions.

The molecular design of the environment-sensitive fluorescent probes often benefits from the dynamic behavior of *D*–π–*A* or similar architectures, *i.e.*, when the π-connected electron accepting and donating moieties modulate the ICT process. Following this rationale, Yamaguchi *et al.*, combined benzophosphole $\lambda^5\sigma^4$-oxide (**60**), -sulfide (**61**), and $\lambda^4\sigma^4$-salt (**62-OTf**), (*A*), with triphenylamine group (*D*) (Figure 16).[158] The resulting *D-A* molecules demonstrated discernible solvatochromism (*e.g.*, **60** λ_{em}, Φ_{em}: 528 nm, 94% in toluene; 553 nm, 94% in chloroform; 575 nm, 84% in acetone; 601 nm, 64% in DMSO). The red-shift of the emission was expectedly more pronounced for phospholium salt **62** (λ_{em} 672 nm in toluene → 702 nm in DMSO). Rigidification of **60** *via* diphenylmethylene or diphenylsilylene bridges drastically improved the photostability of the fluorophores, which is crucial for bioimaging.[159,169] The photophysical parameters of carbon-bridged **63** were similar to those of parent **60**, except for the 1.5–2.0-fold higher quantum yields in polar solvents, whereas the silicon-modified analogue **64** displayed a 35 nm emission red-shift, explained by the decreased LUMO energy.
The introduction of the electron-rich group into the second position of phosphole **65** or benzo-ring (**66–68**) resulted in decreased ICT character and increased emission energy (Figure 16). For compounds **66–68**, Yoshikai *et al.*, illustrated optical tuning using different spacers (none, ethylene, and acetylene) between the dimethylaniline-donor and phosphole-acceptor moities.[167]

The phosphonium-borate stilbenes are intriguing examples of zwitterionic *D-A* heterocyclic luminophores (Figure 17A).[30,161]

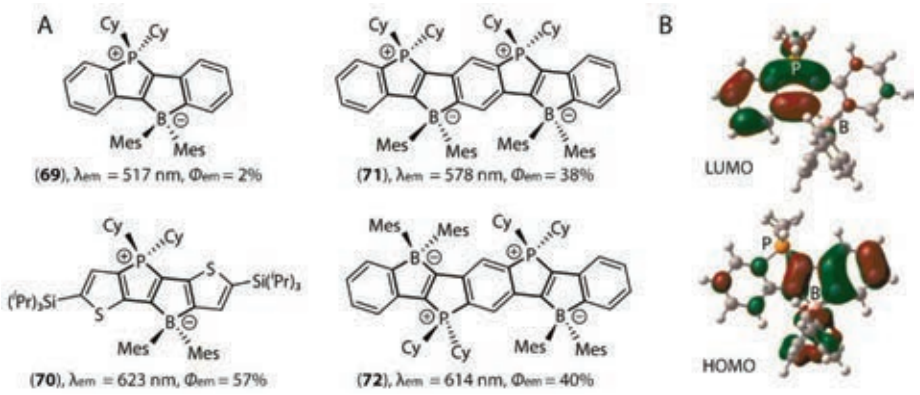

Figure 17. A: Schematic structures and emission properties of the *A-D* **69**, **70**; *A-D-A-D* **71;** and *D-A-A-D* **72** molecules (Cy = cyclohexyl, Mes = mesityl) and B: Kohn-Sham HOMO and LUMO of **69**.[30,161]

The planar scaffolds **69–72** are stable toward oxygen and moisture. Zwitterion **69** displayed green emission (Φ_{em} = 2%), owing to the ICT from the borate donor to the phosphonium acceptor (Figure 17B. This could be facilitated by utilizing the silyl-substituted thiophene (**70**) instead of the benzene to produce an intense orange-red fluorescence (λ_{em} = 623 nm, Φ_{em} = 57%). Moreover, extending the conjugated system in **71** and **72** also resulted in a significant change in the emission to orange with Φ_{em} ~40%.

An alternative structural configuration has been proposed by Yamaguchi[170] and Imahori,[171] which involved double merging of the electron-accepting phosphine oxides with the PAH core, shifting the emission to ≤700 nm.

Rare examples of fluorescent $\lambda^3\sigma^2$ oxa- and azaphospholes have also been reported.[172,173] This remarkably rich variability of the phosphole-based chromophores allowed the realization of a wide range of important phenomena of absorption/emission dynamic behavior, such as white-light generation and dual emission;[17,174] photochromism;[164,175,176] proton transfer;[160] anion, solvato, and pH response;[17,177] and circularly polarized emission.[178] Furthermore, the peripheral functionalization afforded intriguing phosphole-lipid dendritic architectures with mechano-responsive properties, liquid crystals, and gels as well as self-assembled micro-/nanostructures, which have been intensively studied as promising energy converting materials.[137,146,179,180]

1.3.2 Six-membered luminescent phosphacycles

Embedding of the phosphorus center into a six-membered ring is still not a trivial task. Compared to the extensively studied phospholes, synthetic approaches to six-membered phosphacycles have been much less explored and generalized (Scheme 4).

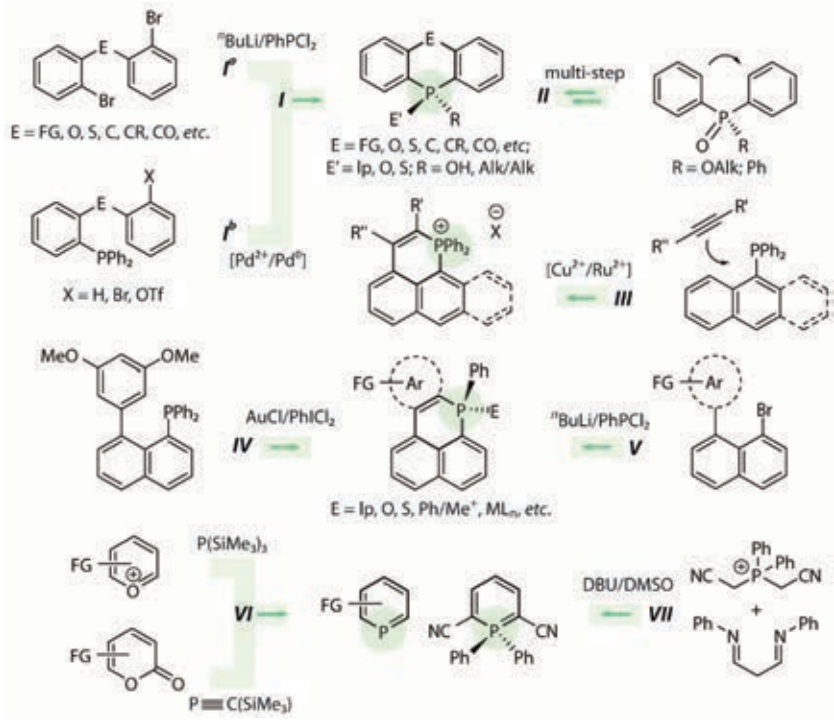

Scheme 4. Synthetic approaches to six-membered phosphacycles; procedure details: ***I***^{a} *i*) $^{n/t}$BuLi, THF/Et_2O, -78 °C and *ii*) $PhPCl_2$, -78 °C to rt; ***I***^{b} $Pd(OAc)_2/Pd(PPh_3)_4$, $(Me_3Si)_3SiH$, DMF, 130 °C, 12 h; ***III*** $Cu(BF_4)_2{\cdot}6H_2O/RuCl(C_6Me_6)$, MeCN, 100 °C, 12 h/DCE, 70 °C, 24 h; ***IV*** *i*) ^{n}BuLi, THF/Et_2O, -78 °C and *ii*) $PhPCl_2$, -78 °C to rt; ***V*** AuCl, $PhICl_2$ or $PhICl_2$, DCM, rt; and ***VI*** MeCN, rt or toluene, rt; ***VII*** 17 h, 85 °C.

Similar to the original synthesis of phospholes, general method ***I***^{a} comprises the dilithiation of an aryl dibromide and its further treatment with dichlorophenylphosphine.[181–185] The structural analogues can be obtained through P–C bond cleavage and the reductive elimination of the metalated phosphine from the Pd center (route ***I***^{b}).[186,187] In a more sophisticated multi-step route (***II***) the closure of the six-membered ring occurs *via* the addition of a bridging atom or functional group to the *ortho*-carbons next to the phosphorus center.[188–190] However, the applicability of methods ***I*** and ***II*** is limited by a low degree of accessible functionalization, poor overall yields, and the necessary synthesis of elaborate precursors. For instance, Wang *et al.*, prepared near-infrared-emitting $\lambda^5\sigma^4$-phospha-fused rhodamines **73–75** by four- and five-step procedures (Scheme 5), namely, nitration, reduction, alkylation, and cyclization/condensation, to attain total yields of only 1–5%.[188]

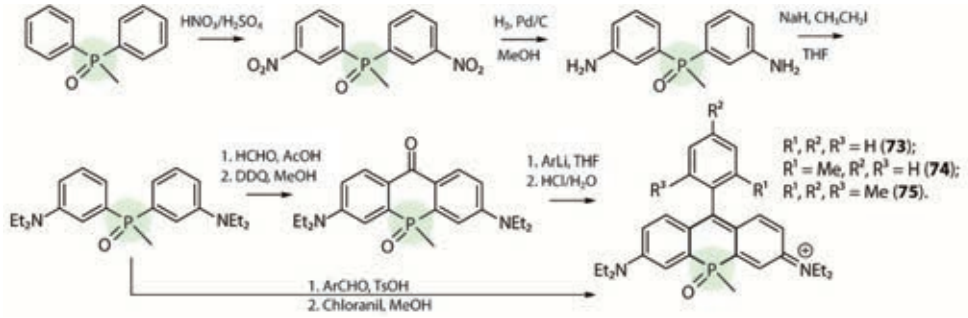

Scheme 5. Synthesis of $\lambda^5\sigma^4$ fused phospha-rhodamines **73–75**.

Despite the inefficient synthesis, the physical impact of including the P-atom into the chromophore was significant. Dyes **73–75** demonstrated a bathochromic shift of both absorbtion and emission with respect to oxygen- and silicon-bridged rhodamines ($\Delta\lambda_{abs}$ = 43-140 nm, $\Delta\lambda_{em}$ = 42-140 nm), owing to the electron-withdrawing property of the phosphine oxide group. The near-infrared emission of **73–75** (λ_{em} = 702 nm, DCM; λ_{em} = 712 nm, PBS) has been utilized for multicolor *in vivo* imaging of subcutaneous tumors in mice.

Six-membered phosphaphenalenium salts are typically assembled following methods ***III*** and ***IV*** *via* metal-mediated (Cu^{2+},[191,192] $Au^{+/3+}$,[193] and Ru^{2+} [194, 195]) P–C bond formation. Additionally, according to Toste, phospha-cyclization is also possible by using only the $PhICl_2$ oxidant, with no need to generate gold intermediates.[193]
The Lewis acid-free protocol ***V***, realized by Romero-Nieto *et al.*, in 2015, is suitable for the synthesis of phosphaphenalene derivatives with accessible variation of the aromatic backbone [Scheme 4, Ar = benzene, (benzo)thiophene, furan, pyridine, and pyrrole][196,197] to alter the fluorescence within the UV/blue region. In 2018, the same group proposed the larger linearly fused diphosphahexaarenes, achieved by method ***I***^{a}.[183] However, the increase in the conjugation, incorporation of two phosphorus atoms, as well as further post-modification[198] modulated the emission only in a narrow blue range of the visible spectrum. As an alternative avenue, the tandem phospha-Friedel-Crafts annulation in the presence of $AlCl_3$ afforded the families of optically active "peri-fused" phospha-angulenes,[199–201] helicenes,[202] and porphyrins.[29]

The heavier analogues of pyridine, $\lambda^3\sigma^2$-phosphinines, were accessed by protocol ***VI*** using classical pyrylium salt-exchange[203,204] and [4+2] cycloaddition reaction of 2-pyrone with $Me_3SiC{\equiv}P$/$NaOC{\equiv}P$ (Scheme 4).[205,206] The simple one-pot reaction ***VII*** to form fluorescent 2,6-dicyano-$\lambda^5\sigma^4$-phosphinines has been reported by Hayashi *et al.*, in 2018 (Scheme 4 and Figure 18).[207] Initially cyan (λ_{em} = 491 nm, solution) and green (λ_{em} = 561 nm, solid) emissions of **76** could be altered by selective functionalization at the C_4 atom. The electron-withdrawing group decreased the fluorescence wavelength to 463 nm (**77**), whereas electron-donating

substituents in **78–81** led to bathochromic-shifted emissions ranging from 519 to 581 nm. The solid-state luminescence of **76–81** was less intense and more red-shifted.

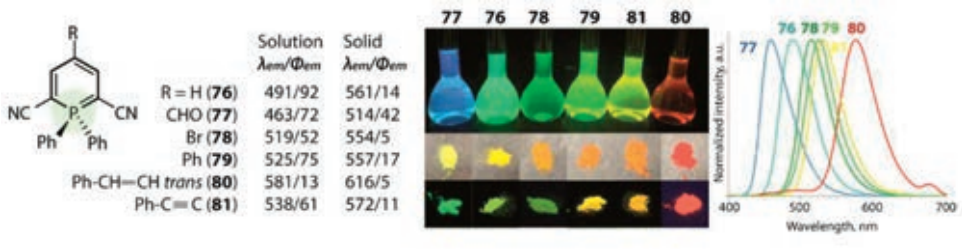

Figure 18. Family of 2,6-dicyano-λ⁵σ⁴-phosphinines **76–81** (left) and their fluorescence behavior in solution and solid state (center); solution emission spectra of **76–81** ($CHCl_3$, right).[207]

Other phosphinine post-functionalizations, *e.g.*, by amination, polymerization, and coordination to Cu^+ resulted in moderately luminescent materials with ICT character.[205,208,209] Moreover, apart from the abovementioned fluorophores, merging of the six-membered phosphacycle into an anthracene-like backbone produced 9-acridophosphines and 9-phosphaanthracenes, which demonstrated low fluorescence efficiencies.[181,210]

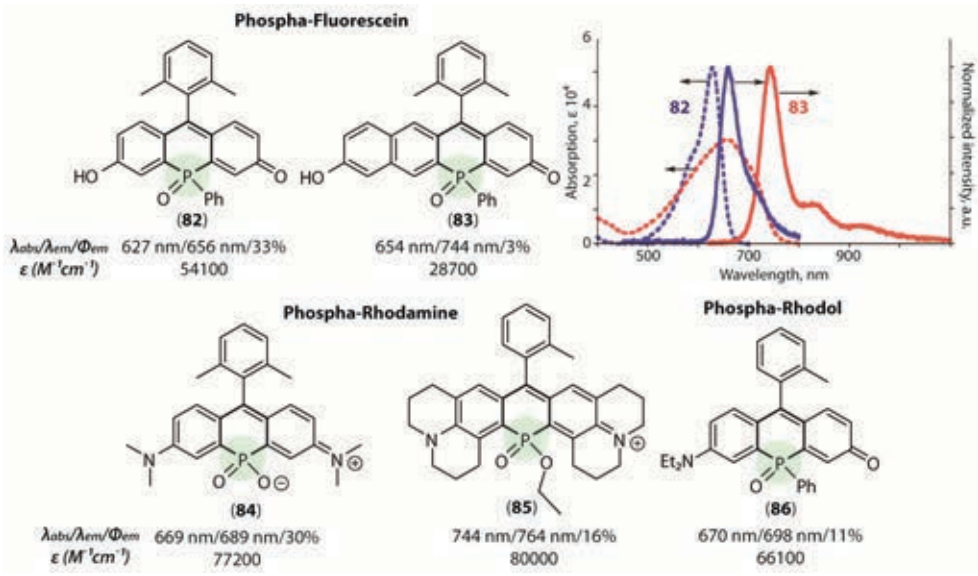

Figure 19. Phospha-cyclic fluorophores of xanthene-type compounds (**82–86**) and their photophysical properties (PBS solution, 10 mM, pH 7.4).[184,189]

On the other hand, the fusion of the phosphorus block into the bridgehead position of the well-known fluorophore framework of xanthene-type

(rhodamine,[185,211] rhodol,[190,212] and fluorescein[184,189,190,213]) and (aza)dipyrromethene[214,215] (*i.e.*, BODIPY analogue) compounds has been actively studied since the pioneering report of **73–75** in 2015.[188]

Fukazawa, Taki, and Yamaguchi demonstrated an effective combination of the σ*–π* conjugation of the electron-deficient phenylphosphine oxide with the fluorescein scaffold (Figure 19).[184] Remarkably, the strategy for optical band gap tuning not only perturbed the frontier MOs but also affected their photobleaching properties. Thus, P-cycle **82** displayed enhanced photostability upon continuous irradiation, compared to those of the oxygen- and silica-fluoresceins, and behaved similarly to the commonly used Alexa 633 and 647 dyes. An unsymmetrical structure of seminaphtho-phospha-fluorescein **83** expectedly manifested in a smaller HOMO/LUMO band gap (λ_{em} = 744 nm, $\Delta\lambda_{em}$ = 88 nm) with a 10-fold drop in the emission efficiency compared to that of its congener **82**.[189]

Significantly, the red-shifted absorption/emission spectra reaching the far-red/near-infrared region (NIR) together with the water solubility and low molecular masses of the abovementioned P-containing fluorophores are of great interest to bioimaging applications. Throughout these studies, cytosolic calcium imaging, cellular esterase activity, and enzyme detection were described as a proof-of-concept.[188,190,211,213,216] Notably, an ideal molecular dye for imaging should comply with the following key criteria: (*i*) a large Stokes shift to prevent auto-absorption, (*ii*) absorption and emission in the therapeutic red-NIR window (580–1400 nm) because of minimal cellular auto-fluorescence and a higher penetration depth of this radiation into living tissues, and (*iii*) high stability, permeability, and low toxicity.

In 2016, in the search for improved phosphacycle properties for bioimaging purposes, Stains *et al*., reported on the $\lambda^5\sigma^4$ phosphinate-based rhodamine "paint" **84**, which they called Nebraska red (Figure 19).[185] The use of the phosphinate ether and julolidine donor functionalities in **85** afforded the most red-shifted phospha fluorophore to date operating in aqueous solution (PBS, λ_{em} = 764 nm; brightness, $\varepsilon \times \Phi_{em}$ = 12800 $M^{-1}\,cm^{-1}$). These results, obtained by three groups (Yamaguchi, Wang, and Stains), indicated that in the rhodamine scaffold different phospha-centers slightly impacted on the efficiency of the fluorophore (except for NIR vibrational quenching) but played a major role in the σ*–π* interaction. This resulted in the gradual decrease in the HOMO/LUMO gap in the order: PO(OH) (λ_{em} = 685 nm, Φ_{em} = 38%) > PO(Me) (λ_{em} = 712 nm, Φ_{em} = 11%) > PO(OEt) (λ_{em} = 722 nm, Φ_{em} = 11%) > PO(Ph) (λ_{em} = 731 nm, Φ_{em} = 12%). Additionally, solutions of phospha-rhodamines underwent color changes at pH >10. This indicated that hydrolytic deamination, which has been utilized for the synthesis of rhodol **86** also displays NIR fluorescent character.[190,212]

1.3.3 Other (4-, 7-membered) phosphacycles

Phosphacycles with other ring sizes (*i.e.*, composed of four and seven atoms) are much less spread. Among the four-membered cycles (phosphonio-naphtalenes, 1,3-diphosphacyclobutane-2,4-diyls, and 1,2-dihydrophosphetes),[217–219] only the unsaturated 1,2-dihydrophosphetes decorated with π-donors [naphthalene (**87**), carbazole (**88**), and fluorene (**89**)] displayed reasonable luminescent properties (Figure 20).[219] Similar to other organophosphorus species, the tetrahedral configuration of the P atom in **87–89** largely prevents solid-state aggregation, which is beneficial for the fabrication of uniform amorphous materials for optoelectronics. Thus, as a proof of concept, blue emissive $\lambda^5\sigma^4$-phosphete **89** was used as an emissive layer in a sandwich OLED, which presented EQE_{max} = 2.5% and CIE (0.18, 0.34).

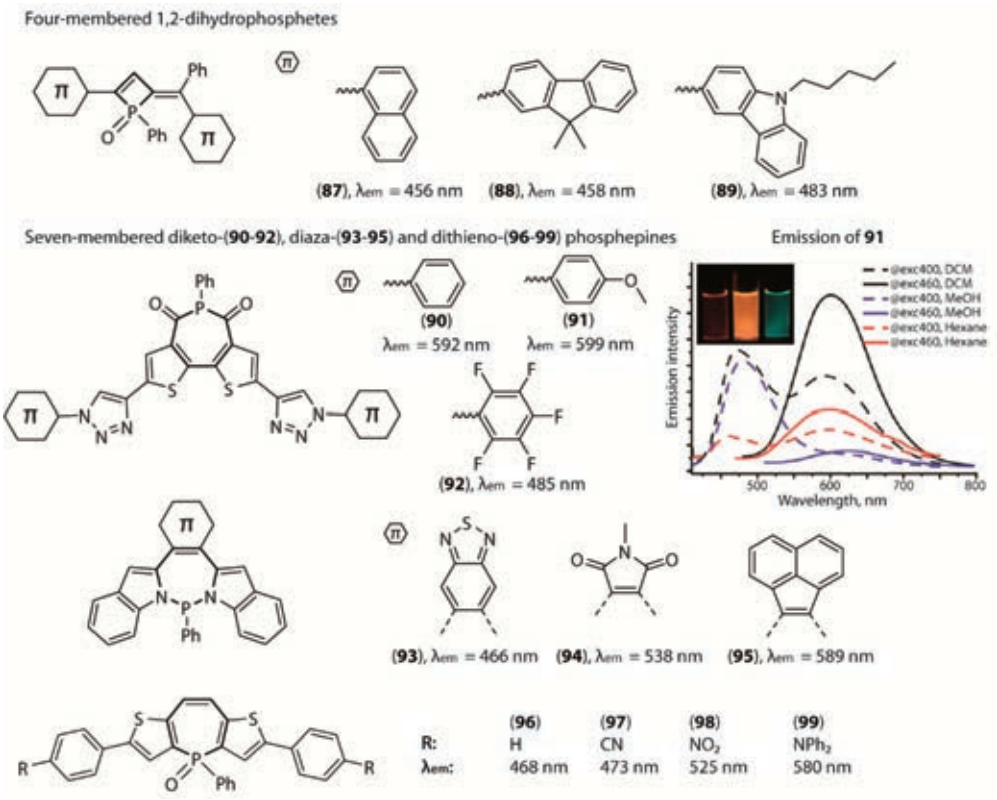

Figure 20. Four- and seven-membered phosphacycles and their emission maxima in DCM solutions; emission spectra of **91** in various solvents under different excitations; inset displays the photo of the compound in (from left to right) hexane, DCM, and MeOH under UV light.[145]

A seminal work on photofunctional seven-membered P-heterocycles was published by Baumgartner *et al.*, in 2013.[145] Dithienophosphepines **90–92**

demonstrated better electron-accepting properties than the related imides and phospholes and the emission variation was achieved through the modification of the lateral substituents on the triazole rings. An interesting feature of these phosphacycles was their dynamic dual emission. For instance, in a DCM solution, the luminescence CIE coordinates for **91** vary from nearly pure white light (0.33, 0.34) under λ_{exc} = 365 nm to orange (0.53, 0.46) at a longer excitation wavelength (λ_{exc} = 460 nm). The authors associated the HE band with phosphepine-localized $\pi\pi^*$ transitions, whereas the LE signal was ascribed to the ICT from the phosphepine core to the peripheral triazoles. In polar solvents, the LE band was significantly quenched (Figure 20), thereby supporting the proposed assignment.

Diazaphosphepines **93–95** were designed by Loo *et al.*, in 2016.[220] Merging of the aromatics (*e.g.*, benzothidiazole **93**, maleimide **94**, and acenaphthylene **95**) with the C=C linker between the indolyl fragments provided access to efficient tuning of the HOMO-LUMO band gap. Unlike the carbon-based phosphepines,[221,222] the $\lambda^3\sigma^3$-diketo- and diazacycles were more resistant toward oxidation and other reactions involving the P-atom. This was attributed to a higher stabilization of the phosphorus lone pair because of the electron withdrawing keto- or diaza group.

A family of luminescent seven-membered dithienophosphepines **96–99** was described by Hissler *et al.*, in 2019 (Figure 20).[222] The absorption and emission characteristics, which were widely altered by varying the pendant donor and acceptor groups, readily linked to the phosphepine backbone by Pd-catalyzed arylation. A boat-like nonplanar conformation of the ring, confirmed by X-ray crystallography, displayed the non-aromatic character of the cycle compared to those observed for phospholes and phosphaphenalenes.

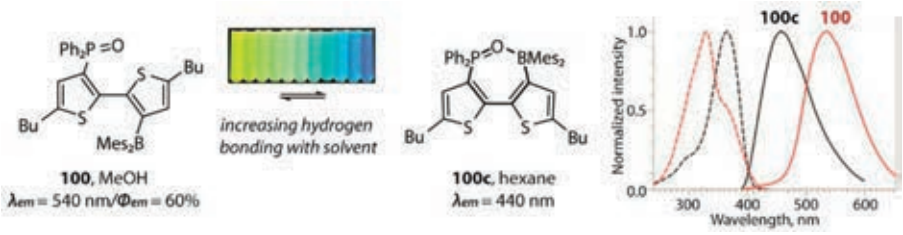

Figure 21. Formation of the seven-membered phosphacycle in a nonpolar solvent; absorbance (dashed lines) and emission (solid lines) spectra of **100** and **100c**.[223,224]

The final example of a seven-membered heterocycle is the unconventional reversible formation of the oxa-boron-phosphorus motif examined by Wolf *et al.*[223,224] Flexible fluorescent Lewis pair **100** underwent structural and emission changes in non-hydrogen bond donating solvents, such as hexane, to afford the cyclic form **100c** (Figure 21). In methanol, **100** demonstrated intense yellow emission (λ_{em} = 540 nm, Φ_{em} = 60%) with a large Stokes shift ($\Delta\lambda$ = 11800 cm^{-1}), thereby indicating the charge-transfer character of fluorescence. Folding of the

molecule in hexanes into a seven-membered cycle is reflected by a substantial hypsochromic shift: a blue band at λ_{em} = 440 nm originating from the bithiophene-localized transitions. In the more polar aprotic DCM, the emission of **100** revealed a mixture of colors.

1.4 AIMS OF THE STUDY

The presented literature analysis illustrates that diverse phospha-synthons combined with π-organic aromatic motifs have been extensively utilized for the construction of unique families of photoluminescent organo-/metalorgano-phosphorus molecular materials. The electronic tunability of the phosphorus center significantly affects the optical band gap and thus, the photophysical behavior of these species can be tuned in a wide range. The preparation of new organophosphorus photoactive compounds possessing "push-pull" *D*–π–*A* molecular architecture is of primary importance; thus, these dyes proved to be superior candidates for optoelectronic devices, optical sensing, and visualization techniques in biological systems. However, most phosphorus-containing organic luminophores are represented by five-membered phosphole derivatives or organic chromophores decorated with pendant –R_2P=E (E = O, S, and Se) group(s), whereas six-membered P-heterocycles (phosphinines, phosphaacenes, etc.) remain scarcely explored. Furthermore, compared to the terminal –R_2P=E (E = O, S, and Se) acceptors, substantially more electron deficient phosphonium building blocks $R_{3-n}P^+$–(chromophore)$_n$ have been randomly utilized for the preparation of photofunctional species. Therefore, the main aim of this study was to develop a new class of efficient and tunable multipolar organo/metal-organophosphorus chromophores, which would allow for the systematic alteration of the π-conjugated core and that contain strongly electron-accepting –R_3P^+/–R_2P^+– or –R_2P–ML_n functions. The specific objectives of the project are formulated as follows:

1. Development of the synthetic approach to polyaromatic systems fused with phosphonium heterocycles. Structural modification of the chromophoric central core to vary the degree of π-conjugation; tailoring the electron-donor moieties to the most promising polycyclic scaffold to alter the emission energy.

2. Construction of ionic donor-acceptor chromophores of a simple linear *D*–π–A^+ architecture, which comprises the pendant strongly electron-accepting phosphonium group –R_3P^+. Studying the effect of the –π– spacer on the photophysical behavior, investigating the ICT process depending on the properties of the medium and counterion.

3. Merging the donor-acceptor fluorophores, which exhibit pronounced charge-transfer character, with metal-based emitters to attain dual luminescence, dynamically dependent on the properties of the environment. Studying the ICT and excitation energy processes between the constituting components.

2 EXPERIMENTAL

2.1 GENERAL INFORMATION

Oxygen-sensitive reactions were performed under a nitrogen atmosphere using standard Schlenk or glovebox techniques. Tetrahydrofuran (THF), diethyl ether (Et_2O), and toluene were distilled over Na-benzophenone ketyl under a nitrogen atmosphere prior to use. Other solvents, ligands, and reagents, purchased from Alfa Aesar, VWR, Merck (Sigma-Aldrich), and TCI Europe were used as received without further purification.

The syntheses of the precursors (*i.e.*, intermediates, *ortho*-bromo-phenylaryls, bromoaryls, phosphines, catalysts, and Eu-complexes) and final products **1c**–**8c** and **9**–**26**, and **12Cbz** (Figure 22) are included in the supporting information (SI) of the original publications.

2.2 CHARACTERIZATION

The purity and identity of all the newly synthesized compounds were proven by NMR and mass spectrometry (MS; in solution), FTIR spectroscopy (**21**–**26**), and CHN microanalyses (in solid state). The solution ^{1}H, ^{1}H-^{1}H COSY, $^{31}P\{^{1}H\}$, and ^{13}C NMR spectra were recorded on Bruker Avance 400 and AMX-400 spectrometers and referenced to the residual solvent signals. The mass spectra were measured on Bruker MaXis, MaXis II, and Solarix XR instruments in the electrospray ionization (ESI^+) and atmospheric pressure photoionization (APPI) modes. The infrared (FTIR) spectra were measured on a Bruker VERTEX 70 FT-IR spectrometer. Microanalyses were performed in the analytical laboratory of the University of Eastern Finland using a vario Micro cube CHNS analyzer (Elementar). TGA analysis of **11**, **12**, **14**–**16**, and **18** was performed using a Mettler Toledo TGA851e instrument. The melting points of **1c**–**6c** were estimated using Stuart SMP10 apparatus.

The structures of **1c**, **2c**, **4c**, **10**, **11**, and **12Cbz** in the solid state were determined by single-crystal X-ray diffraction studies. Suitable materials for crystallographic analysis were obtained by gas-phase diffusion (**1c**, **2c**, and **4c**), recrystallization from hot solvent (**10**), and slow evaporation (**11** and **12Cbz**) methods. The crystals were immersed in cryo-oil, mounted in a nylon loop, and measured at temperatures of 120 K (**4c** and **11**) or 150 K (**1c**, **2c**, **10**, and **12Cbz**). The diffraction data were collected with a Bruker Kappa Apex II Duo diffractometer using Mo Kα radiation (λ = 0.71073 Å). The *APEX2*[225] program package was used for cell refinements and data reductions. The structures were solved by direct methods using the *SHELXS-2013/2014*[226] program with the *WinGX*[227] graphical user interface. A semiempirical

or numerical absorption correction (*SADABS*)[228] was applied to all data. Structural refinements were carried out using *SHELXL-2013/2014* (original publications **I–III)**. The ESI^+ MS of **21–23** were measured by the group of Prof. Janne Jänis (University of Eastern Finland, Finland). The theoretical, electrochemical, biological (cell imaging, and *in-vitro* cytotoxicity) and a part of the photophysical studies were performed by the collaborating colleagues at Aalto-University (Finland, group of Prof. A. Karttunen), Saint-Petersburg State University (Russia, group of Dr. V. Sizov), Ruprecht-Karls-Universität Heidelberg (Germany, group of Dr. C. Romero-Nieto), and the National Taiwan University (Taiwan, group of Prof. P.-T. Chou).

2.3 PHOTOPHYSICAL STUDIES

The photophysical measurements in solution were carried out at concentrations of $1–5\times10^{-5}$ M (10 mm cuvette), while the neat samples were used in the solid-state studies. The steady-state absorption, emission, and excitation spectra were recorded on PerkinElmer Lambda 900 UV/vis/NIR, Hitachi U-3310, and Shimadzu UV-1800 spectrophotometers and Edinburgh FS920, Jasco V66FP6500, Horiba FluoroMax-4, Fluorolog-3, and Avantes AvaSpec-ULS4096CL-EVO fluorimeters, respectively. Both the wavelength-dependent excitation and emission responses of the fluorimeters were calibrated. Xe lamps (300 and 450 W) and LEDs (365 nm) were used as excitation light sources to generate luminescence. The lifetimes in solution were determined by the time-correlated single photon counting (TCSPC) method with an Edinburg FL 900 photon-counting system, using a hydrogen-filled lamp as the excitation source or a HORIBA Fluorolog-3 spectrofluorometer and photon-counting system with an LED (maximum emission at 340 nm) in pulse mode (width 0.9 nm, repetition rate 100 kHz) for the nanosecond domain and a Xe lamp (450 W, repetition rate 10 kHz) for the microsecond domain. The lifetime data were fitted with the HORIBA Instruments software package and the Origin 9.55b program. The relative emission quantum yields in solution were determined by a comparative method using a set of standards (further detail in the SI of the original publications).[229] Absolute quantum yields of the solid samples were measured using an integrating sphere with a Horiba FluroMax-4P luminescence spectrometer as the optical detector.

Different excitation sources were used for the photostability tests (λ_{ex} = 375 nm diode laser, RGB Photonics, MiniLas EVO 375-50; λ_{ex} = 458 nm Argon ion laser; λ_{ex} = 532 nm diode laser, Suwtech, DPGL-2100). The fluorescence intensities at the respective emission maxima were recorded with continuous exposure to the excitation light and collected on an Edinburg FS920 fluorimeter and Zeiss LSM710 NLO confocal spectral microscope.

The CIE 1931 coordinates were calculated from the photoluminescence data using the Origin 9.55b software pack.

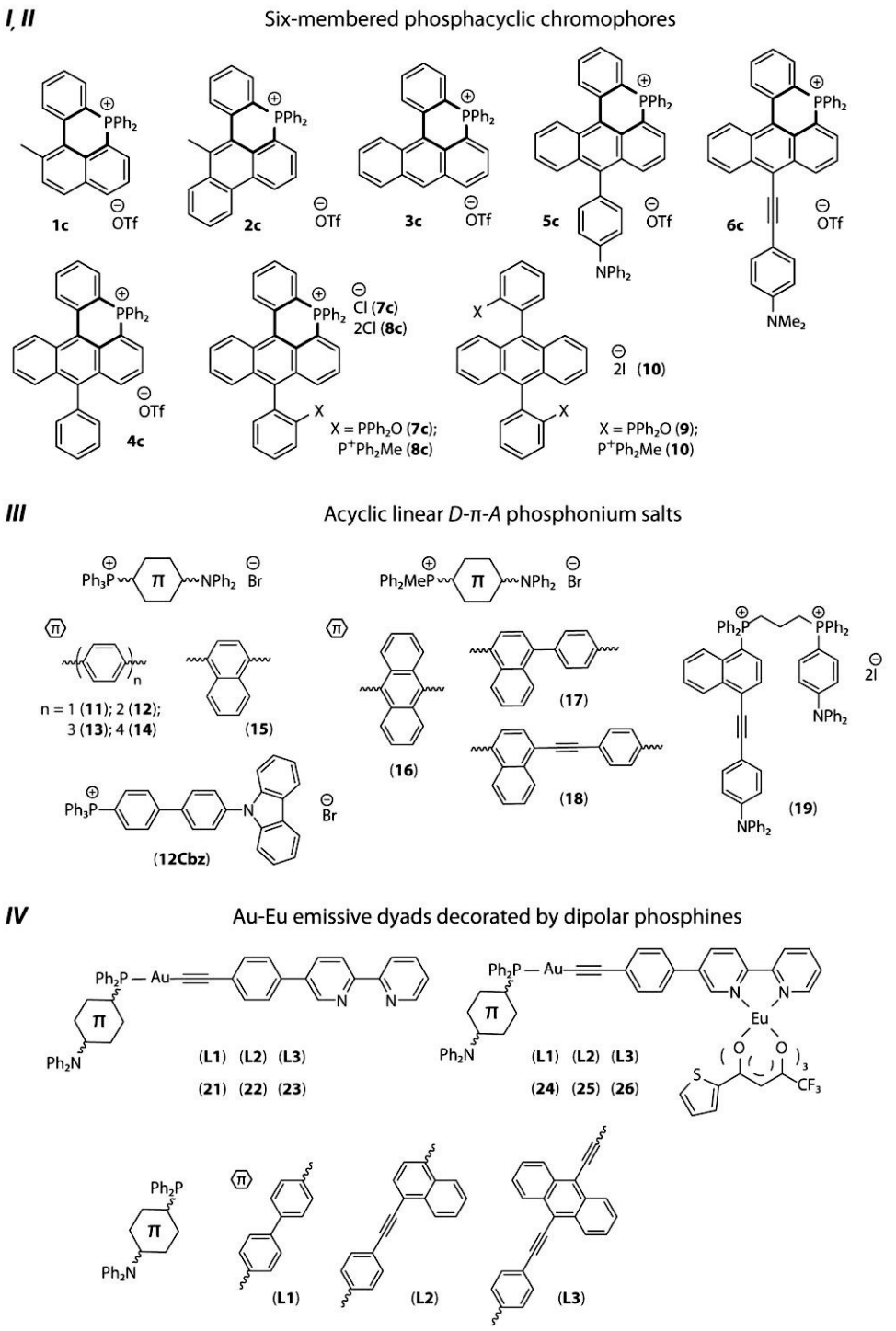

Figure 22. Structures of compounds **1c**–**8c** and **9**–**26** obtained in this study (Roman numbers correspond to the original publications).

3 RESULTS AND DISCUSSION

3.1 POLYAROMATIC SIX-MEMBERED PHOSPHONIUM HETEROCYCLES [I, II]

In view of the poorly explored six-membered P-heterocycles, compared to the five-membered phospholes and conventional acyclic derivatives, the initial focus of this work was on the elaboration of new ionic phospha-polyaromatic fluorophores. The molecular design, depicted in Figure 23, implies the following concepts:

1) Merging a strongly electron accepting $\lambda^4\sigma^4$ phosphonium function (>P$^+$Ph$_2$) with a robust polyaromatic scaffold leads to stable and efficient fluorophores and decreases the energy of the LUMO.
2) Optical properties depend on the size and stereochemistry of the polyaromatic core.
3) Decorating the phospha-scaffold with electron-donating groups induces ICT that dramatically influences the optical gap.

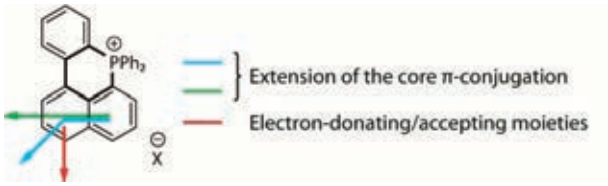

Figure 23. Molecular design strategy to control the physicochemical properties of six-membered cycles.

These structural variations of the central core and lateral functionalities aimed at the wide alteration of the emission energy, ultimately reaching the deep red or near-IR region.

The synthetic method that was applied to merge the positively charged $\lambda^4\sigma^4$ phosphonium group with a polyaromatic core involved intramolecular Cu^{II}-mediated phospha-annulation as a key step (Scheme 6, *b*). The starting *ortho*-bromo functionalized phenylene-acenes (naphthalene, phenanthrene, and anthracene) were synthesized *via* multi-step protocols, which include (*i*) conversion of the acenes into bromo- and iodo-substituted derivatives followed by (*ii*) Suzuki cross-coupling with 2-bromophenylboronic acid. Additionally, the anthracene platform was functionalized at the 10-position by tailoring the substituents with different electron-donating abilities such as phenyl (**4c**), triphenylamine (**5c**), and 4-ethynyl-*N*,*N*-dimethylaniline (**6c**). Similar to PAH-phenylene-*o*-bromides, *ortho*-phenylenephosphines (**1–6**) were obtained in good yields (71–94%) by a procedure

involving conventional lithiation with ^{t}BuLi and successive treatment of the i-intermediate with a diphenylphosphinechloride (Scheme 6, *a*).

The PAH-*ortho*-functionalized phosphines instantly react at room temperature with copper(II) triflate in DCM/MeCN solutions to afford six-membered phosphacycles (**1c–6c**, where "**c**" denotes the cyclization product; Scheme 6, *b*). Regarding the cyclization step, the initial studies started from 1-(2-diphenylphosphinophenyl)naphthalene (non-methylated structural analogue of **1**), which reacted with Cu^{II} to yield a mixture of two products. The mass spectrum of the chromatographically purified mixture presented one signal at *m*/*z* = 387.1, whereas two resonances were observed in the corresponding ^{31}P NMR spectrum (δ = 4.4 and 23.8 ppm), indicating that two constitutional isomers with six- and five-membered P-rings were formed in a 70/30 ratio. Unfortunately, these isomers could not be separated. To exclude the formation of the product mixture, the methyl-substituted analogues of unsymmetrical naphthalene- and phenanthrene-phenylenes were further utilized.

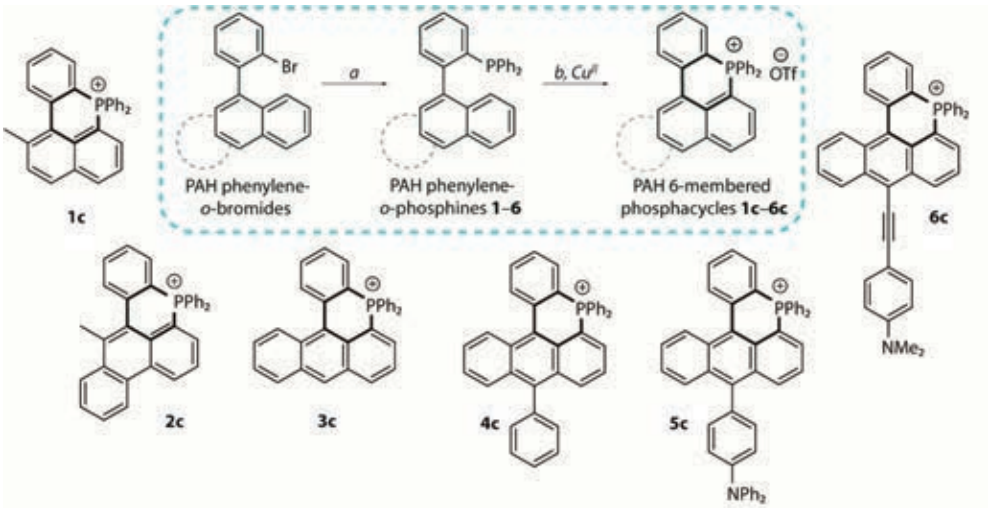

Scheme 6. Synthetic route to six-membered phosphacycles **1c–6c**: *a* (*i*) ^{t}BuLi, 1.7 M, THF, –78 °C, 40 min; (*ii*). PPh_2Cl, –78 °C → rt, 1 h, 71–94% and *b* $Cu(OTf)_2$ anhyd, DCM/MeCN, 10 min, 30–79%.

The efficiency of the cyclization reaction depended on the nature of the Cu^{II}-mediator, as illustrated by phosphine **3** (Table 1). The copper(II) bromide and acetate did not convert **3** into the desired product **3c** and only trace amounts of the cyclized derivative were observed, even after six hours. A visibly better conversion was demonstrated by the copper(II) chloride (48%) and perchlorate (25%) hydrates in the 1/1 DCM/MeOH mixture. The reaction proceeded most efficiently when anhydrous copper(II) triflate served as the mediator (79% yield). As a result, $Cu(OTf)_2$ was used for the synthesis of all the phosphacycles (**1c–6c)**. These findings can be

rationalized by a lower solubility of the copper(II) bromide and acetate, which evidently decreased the overall oxidative activity of the Cu^{II} reactant. The counterion might also play a non-negligible role in the stabilization of the reaction intermediates.

The $Cu(OTf)_2$-mediated phosphacyclization resulted in good phosphonium salt yields (**1c**–**4c**; 62–79%). However, in the case of *ortho*-phosphines **5** and **6** decorated with donor groups, the yields of **5c** and **6c** substantially dropped to 38 and 30%, respectively. This was attributed to their lower stability, which caused significant losses during purification by column chromatography.

Table 1. Cyclization of **3** mediated by Cu^{II} salts at 298 K in different solvent mixtures.

Cu^{II} salt[a]	Solvents	Yield of 3c %[b]
$CuCl_2{\cdot}2H_2O$	DCM/MeOH 1/1	48
$Cu(OCl_4){\cdot}6H_2O$	DCM/MeOH 1/1	25
$Cu(OTf)_2$ (anhyd)	DCM/MeCN 1/1	79
$CuBr_2$(anhyd)	DCM/MeOH 1/1	–[c]
$CuBr_2$(anhyd)	DCM/MeCN 1/1	–[c]
$Cu(OAc)_2{\cdot}2H_2O$	DCM/MeOH 1/1	–[c]
$Cu(OAc)_2{\cdot}2H_2O$	DCM/MeCN 1/1	–[c]
$Cu(OTf)_2$ (anhyd) + TEMPO (5 eq.)	DCM/MeCN 1/1	–[c]

[a]2.05 eq. of Cu^{II} salt; [b]isolated yield; [c]trace amount of product observed.

On the other hand, the symmetric architecture of the diphosphine analogue of **3**, 9,10-bis(2-diphenylphosphinophenyl)anthracene (dpa**P²**, Scheme 7), was potentially suitable for double cyclization. The reaction of dpa**P²** with the copper salt however led to the formation of the monocyclic product, which was easily transformed into the $\lambda^5\sigma^4/\lambda^4\sigma^4_{cyclic}$ (**7c**) and $\lambda^4\sigma^4/\lambda^4\sigma^4_{cyclic}$ (**8c**) compounds in moderate yields (46 and 32%, respectively) by treating the second phosphine group with hydrogen peroxide or methyl iodide, respectively (Scheme 7). The main side products of the phosphacyclization reaction, phosphine oxide **9** and diphosphonium salt **10**, could be obtained directly from dpa**P²** by reacting with an excess of hydrogen peroxide or methyl iodide (Scheme 7). Surprisingly, even an excess of the copper salt did not lead to the formation of the 1,4- or 1,5-dicyclic products. Trace amounts of these substances (yield <1%) were obtained under modified conditions (benzonitrile, 80 °C). The ESI^+ MS of the highly emissive red species displayed one signal of a doubly charged ion (m/z = 348.1), while two peaks were observed in the ^{31}P NMR spectrum (δ = 4.3 and 5.5 ppm). All attempts to separate the isomers were unsuccessful. Other P-cyclization methods, such as the gold(I)-based procedure reported by D. Toste[193]

and the metal-free protocol reported by C. Romero-Nieto,[196] also failed in the preparation of these dicycles.

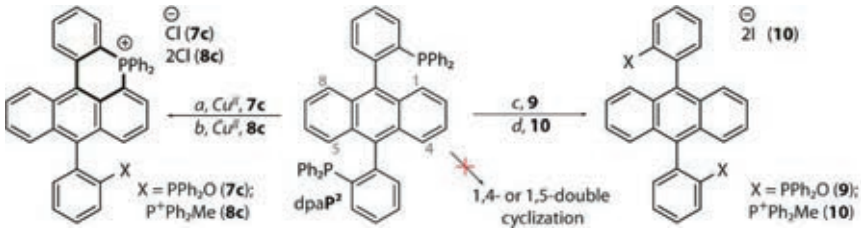

Scheme 7. Synthesis of phosphacycles **7c**, **8c**, diphosphine oxide **9**, and diphosphonium salt **10** from dpa**P²**: *a* (*i*) $CuCl_2{\cdot}2H_2O$, DCM/MeOH; (*ii*) H_2O_2 aq. 30%, 46%; *b* (*i*) $CuCl_2{\cdot}2H2O$, DCM/MeOH; (*ii*) MeI, 32%; *c* DCM/H_2O_2 aq. 30%, 91%; and *d* DCM/MeI excess, 88%. The dpa**P²** structure illustrates the numbering of the carbon atoms available for cyclization.

To rationalize this problem, a mechanism based on the analysis of metal-free and metal-mediated cyclization reactions was proposed (Scheme 8). In brief, the highly reactive phosphoniumyl radical cation $\boldsymbol{P}^{+\cdot}$, formed *via* single electron transfer (SET), generates the polycyclic annulated intermediate $\boldsymbol{P}_{CH}^{+\cdot}$. This is followed by the second oxidation and proton elimination from the $\boldsymbol{P}_{CH}^{+}$ species to form the final cyclization product $\boldsymbol{P}_C$. The involvement of radicals in the key steps was supported by the addition of the radical scavenger 2,2,6,6-tetramethylpiperidine *N*-oxide (TEMPO) to the mixture of Cu^{II} and phosphine **3** reactants, which completely suppressed the cyclization process (Table 1). In view of the proposed mechanism, the second electrophilic annulation in case of dpa**P²** seems to be unfavorable because the formation of the first cationic phosphonium cycle probably decreases the nucleophilicity of the anthracene core.

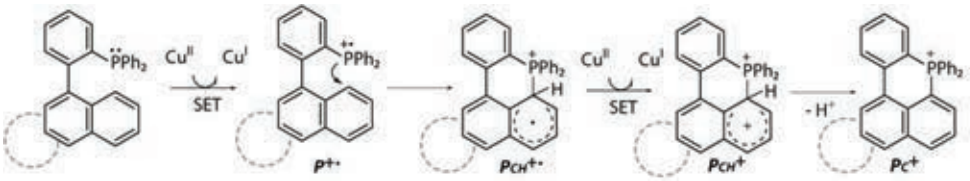

Scheme 8. Proposed mechanism for the Cu^{II}-mediated phosphaannulation.

The ^{31}P NMR singlet resonances of the phosphaannulated fragments of **1c–8c** were observed in the range 4.1–5.7 ppm, which agreed with the data for six-membered P-cycles of the same stereochemistry.[195,198] Additionally, phosphacycles **7c** and **8c**, bearing the second (acyclic) acceptor group, displayed low-field signals at δ = 24.0 ($\lambda^5\sigma^4$ –P(O)Ph_2) and δ = 19.8 ppm ($\lambda^4\sigma^4$ –P^+Ph_2Me). The positions of the high-frequency signals correlate with those of **9** (δ = 25.7 ppm) and **10** (δ = 20.8 ppm). The expected molecular compositions of the ionic compounds were con-

firmed by high-resolution ESI$^+$ MS. The corresponding data revealed the peaks of singly (cycles **1c–8c**) and doubly (dication **10**) charged molecular ions (m/z = 401.1, 451.2, 437.1, 513.2, 680.3, 580.2, 713.2, 356.1, and 364.1, respectively), in accordance with the proposed structures.

The solid-state structures of **1c**, **2c,** and **4c**, determined by single-crystal X-ray diffraction analysis, are illustrated in Figure 24. The phosphorus atom, integrated into the six-membered ring, adopted a slightly distorted tetrahedral geometry. The *endo* C–P–C angles were close to the idealized value of 109°, whereas significant deviations were observed for the *exo* parameters inside the cycle. The phosphorus centers were positioned slightly out-of-plane in the twisted hydrocarbon backbones of **1c**, **2c**, and **4c**, resulting in a boat-like phosphacyclic motif. This arrangement was similar to that observed in the acridophosphine family;[210] however, it is not typical for other six-membered congeners.[181,198,208,211,230]

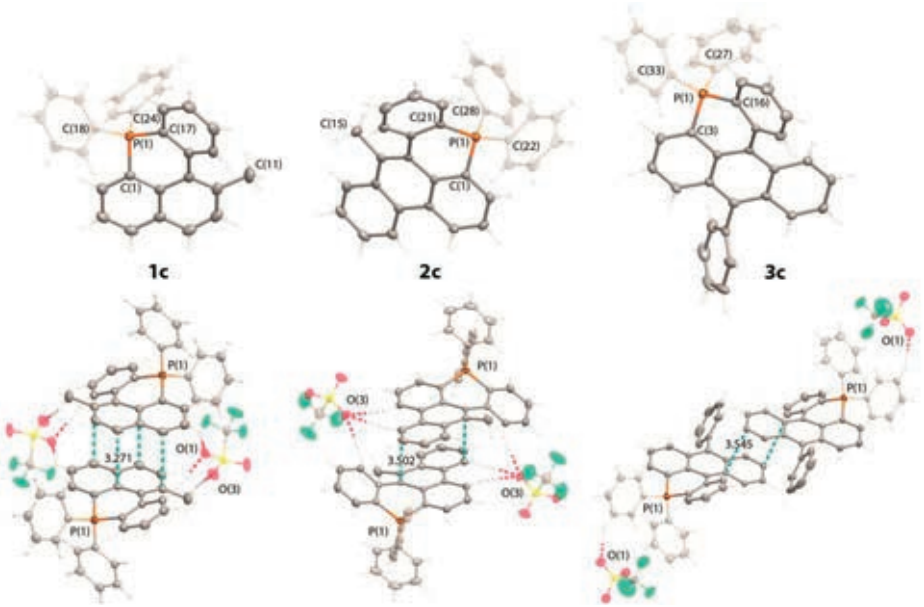

Figure 24. Molecular views of phosphacycles **1c**, **2c,** and **4c** (top; triflate counterions are omitted for clarity) and their dimers in the crystals (bottom). Thermal ellipsoids are shown at the 50% probability level.

Despite the tetrahedral geometry of the phosphorus atom, the crystal packing of molecules **1c**, **2c**, and **4c** featured dimer pairs arranged in a "head-to-tail" fashion, as well as the extensive hydrogen bonding S=O···H–C, which involved triflate counterions. The C–P bond lengths in **1c**, **2c**, **4c**, and **10** were quite similar to those of the recently studied $\lambda^5\sigma^4/\lambda^4\sigma^4$ phospha-oxides and phosphonium salts.[193,197,212]

Salts **1c–4c** were moderately soluble in water (0.05–0.3 mg/mL at 298 K), whereas **5c**, **6c**, and **9** were more hydrophobic. Compounds **7c**, **8c**, and **10**, comprising hy-

drophilic Cl^- and I^- counterions, demonstrated better aqueous solubilities (0.5–0.8 mg/mL at 298 K).

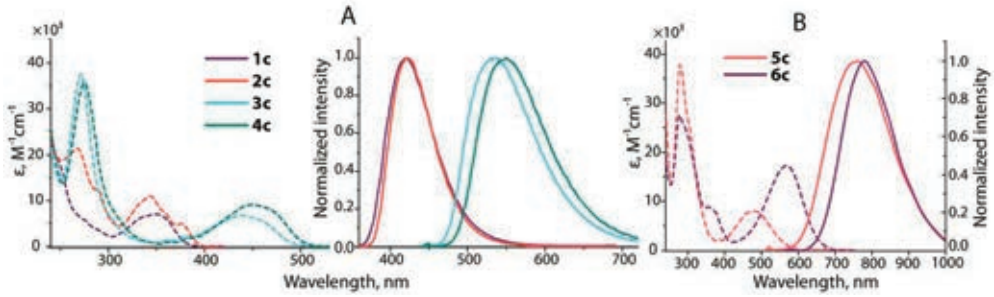

Figure 25. A: Absorption (dashed lines) and emission (solid lines) spectra of **1c–4c** (H_2O) and B: Spectra of **5c**, **6c** (DCM).

The optical behavior of **1c–4c**, **7c**, **8c**, and **10** were investigated in water solutions. Owing to poor solubility, hydrophobic **9** was analyzed in MeOH; moreover, the photophysical properties of **5c** and **6c** were studied in DCM, water, and phosphate buffered saline (PBS) containing 5% DMSO as a co-solvent. The data are summarized in Table 2 and depicted in Figures 25 and 26 (complete data in original publications **I, II**). The absorption profiles of **1c–4c**, **7c**, and **8c** displayed high-energy (HE) bands in the region 268–275 nm with the molar extinction coefficients changing from 5900 to 37600 M^{-1} cm^{-1}. Modification of the anthracene core **3c** by the phenyl (**4**) or acceptor–phenylene (**7c**, **8c**) substituents did not affect the position of the HE band; however, a gradual decrease in the absorption intensity was observed, especially for **8c** (ε = 15200 M^{-1} cm^{-1}). In turn, the low-energy (LE) bands exhibited moderate absorptivity (ε = 4800–10800 M^{-1} cm^{-1}). The LE maxima were progressively red-shifted upon extension of the conjugated system: naphthalene (**1c**; 348 nm), phenanthrene (**2c**; 375 nm), anthracene (**3c**; 438 nm), and phenylanthracene (**4c**, **7c**, and **8c**; 448–450 nm).

According to the TD-DFT calculations, the HE absorption resulted from mixed HOMO–2 to LUMO+2 transitions. The LE broad band was correlated with the HOMO→LUMO transition, which mainly occurred within the PAH fragment and phenylene ring, suggesting charge-transfer character.

Table 2. Photophysical data of **1c–8c**, **9**, and **10** in solution at 298 K.

	λabs, (ε, 10^3 M^{-1} cm^{-1})	**λem, nm**	**Δν, cm^{-1}**	**τ, ns**	**Φem, %**	**δ_2,[f] GM**	**δ_2×Φem, GM**
1c[a]	275 sh (5.9), 344 (7.0)	420	5260	3.3	38	277	105
2c[a]	268 (21.7), 290 (12.3), 344 (11.2), 375 (5.1)	425	3137	3.5	49	183	90
3c[a]	272 (37.6), 360 (1.1), 379 (2.3), 438 (6.7)	533	4070	16.0	99	637	630
4c[a]	274 (35.8), 362 (0.7), 383 (1.8), 450 (9.1)	547	3941	9.3	69	634	437
5c[b]	280 (38.0), 307 sh (24.5), 480 (7.9)	**760**	7676	3.4	10	-	-
5c[c]	281 (31.2), 472 (7.1)	640	5561	3.5	2	151	~3
5c[d]	280 (29.5), 472 (6.9)	640	5561	3.3	2	-	-
6c[b]	276 (27.6), 367 (8.5), 570 (17.4)	**780**	4723	1.5	18	-	-
6c[c]	277 (28.3), 365 (7.9), 540 (14.5)	665	3481	-	<1	266	~2
6c[d]	272 (32.3), 374 (7.2), 555 (10.3)	690	3526	-	<1	-	-
7c[a]	274 (28.9), 450 (9.4)	536	1014	16.1	99	423	419
8c[a]	275 (15.2), 448 (4.8)	527	1333	16.1	99	310	307
9[e]	365 (4.0), 379 (6.6), 401 (6.5)	418	3566	8.4	99	-	-
10[a]	367 (5.9), 382 (9.1), 404 (9.0)	427	3346	13.5	99	640	634

[a]In H_2O; [b]in DCM; [c]in H_2O/DMSO (5%); [d]in PBS/DMSO (5%); [e]in MeOH; [f]averaged value of three replicas measured at 800 nm

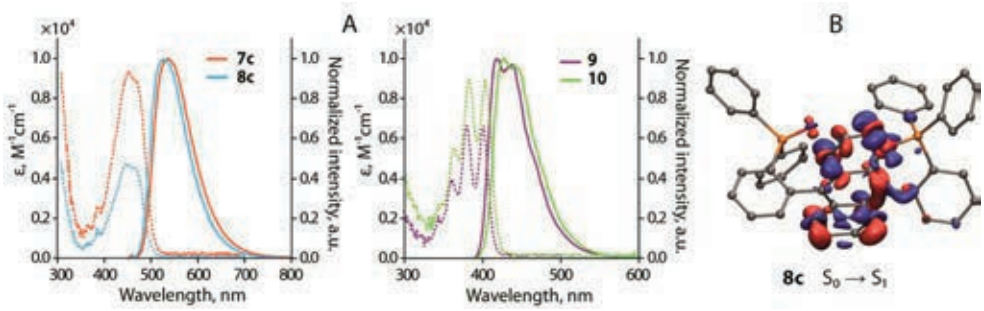

Figure 26. A: Absorption (dashed lines) and emission (solid lines) spectra of **7c**, **8c** in (left) H_2O and **9**, **10** (right) H_2O and MeOH and B: Electron density difference plot for the lowest energy singlet excitation ($S_0 \rightarrow S_1$) of **8c**.

The electronic absorption spectra of the red **5c** and violet **6c** generally resembled those of **3c**, **4c**, **7c**, and **8c**. The HE bands positioned at 272–281 nm were nearly insensitive to the polarity of the solvent and in a similar manner were attributed to the HOMO–2→LUMO+2 transitions. The LE maxima were significantly red-shifted with respect to the congeners at λ_{abs} ≤480 nm for **5c** and λ_{abs} ≤570 nm for **6c** in DCM,

probably because of a more pronounced ICT caused by the *D–A* architecture (Figure 25B); this is in agreement with the TD-DFT results. Notably, the dimethylaniline donor of **6c** should be more susceptible to the formation of $Me_2N\cdots H_2O$ hydrogen bonding than the triphenylamine unit of **5c**. This might cause a more effective stabilization of the ground state and a more distinct impact of the protic solvents on the energy of the CT band [λ_{ICT} = 540 nm in H_2O/DMSO (5%); 555 nm in PBS/DMSO (5%); and 570 nm in DCM].

The HOMO-LUMO gaps for **1c–6c** gradually decreased upon the extension of the π-conjugated motif, enhanced by the increased *D–A* character of **5c** and **6c** (Figure 27). This was in line with the absorption data and confirmed the validity of the chosen molecular design. The introduction of the $\lambda^4\sigma^4_{cyclic}$ cationic phospha-group into the phenylnaphthalene scaffold better stabilized both frontier orbitals (HOMO and LUMO) in **1c** compared to its $\lambda^5\sigma^4_{cyclic}$ phospha-oxide analogue (Figure 27A).[197] Thus, a large reduction in the optical gap from 3.975 eV (**1c**) to 2.215 eV (**6c**; Figure 27) was successfully achieved via rational structural variations.

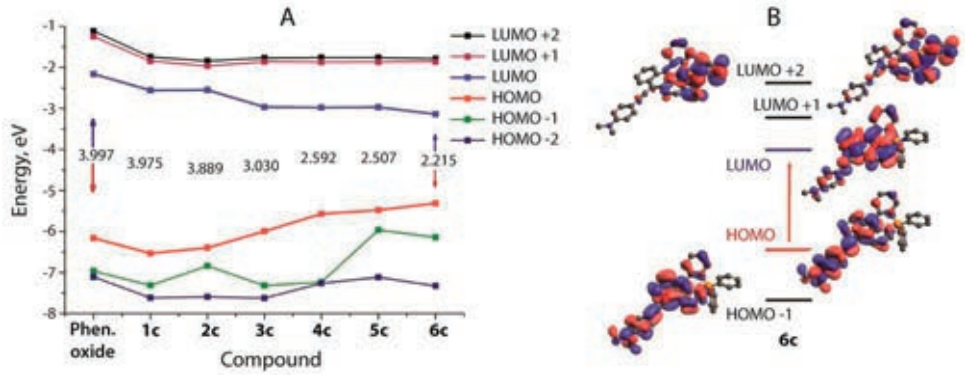

Figure 27. A: energies of the molecular orbitals and HOMO-LUMO gap for **1c–6c** obtained by TD-DFT calculations and B: Orbitals involved in the LE photoinduced electronic transitions for **6c**.

Acyclic compounds **9** and **10** demonstrated optical behavior similar to that of the diphenylanthracene and its silane-modified analogue.[231] For instance, the electronic spectra of **10** displayed vibronically structured absorption (λ_{abs} = 404 nm) and emission (λ_{em} = 427 nm) profiles with small Stokes shifts of ~23 nm (Figure 26A) and a mono-exponential decay of the excited state (τ = 13.5 ns, Table 2). The highly intense blue emissions (Φ_{em} ~99%) were dominated by the $^1\pi\pi^*$ transitions of the anthracene moiety.

The phosphacyclic compounds **1c–8c** exhibited remarkable luminescence in solution, which covered a wide interval of wavelengths (360 nm or 12103 cm^{-1}) from deep blue (420 nm) to near-infrared (780 nm; Figures 25 and 26A). The structureless fluorescence bands followed the bathochromic shift of the LE absorption bands

caused by π-extension. Naphthalene- and phenanthrene-derived cations **1c** and **2c**, respectively, featured deep blue emissions with maxima at 420 and 425 nm, respectively. Effective delocalization of the HOMO and LUMO over the $\lambda^4\sigma^4_{cyclic}$ R_4P^+ fragment led to double the quantum yield for **1c** (Φ_{em} = 30% in DCM) and ~41 nm emission red shift *vs* the congener $\lambda^5\sigma^4_{cyclic}$ oxide (λ_{em} = 389 nm, Φ_{em} = 14% in DCM).[197] Changing the PAH core to the anthracene (**3c**) decreased the luminescence energy (113 nm or 5047 cm^{-1} bathochromic shift) resulting in bright green emission with a relatively long lifetime and an efficiency close to unity (λ_{em} = 533 nm, Φ_{em} = 99%, τ = 16.0 ns). Further increase in the emission wavelength (~14 nm) was detected for **4c** (λ_{em} = 547 nm), which contained the phenyl substituent in the 10-position of the acene. This also influenced the quantum efficiency of **4c** (Φ_{em} = 69%), presumably due to the increased degree of stereochemical freedom. The unrestricted movement of the phenyl group facilitated the non-radiative decay of the excited state (k_{nr} = 3.3×10^7 s^{-1} for **4c** and 0.1×10^7 s^{-1} for **3c**). Such an effect was recently found for other emitters.[232,233] In accordance with this hypothesis, the rotational dissipation of the excitation energy was blocked by the inclusion of bulky electron-deficient $\lambda^5\sigma^4/\lambda^4\sigma^4$ groups into the *ortho*-position of the phenylene rings [-$P(O)Ph_2$ in **7c**, -P^+Ph_2Me in **8c**]. This restored the efficiency to unity (k_{nr} = 0.1×10^7 s^{-1} for **3c** ≈ for **7c** and **8c**) with some hypsochromic shifting (11–20 nm; λ_{em} = 536 and 527 nm for **7c** and **8c**, respectively). The blue-shifted emission maximum for **8c** with respect to that of **7c** suggested larger HOMO stabilization by a stronger phosphonium acceptor.

The luminescence features of compounds **5c** and **6c** were determined by their donor–acceptor configuration. Thus, **5c** with a $-NPh_2$ electron-rich function displayed broad emission bands in water/DMSO and PBS/DMSO solutions maximized at 640 nm. The rather low efficiency (2%) indicated fast rotational/vibrational relaxation (k_{nr} = 28.0×10^7 s^{-1}) and the presence of the solvent polarity effect, typical for many organic fluorophores with ICT.[31,167,190,233] In line with the absorption behavior, the emission maximum for **6c** was more sensitive to the properties of the medium than that for **5c**. Thus, in the water/DMSO mixture, the former presented a band at ~665 nm that was red-shifted in a more ionic PBS/DMSO solution to ~690 nm. As compared to that in the aqueous medium, the luminescence of **5c** and **6c** in DCM was considerably more intense and simultaneously red-shifted (λ_{em} = 760 nm, Φ_{em} = 10% for **5c** and λ_{em} = 780 nm, Φ_{em} = 18% for **6c**). Furthermore, in aprotic DCM, **5c** and **6c** were among the most efficient and lowest-energy fluorophores found within the family of organophosphorus dyes.[185,188,211,212,216]

The emission maxima for the powder samples of phosphacycles **1c–4c** displayed 10–20 nm bathochromic shifts with respect to the DCM solutions [λ_{em} (nm) = 430 **1c**, 450 **2c**, 541 **3c**, and 556 **4c**], which probably resulted from the dimer formation as a solid-packing effect. More drastic changes were observed for **6c**, which presented an emission band at 825 nm and superior Φ_{em} (7%), arising from the lack of solvent quenching.

Importantly, the pronounced CT nature of the excited states for **5c** and **6c** ensured the respective large Stokes shifts 280 nm (7676 cm^{-1}) and 230 nm (4723 cm^{-1}; Figure 24, Table 2), thereby producing negligible overlap of the absorption and emission profiles (*i.e.*, minimizing the reabsorption) that is crucial for imaging applications.

Essentially, all the ionic compounds (**1c–8c** and **10**) exhibited moderate to high two-photon absorption (TPA) cross sections at the excitation wavelength 800 nm (δ_2 = 151–640 GM, Table 2). These data were similar or considerably higher than the TPA values of the commonly used coumarin 485/480 and rhodamine 6G/B dyes (δ_2 = 36–160 GM).[234–236] The phosphonium species displaying good one- and two-photon excited brightness ($\varepsilon \times \Phi_{em}$ and $\delta_2 \times \Phi_{em}$, Table 2) served among the best mitochondrial probes (*e.g.*, 2 and 3 GM for MitoTracker green and red, respectively).[237]

Furthermore, the aerated solutions of the phosphacycles exposed to continuous high-power irradiation revealed their excellent photostability. The changes in the initial intensities (I/I_0) of dyes **3c**, **4c**, and **7c** were compatible with those observed for coumarin 480 and fluorescein. On the other hand, **1c**, **5c**, **6c**, and **8c** demonstrated visibly slower degradation (original publications **I, II**).

The combination of the ionic nature (*i.e.*, solubility in aqueous medium) with outstanding optical behavior and good photostability make the title phosphonium dyes potentially suitable for cellular bioimaging. Thus, as a proof of concept **4c**, **6c–8c**, and **10** were tested for *in vitro* imaging of the HeLa and CCD cells. The positively charged phospha-salts demonstrated high cell viability and permeability in the 1–5 μm concentration range.

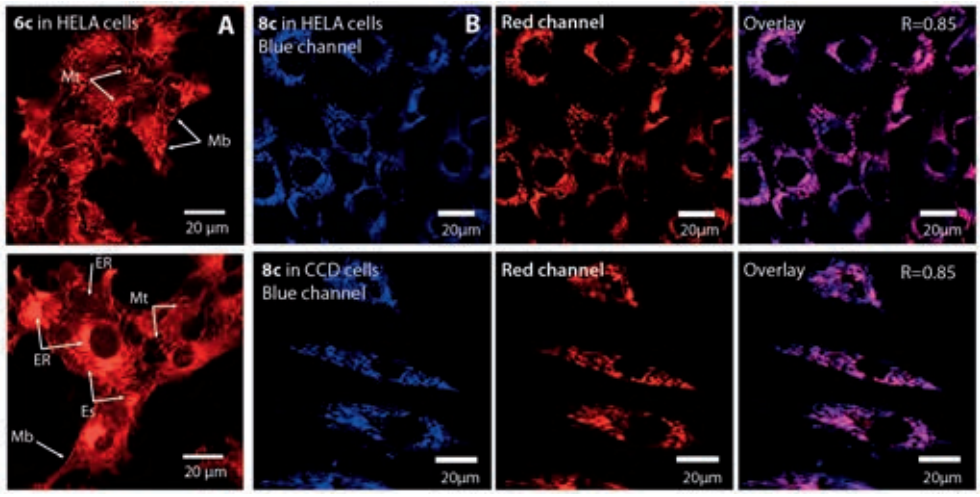

Figure 28. A (first column): Two-photon confocal images of living HeLa incubated with **6c** (λ_{ex} = 800 nm) for 10 min (top) and 2 h (bottom) and B (next three columns): confocal images of HeLa (top row) and CCD cells (bottom row) labeled with **8c** and MitoTracker (blue channel: 460–620 nm, λ_{ex} = 458 nm; red channel: 640–740 nm, λ_{ex} = 633 nm).

For instance, the results for **6c** are illustrated in Figure 28A. The two-photon fluorescence images obtained at the excitation wavelength 800 nm displayed strong red emission in the living HeLa cell cultures. The dyes were localized primarily in mitochondria (Mt) organelles after 10 min incubation. However, after 2 h of co-culturing, the lipid-rich endoplasmic reticulum (ER) and endosome (Es) membrane were labeled too (Figure 28A). The selective mitochondrial uptake was additionally studied by co-localization of diphosphonium **8c** with commercial MitoTracker deep red dye in both HeLa and CCD cells. Figure 28B reveals that the overlay images presented the Pearson's correlation coefficient R = 0.85, demonstrating highly specific location of the dyes in mitochondria.

In summary, the strategy to alter the photophysical properties by incorporating the $\lambda^4\sigma^4$ phosphonium ($^+PR_4$) unit into the naphthalene-, phenanthrene-, and anthracene- polyaromatic scaffolds *via* intramolecular Cu^{II}-mediated phospha-annulation was successfully realized. The novel phosphacycles demonstrated rich possibilities for emission tuning from deep blue (420 nm) to near-infrared (780 nm) in solution, which was extended up to 825 nm for the pristine solid. As proof of principle, the water-soluble dyes were demonstrated to be useful for the visualization of the biological samples.

3.2 DYNAMIC *D–A* PHOSPHONIUM FLUOROPHORES [III]

A literature analysis revealed that the $\lambda^4\sigma^4$ phosphonium unit ($-P^+R_3$) has been poorly utilized as a strong pendant acceptor (*A*) for the construction of acyclic fluorophores having the simplest linear *D*–π–*A* architecture (Figure 29). To fill this gap, a systematic study of the family of Ph_2N–π–P^+Ph_3 ionic dyes was next carried out. Aimed at the modulation of the ICT properties and optical gap, the structural tuning of these chromophores mainly focused on the variation of the polarizable π-spacer system.

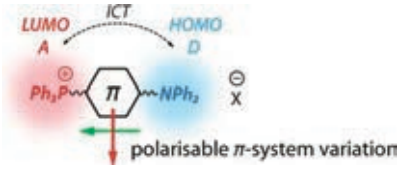

Figure 29. Illustration of the concept: systematic HOMO-LUMO and ICT alteration in linear "push-pull" phosphonium salts.

Following this strategy, the bromoarylamine intermediates (Br–π–*D*) were synthesized according to standard protocols. In brief, the procedure involves *N*-arylation of the secondary amines (diphenylamine and carbazole) and Suzuki and Sonogashira cross-coupling of the aryl dihalide derivatives with triphenylamine-*p*-ethynyl or boronic acid precursors (synthetic details in original publication **III**).[238–240]

Similar to bromoarylamines, the target *D*–π–*A* phosphonium salts **11**–**15** and **12Cbz** were prepared *via* the Ni-catalyzed Charette and Maroux P–C bond forming reaction[110] in moderate to high yields (34–92%; Scheme 9, method *I*). A perceptible drop in the reaction efficiency was observed for the extended oligophenylene and naphthalene derivatives (quaterphenyl **14**, 40% and naphthalene **15**, 34%). Firstly, these lower yields were attributed to a gradual decrease in the solubility of the bromoarylamines in ethylene glycol upon the extension of the hydrocarbon π-spacer. Secondly, oxidative addition to the reactive nickel center should be sensitive to the steric hindrance and electronic factors and is therefore inhibited by the bulky naphthalene motif.

In the case of 10-bromo-9-(*N*,*N*-diphenylamino)-anthracene, no expected quaternized salts were observed in both the Ni- and Pd-catalyzed reactions,[109,111,241] which was in line with the aforementioned results. Alternatively, a two-step procedure (Scheme 9, method *II*) was utilized. Thus, anthracene-**16** and extended naphthalene-based **17** and **18** $\lambda^4\sigma^4$ phosphonium salts were obtained in satisfactory 35–51% yields from the corresponding phosphines quaternized with excess methyl iodide.

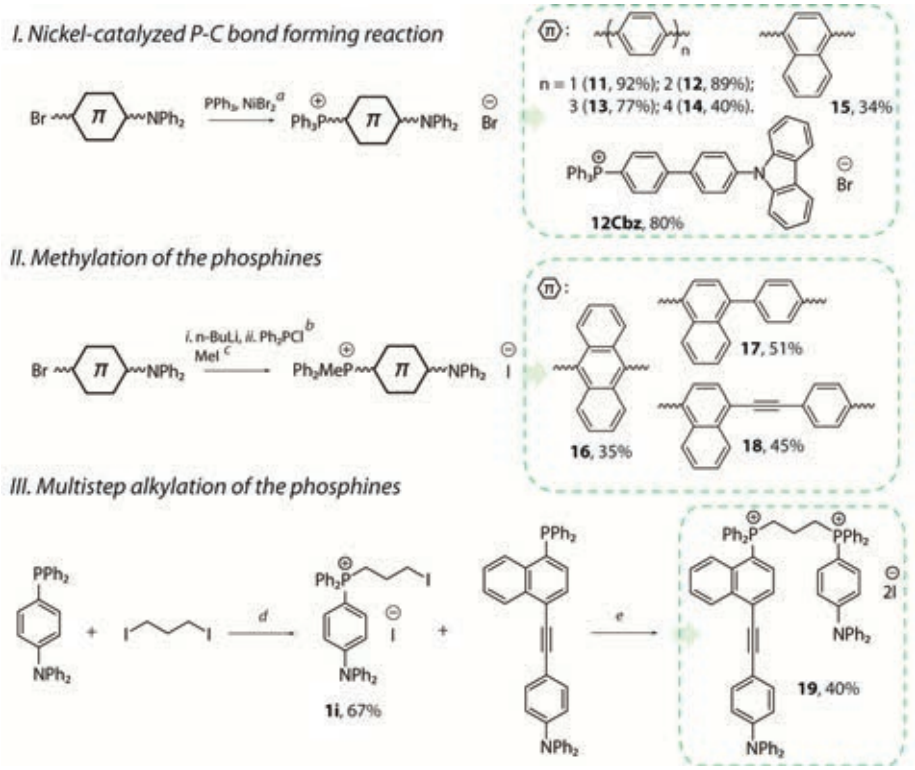

Scheme 9. Synthesis of phosphonium salts **11–19** and **12Cbz**: *a* PPh_3, $NiBr_2$ anhyd, ethylene glycol, 180–200 °C, 5 h; *b* (*i*) ^{n}BuLi, 2.5 M, THF, –78 °C, 1 h followed by (*ii*) PPh_2Cl, –78 °C → rt, 2 h; *c* MeI, DCM, 2 h; and *d* DCM, reflux, 4 h. *e* DMF, 120 °C, 12 h.

In turn, diphosphonium salt **19,** which bears two different *D*–π–*A* fragments connected by the –$(CH_2)_3$– spacer, was synthesized in an overall yield of 27% yield by a two-stage alkylation protocol (Scheme 9, method *III*). The first step proceeded *via* refluxing with DCM, whereas the second alkylation required more severe conditions (DMF, 120 °C, 12 h).

The ^{1}H, ^{13}C, and ^{31}P{^{1}H} NMR spectroscopic measurements in solution confirmed the composition of the salts. Particularly, the phosphorus spectra of **11–18** and **12Cbz** demonstrated singlet resonances in the range 17.8–23.7 ppm, in accordance with the data for the previously reported tetraaryl/triarylalkyl phosphonium derivatives.[42,119,120,129] Two distinct phosphonium groups in **19** generated two doublets (δ = 23.4 and 22.0 ppm) with the clearly resolved long-range coupling constant $^4J_{P\text{-}P}$ = 9.9 Hz. The ESI$^+$ MS of the mono- (**11–18** and **12Cbz**) and dicationic (**19**) species displayed dominating signals at *m*/*z* = 506.2, 582.2, 658.3, 734.3, 556.2, 544.2, 570.2, 594.2, 525.2, and 580.2, respectively. The masses and observed isotopic distributions completely matched the simulated patterns for these molecular ions.

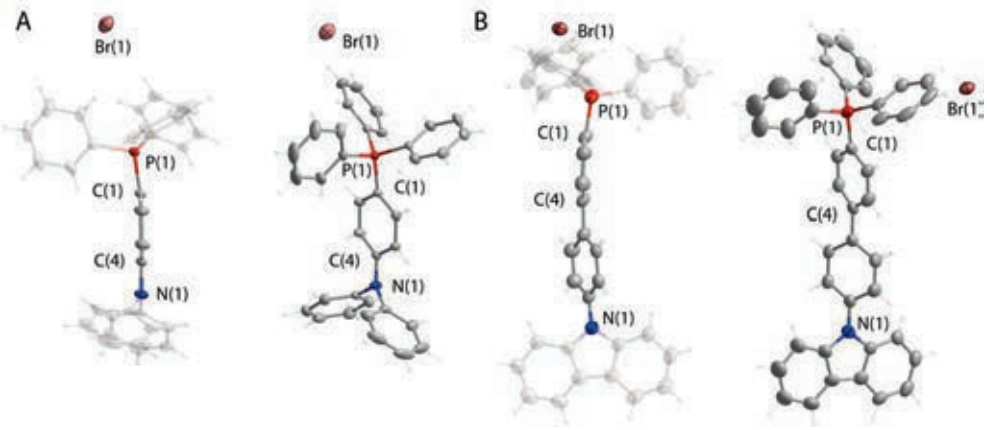

Figure 30. A: Molecular views of phosphonium salts **11** and B: Of **12Cbz** (only one of two independent molecules found in the unit cell is depicted). Thermal ellipsoids are shown at the 50% probability level.

The X-ray crystallographic studies confirmed that the quaternized phosphorus atoms in **11** and **12Cbz** (Figure 30) adopted a tetrahedral geometry with ∠C–P–C and C–P bond lengths in the range 107.9–112.5° and 1.781(2)–1.812(2) Å, respectively. These structural parameters agreed with those of the other $\lambda^4\sigma^4$ tetraarylphosphonium centers.[242,243]

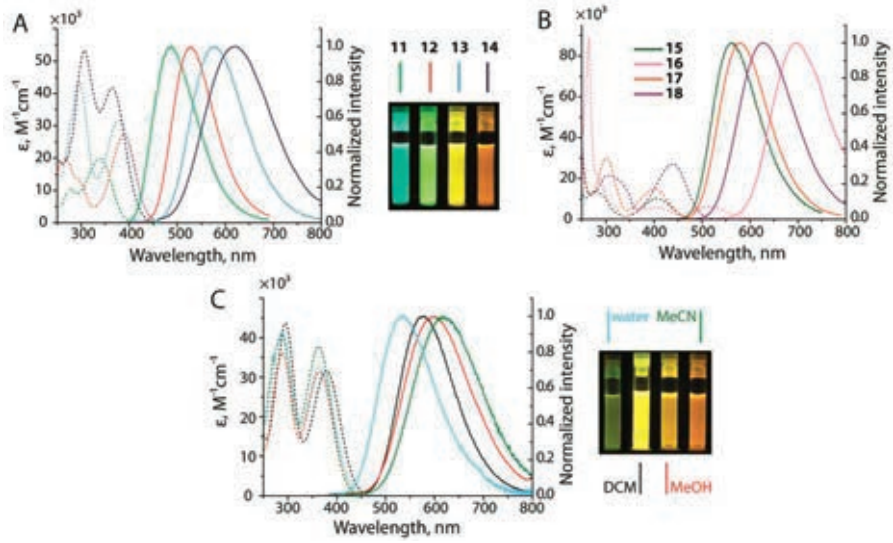

Figure 31. Absorption (dashed lines) and emission (solid lines) spectra of the **11**–**14** (A) and **15**–**18** (B) in DCM and salt **13** in different solvents (C; water, DCM, MeOH, and MeCN). The photos reveal the appearance of the corresponding solutions under 365 nm excitation.

Table 3. Photophysical data of **11–19** and **12Cbz** in solution at 298 K.

	λabs, nm (ε, 10^{-3} M^{-1} cm^{-1})	**λabs.calc, nm**	**λem, nm**	**Δν, cm^{-1}**	**τ, ns**	**Φem, %**	**k_r, 10^7 s^{-1}**	**k_{nr}, 10^7 s^{-}**
11[a]	275 (10.3), 333 (19.8)	316	487	9496	9.2	72	7.8	3.0
12[a]	268 (20.2), 387 (27.2)	349	528	6900	4.4	88	20.0	2.7
[b]	262 (20.1), 375 (28.6)	-	538	8583	3.8	84	22.1	4.2
[c]	260 (21.5), 372 (26.8)	-	555	8864	4.1	51	12.4	12.0
[d]	256 (21.0), 369 (26.1)	-	568	9495	0.4	7	17.5	232.5
12Cbz[a]	261 (28.9), 343 (13.9)	-	488	8663	-	85	-	-
13[a]	294 (43.9), 379 (32.0)	341	577	9054	4.2	71	16.9	6.9
[b]	290 (36.3), 365 (31.5)	-	598	10675	1.6	44	27.5	35.0
[c]	288 (41.1), 364 (38.0)	-	617	11265	2.4	54	22.5	19.2
[d]	286 (40.8), 362 (32.7)	-	534	8898	4.4 (88); 23.2 (12)	11	0.9	8.0
14[a]	305 (53.4), 364 (42.0)	333	619	11317	4.3	95	22.1	1.2
[b]	299 (42.8), 353 (41.7)	-	670	13403	0.1	~1	10.0	990.0
[c]	298 (46.4), 354 (47.0)	-	687	13693	0.2	~1	5.0	495.0
15[a]	278 (13.9), 407 (10.6)	420	560	6713	14.2	29	2.0	5.0
16[a]	264 (89.6), 398 (5.9), 519 (6.2)	465	696	4900	2.5	2	0.8	39.2
17[a]	301 (30.8), 402 (15.0)	398	579	7604	6.8	95	14.0	0.7
18[a]	310 (21.6), 438 (27.4)	449	626	6857	4.1	81	19.8	4.6
19[a]	332 (43.6), 437 (31.2)	-	627	6934	4.1	89	21.7	2.7

[a]In DCM; [b]in MeOH; [c] in MeCN; and [d]in H_2O.

The relevant photophysical data for **11–19** and **12Cbz** in polar solvents are displayed in Figure 31 and listed in Table 3 (complete dataset in original publication **III**). The lowest energy CT band in the absorption spectra of the phosphonium salts was attributed to the donor-acceptor architecture, which was confirmed theoretically (Table 3). This absorption demonstrated a gradual bathochromic shift (≤186 nm, 10760 cm^{-1}) along with the extension of the polarizable spacer [$\lambda_{abs(ICT)}$ = 333 nm for **11** (–π– is phenylene); 387 nm for **12** (–π– is biphenylene); 519 nm for **16** (–π– is anthracene)]. On the other hand, the elongation of the oligophenylene spacer caused a slight blue shift (I) in the range 8–13 nm (DCM) with an expected rise in the extinction coefficient [λ_{abs} (ε M^{-1} cm^{-1}) = 387 (27200), 379 (32000), and 364 (42000) nm for **12**, **13**, and **14**, respectively]. The maximum of the ICT absorption band for **12Cbz** shifted to 343 nm as a result of a lower donicity of the carbazole function compared to that of the diphenylamine in **12**. The absorptions of the close conge-

ners $Ph_{3-n}P(E)–[(C_6H_4)_m–NPh_2]_n$ (E = O, S, Se, and AuC_6F_5; n = 1 or 3; m = 1–3)[73,80] systematically appeared at higher energies. This pointed towards a higher degree of ICT in the ionic dyes because of a stronger electron-accepting ability of the $–P^+Ph_3$ group. The absorption bands of all the title phosphonium salts demonstrated modest negative solvatochromism upon increasing the solvent polarity (*e.g.*, $\lambda_{abs(ICT)}$ for **13** = 379 nm in DCM, 365 nm in MeOH, 364 nm in MeCN, and 362 nm in water), which is consistent with the properties of the reported push-pull phosphonium and pyridinium compounds.[122–124,244]

The emission maxima for molecules **11–19** and **12Cbz** also varied as a function of the medium nature and size of the conjugated system (Figure 31). All the compounds displayed structureless emission profiles with fluorescence lifetimes of 2.5–14.2 ns (DCM) and luminescence colors covering the entire visible range (λ_{em} = 487–696 nm, DCM). The quantum yields of fluorophores **11–14**, **17**, **18**, and **12Cbz** in DCM solutions fell in the range 71–95%. On the other hand, dyes **15** and **16** with naphthalene and anthracene polyaromatic cores, demonstrated lower efficiencies of 29 and 2%, respectively, owing to the visibly smaller radiative and higher non-radiative rate constants along this series (Table 3). A notable bathochromic shift of the emission (~132 nm, 4378 cm^{-1}) was observed for oligophenylene phosphonium salts: blue emission observed for **11** (487 nm) changed upon elongation of the phenylene chain to green for **12** (528 nm), yellow for **13** (577), and orange for **14** (619 nm), as illustrated in Figure 31A. The weaker donor carbazole substantially increased the emission energy for **12Cbz** (478 nm in DCM) *vs* **12**. The emissions of salts **15** and **16** with polyaromatic backbones expectedly revealed an energy reduction to 560 and 696 nm, respectively; notably, the latter wavelength was the most red-shifted within the series **11–19**. The quantum efficiency of **15** was improved by inserting the phenylene (**17**) or ethynyl-phenyl (**18**) spacers to produce the remarkable values Φ_{em} = 95 and 81% together with significant red-shift of the emission maxima (λ_{em} = 579 nm for **17** and 626 nm for **18**). In turn, di-phosphonium salt **19** mimicked the fluorescence of **18** with a slightly higher quantum yield (8% increase). The absence of dual emission denoted a complete excitation energy transfer from the phenylene to the naphthalene moiety.

The luminescence of the given phosphonium salts was sensitive to the solvent properties (Figure 31C, Table 3). Increasing the polarity from DCM to MeOH and MeCN led to a bathochromic shift of the emission. For instance, the emission of biphenyl dye **12** demonstrated a shift of ~10 nm in methanol (λ_{em} =538 nm) and ~27 nm in MeCN (λ_{em} =555 nm), reaching the largest value of ~40 nm in water (λ_{em} =568 nm), compared to that of the DCM solution (Table 3). Such a decrease in energy was accompanied by substantial fluorescence quenching, caused by static interactions with the water molecules.[245] Anthracene salt **16** reached NIR emission in MeCN (709 nm), which presented low efficiency (<1%), attributed to a lowered energy gap (energy gap law).[246]

For salts with longer aromatic spacers, *i.e.*, **13**, **14**, **17**, and **18**, the emissions in water appeared at higher energies than those observed in DCM (*e.g.*, **13,** λ_{em} = 534 nm in water and 577 nm in DCM; Figure 31C). The rise in the optical gap in water can be explained by effective stabilization of the ground state in view of possible HOH···NPh$_2$ and H-O$^{\delta-}$···$^{+}$PR$_4$ interactions.

Broad structureless profiles, emission quenching in the polar medium, pronounced solvatochromism and large Stokes shifts (from 4900 to 11300 cm^{-1}) indicated the pure ICT character of the fluorescence.[61]

Dyes **12–15** and **18** exhibited moderate to high two-photon absorption properties measured under 800 nm excitation in water (δ = 263, 299, 321, 313, and 977 GM), which have application potential for bioimaging.[121]

Unexpectedly, investigation of the photophysical properties of salts **11–13, 17**, and **12Cbz** in nonpolar toluene revealed unusual dual emission (Figure 32A, Table 4). While compound **11** demonstrated only visible broadening and asymmetry of the emission profile (λ_{em} = 480 nm, Φ_{em} = 7%), two distinct bands, F$_1$ (high energy) and F$_2$ (low energy), were identified in the spectra of salts **12**, **12Cbz**, **13**, and **17** in toluene. The ratio of the F$_1$/F$_2$ intensities and the energy of the F$_2$ band were evidently dependent on the length of the conjugated –π– spacer and the strength of the donor group. The emission of **12** was comprised two complementary bands with maxima at λ(F$_1$)= 480 nm and λ(F$_2$) = 600 nm and the F$_1$/F$_2$ ratio 1.9. This resulted in white light with the CIE coordinates (0.29, 0.34), which are close to those of pure white. The intensities of the F$_2$ bands for **12Cbz** and **13** were substantially lower and presented F$_1$/F$_2$ values of 10.0 and 5.6, respectively. Moreover, the elongated terphenylene chain in **13** decreased the F$_2$ energy to λ_{em} = 674 nm and the total quantum yield for **13** improved to 37% compared to that of **12** (Φ_{em} = 17%). Notably, salt **14**, which bears a quaterphenylene spacer did not demonstrate any dual emission.

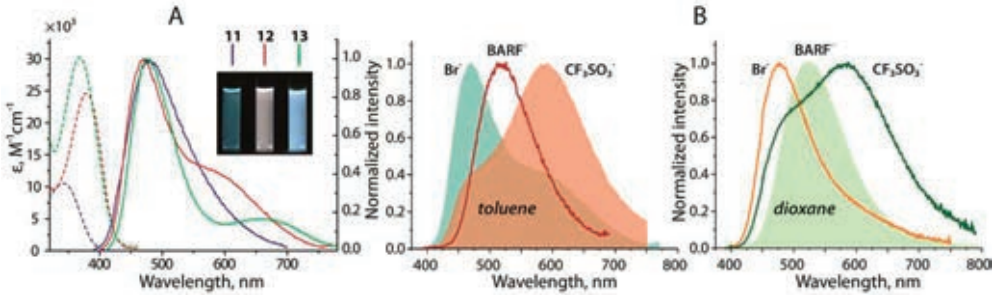

Figure 32. A: Absorption (dashed lines) and emission (solid lines) spectra of **11–13** in toluene (inset: corresponding solutions under 365 nm excitation) and B: Emission profiles of **12[X]**, X = Br, BARF, and CF_3SO_3 in toluene (left) and 1,4-dioxane (right).

To gain insight into the observed phenomenon, compound **12** was selected as a model for additional studies because of its appropriate F$_1$/F$_2$ ratio and superior sol-

ubility. Firstly, the dual emission resulting from micelle-like aggregation or excimer formation could be excluded because of the: (*i*) constant F_1/F_2 ratio at variable concentrations; (*ii*) identical excitation spectra, monitored at both high and low energy emission maxima; and (*iii*) presence of only one emission band in the solid state (λ_{em} = 510 nm).

Table 4. Photophysical data of **12[X]**, **12Cbz**, and **13** in toluene, 1,4-dioxane, and CCl_4 solutions at 298 K.

	λem, nm	**F_1/F_2** [a]	**τ (F_1), ps** [b]	**τ (F_2), ps** [c]	**Φem, %**	**CIE** [d]
12[Br]/1.81 Å [e]						
Toluene	468, 592	1.85	67 (63), 459 (37)	93 (-49),792 (36), 2439 (15)	17	0.29, 0.34
1,4-dioxane	477	-	73 (56), 600 (44)	73 (-51), 652 (37), 2066 (22)	15	0.23, 0.31
CCl_4	450, 606	8.33	-	-	14	0.21. 0.17
12[OTf]/2.48 Å [e]						
Toluene	468 sh, 589	0.39	150 (73), 660 (27)	298 (-45), 3807 (55)	47	0.42, 0.43
1,4-dioxane	482 sh, 584	0.69	265 (70), 917 (30)	431 (-46), 3063 (54)	35	0.39, 0.43
CCl_4	450, 590	2.27	-	-	26	0.29, 0.26
12[OCl_4]/2.22 Å [e]						
Toluene	468 sh, 587	0.33	86 (70), 503 (30)	219 (-46), 3948 (54)	44	0.43, 0.44
1,4-dioxane	480 sh, 586	0.59	144 (63), 678 (37)	358 (-47), 3167 (53)	34	0.40, 0.43
CCl_4	450, 590	2.08	-	-	20	0.29, 0.27
12[CF_3COO]/2.35 Å [e]						
Toluene	468 sh, 588	0.43	128 (68), 744 (32)	274 (-48), 3574 (52)	45	0.41, 0.43
1,4-dioxane	483, 590	1.09	235 (60), 784 (40)	412 (-44), 2163 (56)	25	0.35, 0.39
CCl_4	450, 580	1.72	-	-	25	0.30, 0.30
12[BARF]	493/518/522 [f]	-	-	-	81	-
12Cbz	382, 550	10	-	-	10	-
13	500, 674	5.55	120 (39), 780 (61)	120 (-39), 2540 (61)	37	0.21, 0.29
17	495, 650	2.86	-	-	-	

[a]Calculated using intensities of the emissions at 470 and 600 nm for F_1 and F_2, respectively. [b]Monitored at 430 nm, [c]monitored at 650 nm; [d]calculated from the emission spectra; [e]calculated thermochemical radii of the anions,[247] and [f]in CCl_4, toluene, and 1,4-dioxane, respectively.

Secondly, the F_1/F_2 emission ratios were found to be highly dependent on the nature of the counterion (Figure 32B, Table 4). The anion exchange afforded a family of the phosphonium salts **12[X]**, where X = Cl^-, I^-, NO_3^-, ClO_4^-, PF_6^-, $CF_3SO_3^-$,

CF_3COO^-, and $BARF^-$ [tetrakis(3,5-bis(trifluoromethyl)phenyl)borate]. Thus, substitution of the halide for the bulkier trifluoromethanesulfonate enhanced the overall quantum yield and F_2 intensity, leading to the marked emission color changes and CIE coordinates of the toluene solutions [**12**[**Br**] white, (0.29, 0.34) → **12**[**OTf**] yellow, (0.42, 0.43)]. Notably, in 1,4-dioxane and CCl_4, dual emission of **12**[**X**] was observed with a noticeable drop in the intensity of the F_2 band (Figure 32B, Table 4). In fact, the HE F_1 emission maxima varied in the order CCl_4 > toluene > 1,4-dioxane for the **12**[**X**] series, *i.e.*, according to the solvation/stabilization effect of the ICT in the *D*–π–*A* systems. On the other hand, the LE F_2 band was almost insensitive to the polarity of the medium. A larger $BARF^-$ anion completely suppressed dual emission to produce one band maximized at 493/518/522 nm in CCl_4/toluene/1,4-dioxane, respectively, behaving as a "normal" dye molecule with ICT character.

Two decay components (τ_1 = 67 ps and τ_1 = 450 ps) were retrieved from the time-resolved measurements of **12**[**Br**] in toluene for the HE band F_1 (*i.e.*, at ~430 nm). From the experimental data monitored at the maximum of the F_2 band, one rise component (τ_1 = 93 ps) and two relatively long decay times (τ_2 = 792 ps and τ_3 = 2439 ps) could be resolved. Similar behavior was observed along the **12**[**X**] series with the rise of the decay component monitored at 650 nm (Table 4). The results of the spectral temporal evolution for **12**[**Br**] in toluene (Figure 33) demonstrated continuous spectral evolution and absence of an isosbestic point, indicating the presence of several emitting species during the relaxation period.

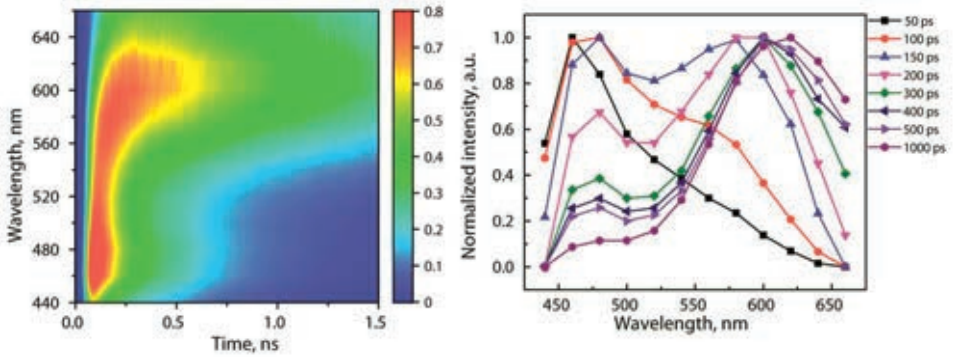

Figure 33. Time-resolved emission spectra of **12**[**Br**] in toluene at 298 K.

Thus, in polar solvents, the emission of the studied phosphonium salts was virtually independent of their counterion nature. The photophysical behavior of the solvent-separated ion pairs (Scheme 10A) was mainly determined by the solvation effect and change in the dipole moment upon excitation (Δμ between the excited and ground states), results that comply with the literature data for the $\lambda^4\sigma^4$ phosphonium salts.[130,158,177]

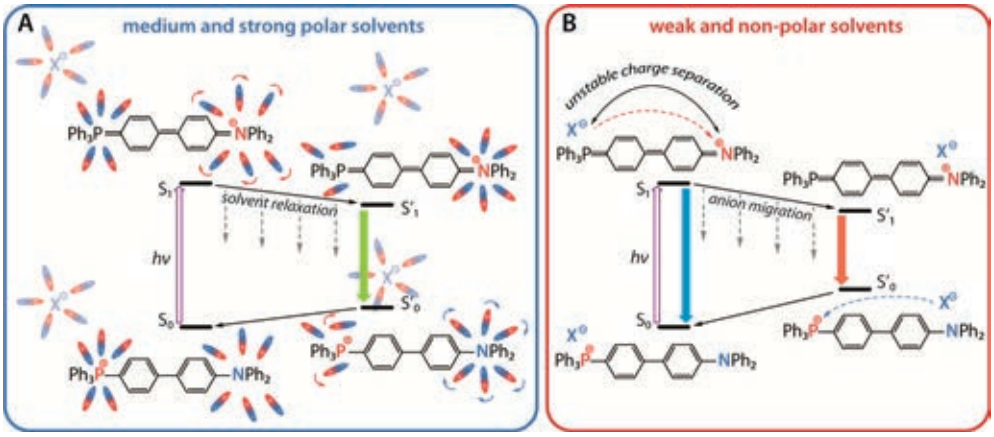

Scheme 10. A: Proposed energy diagram of the excited state relaxation mechanism in polar and B: In nonpolar solvents for salts **12[X]**.

The observations for the weakly polar and nonpolar solvents allowed the elucidation of the relaxation mechanism (Scheme 10B), using the phosphonium salt **12**[**X**] as a prototype. The poor dipole interaction with the solvent and appreciable electrostatic attraction suggested that the salt probably existed in the form of a contact phosphonium-anion pair. The excitation–relaxation cycle is initiated *via* photon absorption by the non-separated species. Consequently, because of the fast ICT (*i.e.*, the donor –NPh_2 and acceptor –$^{+}PR_3$ moieties became more positively charged and neutral, respectively), two emissive states could be considered. The first one (S_1) with unfavorable charge separation mainly acted as a locally excited state and generated the HE emission band F_1. The formation of the second state (S'_1) was supposed to result from anion X^- migration promoted by Coulomb forces from the less positive "=PPh_3" part to the formally (in the extreme representation) "+vely" charged =$^{+}NPh_2$ group. Therefore, the second bathochromically shifted emission band F_2 arose from the stabilization of the excited state simultaneously accompanied by the destabilization of the "hot" ground state (S'_0).

According to the hypothesized mechanism, the characteristics of the anions (*e.g.*, size and charge distribution) would play a major role in the behavior of the nondissociated pair and govern the migration and relaxation processes. Hence, the larger thermochemical radii[247] of the X^- anions corresponded to longer decays of the F_1 band (*e.g.*, **12**[**Br**] r = 1.81 Å, τ = 67, 459 ps; **12**[**CF_3COO**] r = 2.35 Å, τ = 128, 744 ps; Table 4 and Figure 34A). Apparently, a larger counterion increased the probability of migration, which in turn decreased the F_1/F_2 ratio. The exceedingly large size of the $BARF^-$ anion disfavored the relaxation dynamics described in Scheme 10B and suppressed dual emission. Moreover, the solvent viscosity also effected the migration rate and population of the S'_1 state (Figure 32, Table 4). Thus, toluene with its smaller viscosity parameter (0.56 cp) demonstrated accelerated anion motion compared to that of 1,4-dioxane (1.19 cp). This was revealed in the reduced F_1/F_2 ratio

and faster decay times. Additionally, monitoring the emission at different temperatures in the 1,4-dioxane and toluene solutions of **12**[**OTf**] revealed that the intensity of the F_2 band systematically increased upon heating as a result of the decreased viscosity (Figure 34B). This dynamic emission indicated the possibility for such molecules to serve as molecular thermometers.[248]

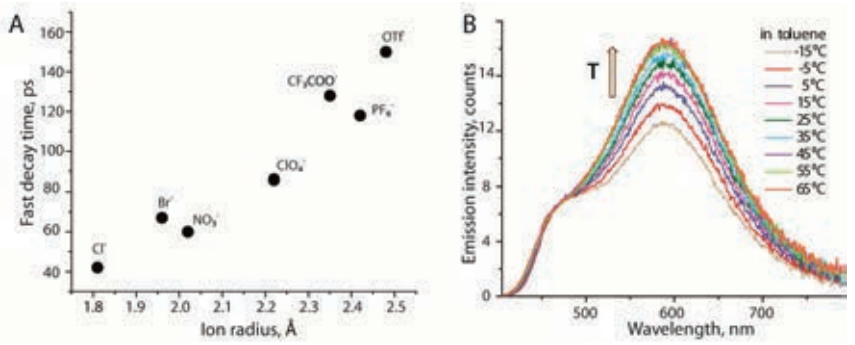

Figure 34. A: Dependence of the fast decay time component of the HE band F_1 for **12**[**X**] on the anion thermochemical radius[247] and B: Temperature-dependent emission spectra for **12**[**OTf**] in toluene.

In summary, the combination of the electron-poor $\lambda^4\sigma^4$ phosphonium group (–$^+PR_3$) and diphenylamine/carbazole (–NPh_2/-Carb) donors with different aromatic spacers produced highly emissive fluorescent dyes **11–19** and **12Cbz** spanning over the whole range of the visible spectrum. Such *D*–π–*A*-type molecules demonstrated pronounced solvatochromism in polar solvents. More importantly, in nonpolar media, salts **11–13, 17**, and **12Cbz** exhibited dual emission, which was dependent on the counterion nature, size of the conjugated spacer, and viscosity of the fluid. To the best of our knowledge, this unusual approach to attain dual emission has been virtually unexplored to date. Furthermore, the counterion migration mechanism reminisced the charge-induced translational motion machines,[249] paving a new avenue for controllable panchromatic light generation and the relevant optical functionalities.

3.3 (PHOSPHINE-AU)-EU EMISSIVE DYADS [IV]

This last chapter is devoted to the utilization of donor-functionalized phosphine ligands for the construction of push-pull phosphine—Au fluorophores *(D*–π–R_2P–AuL), which were merged with luminescent $Eu(tta)_3$ f-block (tta = 3-thenoyltrifluoro-acetonate) compounds. The proposed design (Figure 35) represents a simple pathway for the combination of an ICT chromophore and lanthanide emitter with the aim to achieve tunable dual luminescence.

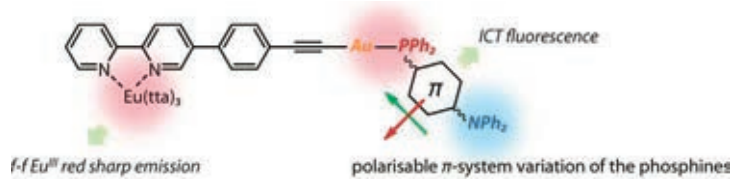

Figure 35. (Phosphine-Au)-Eu dyads capable of multiple emissions.

The phosphines **L1**–**L3**, which comprise a diphenylamine-functionalized π-spacer (biphenyl **L1**, naphthalene-ethynylphenyl **L2**, and ethynyl-anthracenyl-ethynylphenyl **L3**) were synthesized from the corresponding bromoarylamine precursors according to a conventional two-step procedure (*a*, Scheme 11). **L1** and **L2** were related to the phosphonium salts **2** and **18**, discussed in the previous chapter. Depolymerization of $[Au(epbpy)]_n$ [epbpy = 5-(4-ethynylphenyl)-2,2′-bipyridine] with **L1**–**L3** under an inert atmosphere afforded the metalloligands **21**–**23** in high yields (86–95%; *b*, Scheme 11).

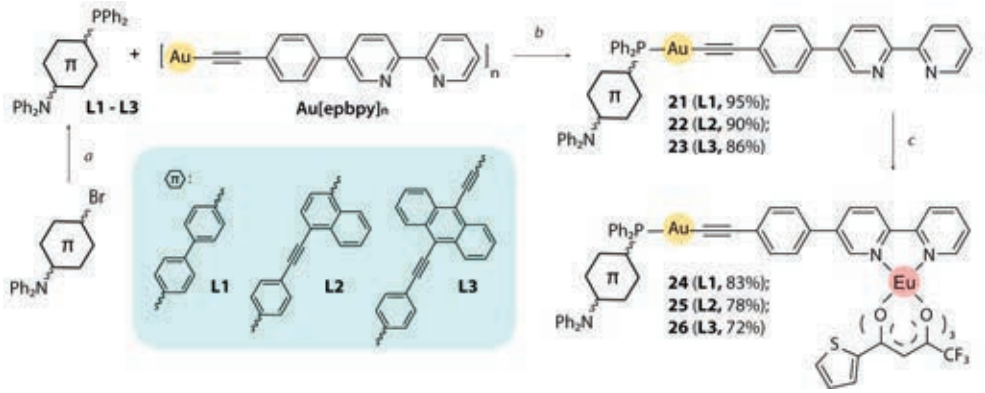

Scheme 11. Synthesis of **21**–**26**: *a) n*-BuLi 2.5 M, THF, –78 °C, 1 h for **L1** and **L2**; *n*-BuLi 1.6 M, diethyl ether/THF (1/1) –85 °C, 1 h for **L3** followed by PPh_2Cl, –78 °C → rt, 2 h; *b)* DCM, 1 h, 298 K; and *c)* $Eu(tta)_3{\times}2H_2O$, DCM, 1 h, 298 K.

Gold(I) complexes **21–23** with a diimine function underwent chelating coordination and readily produced the Au–Eu dyads **24–26** by reaction with $Eu(tta)_3$, in a 1:1 ratio, under mild conditions (72–83%; *c*, Scheme 11). Compounds **21–26** were stable in the solid state and in solution, whereas the phosphines were susceptible to oxidation when dissolved in air.

Singlet resonances of **L1–L3** in the $^{31}P\{^1H\}$ NMR spectra (δ = –6.2 to –32.8 ppm) shifted to a low-field region (δ = 41.7 to 16.5 ppm) upon binding of the $–PPh_2$ group to the Au(epbpy) fragment, reaffirming the formation of metalloligands **21–23**. Further coordination of the bipyridyl functions of **21–23** to the Eu atom did not impact on the position of the ^{31}P signals in **24–26**. The chemical shifts for **21–26** well matched the previously reported values for tertial-phosphine–gold(I) complexes.[43,80,250] Further, the ^1H NMR spectra of the novel ligands and their complexes well agreed with the proposed molecular structures. In particular, the Au–Eu dyads **24–26** demonstrated visible broadening and significantly low-field resonance shifts. These were assigned to the protons adjacent to the Eu-bound N-atoms of the bipyridine moiety, additionally confirming the coordination of the paramagnetic $\{Eu(tta)_3\}$ fragments to precursors **21–23**.

The ESI^+ MS of the metalloligands displayed dominating signals at *m*/*z* = 958.26 (**21**), 1032.28 (**22**), and 1106.29 (**23**), corresponding to the protonated molecular ions. Unfortunately, for the successor dyads **24–26**, only the products of fragmentation were observed.

The FTIR spectra of **24–26** in KBr demonstrated intense absorptions at ~1600 cm^{-1}, attributed to the C=O bond stretching vibration of the coordinated tta ligand.[251,252] Additionally, the IR spectra also demonstrated weak bands in the region 2114–2197 cm^{-1}, assigned to the C≡C vibrations.

Table 5. Photophysical properties of **21–26** in 1,2-dichloroethane (DCE) at 298 K.

	λabs, nm (ε, 10^{-3} M^{-1} cm^{-1})	**λabs, calc**	**λem, nm** [a]	**Δν, cm^{-1}** [b]	**τ, ns** [c]	**τ, μs** [d]	**Φem, %**
21	330 (55.7)	307	460	8560	1.8	-	30
22	324 (67.9), 400 (34.6)	356	525	5950	1.2 (70), 3.5 (30)	-	31
23	264 (54.3), 277 (60.2), 325 (60.7), 495 (31.5)	337, 441	635	4620	4.0	-	29
24	271 (44.1), 339 (100.3)	308	460, 580, 592, 611, 654, 700	7760	2.2	280.0	15 (4) [e]
25	280 (63.2), 337 (139.1), 404 (44.0)	356	525, 611	5700	1.7	434.0	21
26	276 (93.6), 336 (117.8), 495 (35.8)	337, 441	611, 635, 705	4620	4.1	404.1	16

[a] λ_{exc} = 360 nm; [b] Stokes shift; [c] monitored at the fluorescence ICT band; [d] monitored at 611 nm; [e] overall Φ_{em} (Φ_{em} of fluorescence ICT band).

The optical characteristics of metalloligands **21–23** and dyads **24–26** in 1,2-dichloroethane (DCE) solution are summarized in Table 5 and Figure 36. The absorption spectra of **21–23** resembled those of the starting phosphine ligands **L1–L3**, although the LE structureless ICT bands for **22** and **23** exhibited some bathochromic shifts (~15 nm). A decrease in the absorption energy caused by the coordination of the phosphorus atom to the gold(I) center, indicated the enhanced ICT character of the LE excitations as was postulated earlier.[80] These ICT transitions displayed a systematic red-shift in the order **21** (π-spacer = biphenyl, 330 nm) < **22** (naphthalene-ethynylphenyl, 400 nm) < **23** (ethynylanthracenyl-ethynyl, 495 nm), in accordance with the increase in the conjugated system. The absorption bands at 324–330 nm with large extinction coefficients (ε = 55700 M^{-1} cm^{-1} for **21**, 67700 M^{-1} cm^{-1} for **22**, and 60200 M^{-1} cm^{-1} for **23**) were attributed to the intraligand $\pi \rightarrow \pi^*$ transitions localized on the ethynylphenyl-bipyridine fragment.[253] The quantum chemical calculations supported the proposed assignment, although the predicted wavelengths were overestimated.

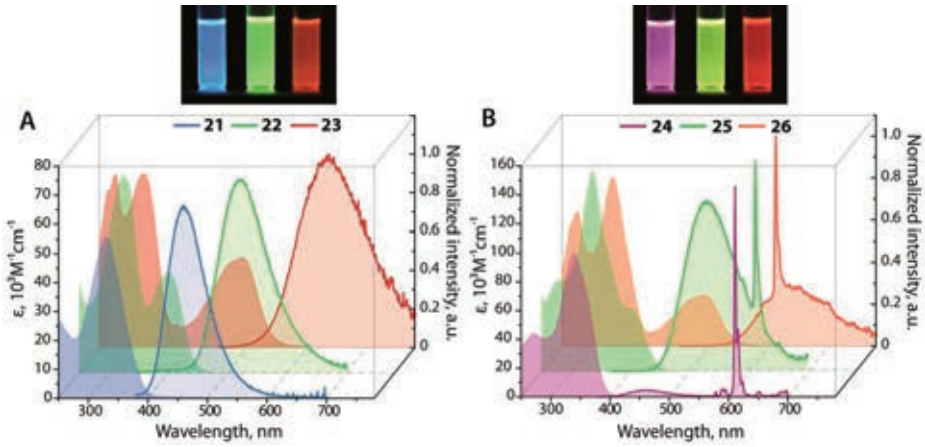

Figure 36.A: UV-vis absorption (left) and emission (right, solid lines) spectra of metalloligands **21–23** and B: Au-Eu dyads **24–26**.

As predicted, the absorption profiles of dyads **24–26** were correlated with those of the gold precursors **21–23** (Figure 36B). The LE CT bands were not affected by the Eu(III) coordination and were positioned at the same wavelengths as those of the parent metalloligands. In turn, the large growth in absorptivity in the range 336–339 nm (ε = 100300–139100 M^{-1} cm^{-1}), which was similar for all three dyads, could be explained as a cumulative contribution of the $\pi \rightarrow \pi^*$ transitions of the diketonate tta ligands. This was proven by the computational results and previous reports[254,255] and indicated the presence of the $Eu(tta)_3$ fragment in dyads **24–26**.

The metalloligands exhibited blue (**21**, λ_{em} = 460 nm), green (**22**, λ_{em} = 525 nm), and orange red (**23**, λ_{em} = 635) intense emissions in DCE with similar quantum effi-

ciencies of ~30% (Table 5, Figure 36A). Structureless broad profiles accompanied by large Stokes shifts (4620–8560 cm^{-1}) are typical for *D*–π–*A*-type molecules, thus indicating the ICT character of the lowest excited state.[61] The close congeners of metalloligand **21**, $Ph_{3-n}P(E)–[(C_6H_4)_2–NPh_2]_n$ (E = O, S, Se, and AuC_6F_5; n = 1 or 3),[73,80] exhibited comparable fluorescence properties with emission maxima in the range 450–457 nm; however, with significantly higher efficiencies (Φ = 80–95% in DCM). With respect to the phosphonium analogues **12** (λ_{em} = 528 nm, Φ_{em} = 88%) and **18** (λ_{em} = 626 nm, Φ_{em} = 81; Scheme 9), the absorption and emission bands of **21** and **22** were at higher energies and exhibited lower intensities. This drop in efficiency might originate from a possible nonradiative ISC process ($S_1 \rightarrow T_1$), induced by the heavy gold atom.[48,49] In turn, the short lifetimes of the excited state of several nanoseconds (τ = 1.8–4.0 ns) indicated prompt fluorescence ($S_1 \rightarrow S_0$) as the radiative relaxation, while phosphorescence was not observed evidently due to the relatively weak SOC.

Figure 36B illustrates that blending of the sharp f→f emissions of the $Eu(tta)_3$ motif with the ICT fluorescence of the metalloligands led to panchromatic luminescence of the dyads **24**–**26**. The corresponding spectrum of **24** consisted of a minor broad band centered at ~460 nm and a major set of signals positioned at 580, 592, 611, 654, and 700 nm. The HE peak originated from the ICT (phosphine) and matched the emission of metalloligand **21**, whereas the LE set resulted from intraconfigurational $^5D_0 \rightarrow {}^7F_n$ (n = 0–4) electronic 4f–4f transitions of the Eu(III) center; the well resolved hypersensitive transition $^5D_0 \rightarrow {}^7F_2$ dominated over other bands. The relatively high ratio of the integral intensities for the $^5D_0 \rightarrow {}^7F_2$ and $^5D_0 \rightarrow {}^7F_1$ transitions (I_2/I_1 = 12) indicated low symmetry of the europium local environment. The overall quantum yield for dyad **24** was 15%, 4% of which was related to the intraphosphine fluorescence and the remaining 11% appeared from Eu(III) emission. The perceptible drop in the fluorescence intensity compared to that of **21** (Φ_{em} = 30%) was associated with the partial energy transfer (ET) from the phosphine-gold(I) moiety to the Eu(III) fragment; results that were in accordance with the TD-DFT calculations. The S_1 levels of the tta, epbpy (E_{S_1} ~32894 cm^{-1}), and **L1** (E_{S_1} ~32467 cm^{-1}) ligands were close in energy and could be populated simultaneously upon photoexcitation. The lowest lying triplet excited state of **21**, localized on the tta ligand (E_{T_1} ~20500 cm^{-1}; *i.e.*, used for sensitization by ET from tta to europium[256]), also suggested possible ET from the triplet states of epbpy (E_{T_1} ~22500 cm^{-1}) and **L1** (E_{T_1} ~23700 cm^{-1}) to the $^5D_0$ level of the Eu(III) ion (E ~17500 cm^{-1}). The emission spectra of dyads **25** and **26**, contrary to that of **24**, exhibited profiles that were dominated by fluorescence bands at 525 and 635 nm, respectively, with sharp Eu(III) peaks at 611 nm (Figure 36B). The calculated energies of the lowest lying triplet states (18000 cm^{-1} for **25** and 10530 cm^{-1} for **26**) confirmed the absence of the ET from the phosphine chromophores to the lanthanide. Moreover, the decrease in the quantum yield for dyads **25** and **26** (21 and 16%, respectively) could be explained by the excitation

transfer from the $^5D_0$ state of the europium(III) ion to the "dark" triplet CT state localized on the gold(I)-phosphine part.

The lifetimes of the dyads measured at the fluorescence maxima conformed with those of the metalloligands. The long lifetimes monitored at 611 nm (τ = 280.0, 434.0, and 404.1 μs for **24**–**26**) agreed well with the data observed for the radiative relaxation of the other Eu(III) complexes.[257]

Owing to the ICT nature of the excited states of the *D*–π–*A* metalloligands **21**–**23** and binuclear Au-Eu dyads **24**–**26**, their photophysical properties (*i.e.*, absorbance and emission) were investigated in solvents of various polarities [cyclohexane (CHX), toluene, DCM, chloroform, diethyl ether, THF, acetone, and MeCN]. The relevant data are summarized in Table 6 and depicted in Figures 37 and 38.

Table 6. Solvatochromic behavior of **22** and **24**–**26** in solution at 298 K.

	CHX	Toluene	Et_2O	$CHCl_3$	THF	DCM	Acetone	MeCN
				22				
λ_{abs} [a]	334, 388	336, 401	332, 393	321, 402	334, 395	321, 400	393	321, 392
λ_{em} [a,b]	428, 450	460	480	495	515	525	560	580
ν_{St}, cm^{-1} [c]	3550	3198	4612	4673	5899	5952	7588	8269
CIE [d]	0.15, 0.08	0.16, 0.19	0.17, 0.30	0.21, 0.40	0.28, 0.50	0.31, 0.53	0.42, 0.51	0.47, 0.48
				24				
λ_{abs}	342	339	337	336	339	338	334	335
λ_{em}	403, 423	425	435	445	450	460	475	490
CIE	0.34, 0.13	0.56, 0.26	0.27, 0.12	0.30, 0.16	0.29, 0.18	0.52, 0.28	0.35, 0.28	0.52, 0.33
				25				
λ_{abs}	334, 405	336, 402	330, 393	321, 402	334, 396	322, 401	393	328, 392
λ_{em}	428, 450	460	480	495	515	525	560	580
CIE	0.22, 0.11	0.28, 0.23	0.39, 0.31	0.35, 0.32	0.40, 0.45	0.34, 0.52	0.51, 0.45	0.53, 0.44
				26				
λ_{abs}	336, 494	337, 498	333, 486	334, 492	336, 488	336, 494	332, 484	333, 483
λ_{em}	520, 555	550	572	590	-[e]	630	-[e]	-[e]
CIE	0.37, 0.58	0.46, 0.53	0.58, 0.41	0.59, 0.39	0.64, 0.36	0.61, 0.38	0.66, 0.33	0.67, 0.33

[a]Measured at 0.15 optical density at the excitation wavelength; [b]fluorescence band λ_{exc} = 365 nm; [c]Stokes shift; [d]calculated from the emission spectra; and [e]only Eu-emission was observed.

The absorption spectra of metalloligands **21**–**23** exhibited little variance in different solvents, except for the small negative solvatochromism (7–13 nm and 296–820 cm^{-1}) that was observed for the ICT band upon increasing the polarity. This

hypsochromic shift was attributed to the effective stabilization of the ground state S_0 by the polar solvents. In turn, the emission spectra of the gold(I) complexes **21–23** demonstrated a perceptible shift of the wavelength maxima and therefore, a wide color diversity. For instance, in nonpolar cyclohexane the luminescence spectra appeared in the blue (λ_{em} = 403, 423 nm for **21**, λ_{em} = 428, 450 nm for **22**) and green (λ_{em} = 520, 555 nm for **23**) regions. The structured bands, with vibronic progressions in the range 1140–1210 cm^{-1}, indicated the radiative relaxation of the locally excited state. The use of more polar solvents (toluene, diethyl ether, *etc.*) led to visible broadening of the fluorescence band, thereby indicating an increase in the CT character of the excited state. Figure 37 illustrates that the emission profiles and calculated CIE coordinates for **22** changed within a wide spectral region, from deep blue (cyclohexane; CIE = 0.15, 0.08) to green (λ_{em} = 515 nm in THF; CIE = 0.28, 0.50) and orange (λ_{em} = 580 nm in MeCN; CIE = 0.47, 0.48), with a maximum red-shift of 152 nm (4719 cm^{-1}). The spectral modulations for **21** and **23** were less pronounced.

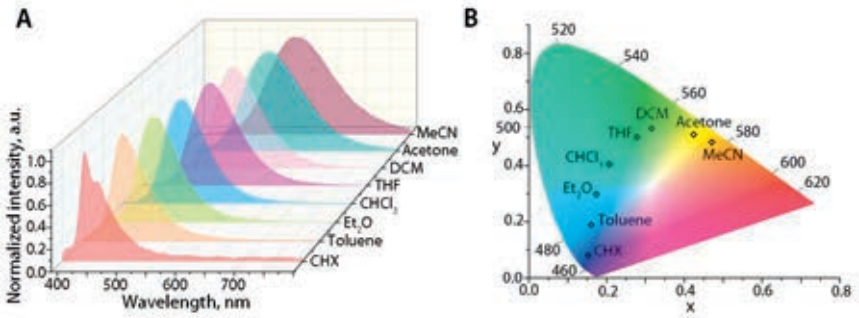

Figure 37. A: Emission spectra and B: CIE 1931 coordinates of **22** in different solvents.

The Stokes shift varied from a minimum of 1177 cm^{-1} (cyclohexane) to the large value 10173 cm^{-1} (MeCN), suggesting considerable stabilization of the ICT excited state S_1. Additionally, the solvatochromic behavior of the metalloligands was studied using the Lippert–Mataga approach.[258,259] The estimated change in the dipole moments upon photoexcitation ($\Delta\mu = \mu_{ES} - \mu_{GS}$) ranged from 24 to 37 D for **21–23**, which is typical for neutral *D*–π–*A* molecules.[61]

The absorption spectra for dyads **24–26** were similar to those of the metalloligands upon solvent variation. The high-energy peak at ~330 nm was almost polarity insensitive, whereas the ICT band revealed a minor hypsochromic shift of 11–13 nm upon polarity growth.

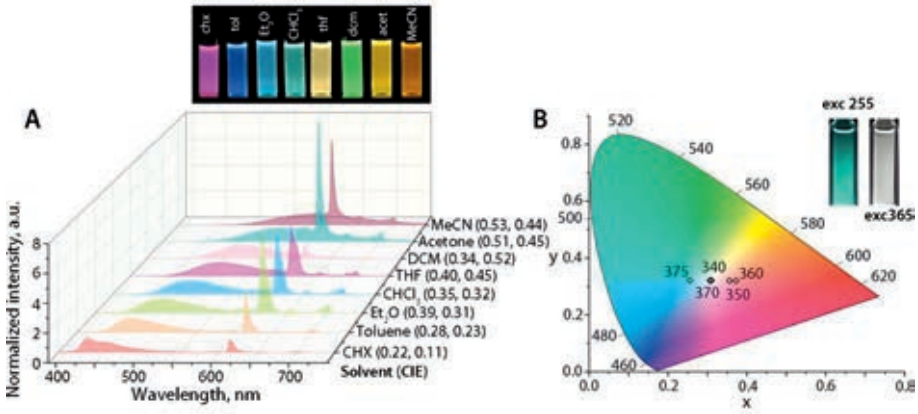

Figure 38.A: Emission spectra and the CIE coordinates for **25** in different solvents and B: CIE coordinates for **25** in chloroform at different excitation wavelengths; inset displays the solution under 255 and 365 nm excitations.

The ICT emissions of the dyads exhibited a bathochromic shift upon the increase in solvent polarity, which was nearly identical to that observed for the metalloligands (Table 6). On the other hand, the energies of the intraconfigurational $^5D_0 \rightarrow {}^7F_n$ (n = 0–4) Eu-centered transitions were not influenced by the solvent, although the relative intensities of the ICT (phosphine) and Eu(III) emissions were significantly varied. This dual emission fluctuation produced diverse luminescence colors. For example, solutions of **24** in acetone (CIE 0.35, 0.28) and **25** in Et_2O (CIE 0.38, 0.31) and $CHCl_3$ (CIE 0.35, 0.32) demonstrated near-pure white light upon 365 nm excitation (Table 6). The less pronounced solvatochromism of dyad **24** covered a smaller sector of the CIE space from violet pink (CIE 0.30, 0.16 in $CHCl_3$) to red (0.56, 0.26 in toluene). Evidently, for **26**, the color coordinates were in the reddish-orange corner of the CIE palette, except for nonpolar CHX (0.37, 0.58) and toluene (0.46, 0.53), where the contributions of the Eu(III) emissions were minimized.

In addition, for **25** in chloroform, which demonstrated white emission, different excitation wavelengths (280–400 nm) were used. Excitations ranging from 320 to 375 nm influenced mostly the *x* coordinates (0.25↔0.37), in particular 340 and 370 nm led to pure white light with CIE = 0.31, 0.32 (Figure 38B). A lower energy excitation (390–400 nm) only resulted in the intraligand fluorescence band that clearly demonstrated the absence of ET from the phosphine moiety to the lanthanide ion.

In conclusion, the combination of the chromophore-containing phosphines **L1**–**L3** with gold(I)-diimine acetylide afforded the highly emissive metalloligands **21**–**23**. Their optical behavior was primarily dictated by the intraphosphine CT that depended on the length of the conjugated spacer. The *D*–π–*A* architecture allowed to achieve ~30% quantum efficiency with color variation from deep blue to orange red (460–635 nm). Consequently, the family of dyads **24**–**26** synthesized by the coordination of complexes **21**–**23** to the $Eu(tta)_3$ fragment demonstrated intriguing

dual emission as a result of incomplete ET from **L1–L3** to the lanthanide ion. The resulting luminophores exhibited marked solvatochromism accompanied by excitation dependence of the emission components, which provided a convenient route for the wide tuning of the emission color.

4 SUMMARY

This study focused on the synthesis and structure-property analysis of novel organophosphorus dyes comprising three types of $\lambda^4\sigma^4$-P accepting blocks.

In the first direction, a facile approach to integrate the electron deficient $\lambda^4\sigma^4$ phosphonium group (>$^+$PPh$_2$) into the polyaromatic scaffold *via* intramolecular Cu^{II}-mediated phospha-annulation was elaborated. This method delivered a family of cationic six-membered P-heterocyclic fluorophores (**1c**–**8c**) with emission quantum efficiencies up to unity. The optical band gap systematically decreased together with the extension of the conjugated framework. The use of the electron-donor functions further led to a noticeable reduction in the HOMO-LUMO separation, owing to a greater CT character of the excited state. As a result, for the donor-modified phospha-anthracene dyes **5c** and **6c**, efficient near-infrared emission was achieved in solution (λ_{em} = 760–780 nm, Φ_{em} = 10–18% in dichloromethane), which is among the best performances for organophosphorus chromophores reported to date. Moreover, in the solid state, **6c** exhibited a superior efficiency of ~7% at the wavelength 825 nm. In contrast, the acyclic diphenylanthracene dyes **9** and **10**, bearing pendant phosphorus accepting units, emitted in the deep blue region, thereby emphasizing the major electronic perturbation brought to the PAH core by the six-membered phosphacycle. As a proof of concept, in view of the intense luminescence, selected dyes with satisfactory two-photon properties, water solubilities, and high stabilities were successfully applied to cell imaging using one- and two-photon excitation. The selected dyes displayed low toxicity against cultures and selective localization in the mitochondrial organelles.

The second avenue was dedicated to acyclic push-pull *D*–π–*A* luminophores. Linking of the electron-poor $\lambda^4\sigma^4$ phosphonium group (–$^+$PR$_3$) with aryl-amine donors (–NPh$_2$/-Carb) *via* different π-aromatic spacers afforded the highly emissive fluorophores **11**–**19** and **12Cbz**. Their photophysical behavior in polar media could be classically rationalized in terms of the ICT excited state. The emission of these push-pull phospha-dyes varied from sky blue (λ_{em} = 487 nm) to red (λ_{em} = 696 nm) in dichloromethane, with a maximum Φ_{em} of 95% and large Stokes shifts reaching ~13693 cm^{-1}. Intriguing dual fluorescence was observed for ionic salts **11**–**13, 17**, and **12Cbz** in non-polar solvents (toluene, carbon tetrachloride, and 1,4-dioxane). This was plausibly ascribed to intramolecular charge-transfer-driven counterion migration, resulting in the appearance of different excited states. The relaxation dynamics were dependent on the counterion size, viscosity, and temperature of the medium as well as on the length of the π-conjugated spacer. Accessible tuning of these parameters paved a new way to unconventional optical functionalities based on light-triggered ion motion. This was exemplified by panchromatic emission, including pure white light generation (0.29, 0.34).

In the last section of this thesis, phosphine ligands **L1–L3**, which adopted the Ph_2P–π-spacer-NPh_2 configuration (π-spacer = biphenyl, naphthalene-ethynylphenyl, and ethynyl-anthracene-ethynylphenyl), were employed to produce the fluorescent gold(I) complexes **21–23**, which acted as metalloligands. The use of the metal-bound $\lambda^4\sigma^4$ organophosphorus (-Ph_2P-Au^I-) fragment as the electron acceptor facilitated photoinduced intraligand CT. The emission behavior of the phosphine–gold species was strongly dependent on the length of the π-spacer (λ_{em} = 460, 525, and 635 nm for **21–23**, respectively) and demonstrated pronounced solvatochromism. Metalloligands **21–23**, comprising a non-coordinated bipyridine function, were combined with the {$Eu(tta)_3$} fragment to deliver the family of Au–Eu dyads **24–26**. The bimetallic assemblies exhibited dual luminescence resulting from the intraphosphine CT fluorescence and intraconfigurational $^5D_0 \rightarrow {}^7F_n$ (n = 0–4) Eu(III) transitions. Owing to the strong solvatochromism of the CT band and the excitation-dependent ratio of the ligand and lanthanide emissions, these dyads offered an unusually wide color variation achieved by a single-molecule emitter.

Overall, the class of $\lambda^4\sigma^4$ phosphorus motifs, particularly those of ionic nature, remain a largely unexplored building block, in view of constructing compounds with advanced optical functionalities. In this study, these electron-deficient units were considered in a systematic manner for the design of tunable push-pull chromophores. The promising photophysical properties of these novel bipolar dyes are expected to provide rich opportunities for further development of the field of luminescent molecular materials.

REFERENCES

(1) Ashley K., Cordell D., Mavinic D. A Brief History of Phosphorus: From the Philosopher's Stone to Nutrient Recovery and Reuse. *Chemosphere* **2011**, *84* (6), 737–746.

(2) Corbridge D. Phosphorous: Chemistry, Biochemistry and Technology **2013**.

(3) Deng B., Frisenda R., Li C., Chen X., Castellanos-Gomez A., Xia F. Progress on Black Phosphorus Photonics. *Adv. Opt. Mater.* **2018**, *6* (19), 1800365.

(4) Mogulkoc Y., Modarresi M., Mogulkoc A., Alkan B. Electronic and Optical Properties of Boron Phosphide/Blue Phosphorus Heterostructures. *Phys. Chem. Chem. Phys.* **2018**, *20* (17), 12053–12060.

(5) Emadi A., Jones R. J., Brodsky R. A. Cyclophosphamide and Cancer: Golden Anniversary. *Nat. Rev. Clin. Oncol.* **2009**, *6* (11), 638–647.

(6) Yoshida T., Stark G. R., Hoogenraad J. Inhibition by N-(Phosphonacetyl)-L-Aspartate of Aspartate Transcarbamylase Activity and Drug-Induced Cell Proliferation in Mice. *J. Biol. Chem.* **1974**, *249* (21), 6951–6955.

(7) Shcharbin D., Shcharbina N., Pedziwiatr-Werbicka E., de la Mata J., Gomez-Ramirez R., Mignani S., Kulchitsky V. A., Munoz-Fernandez M.-A., Caminade A.-M., Majoral J.-P. Phosphorus Dendrimers as Vectors for Gene Therapy in Cancer. Phosphorus Dendrimers in Biology and Nanomedicine. Pan Stanford, **2018**: 227-244.

(8) Reutter S. Hazards of Chemical Weapons Release during War: New Perspectives. *Environ. Health Perspect.* **1999**, *107* (12), 985–990.

(9) Munro N. Toxicity of the Organophosphate Chemical Warfare Agents GA, GB, and VX: Implications for Public Protection. *Environ. Health Perspect.* **1994**, *102* (1), 18–37.

(10) Iaroshenko V. Organophosphorus Chemistry: From Molecules to Applications, **2019**.

(11) Ni H., Chan W.-L., Lu Y. Phosphine-Catalyzed Asymmetric Organic Reactions. *Chem. Rev.* **2018**, *118* (18), 9344–9411.

(12) Guo H., Fan Y. C., Sun Z., Wu Y., Kwon O. Phosphine Organocatalysis. *Chem. Rev.* **2018**, *118* (20), 10049–10293.

(13) Alcarazo M. α-Cationic Phosphines: Synthesis and Applications. *Chem. - A Eur. J.* **2014**, *20* (26), 7868–7877.

(14) Nakajima T., Kamiryo Y., Kishimoto M., Imai K., Nakamae K., Ura Y., Tanase T. Synergistic Cu 2 Catalysts for Formic Acid Dehydrogenation. *J Am Chem Soc*. **2019**, 141(22), 8732-8736.

(15) Vendrell M., Zhai D., Er J. C., Chang Y.-T. Combinatorial Strategies in Fluorescent Probe Development. *Chem. Rev.* **2012**, *112* (8), 4391–4420.

(16) Joly D., Bouit P.-A., Hissler M. Organophosphorus Derivatives for Electronic Devices. *J. Mater. Chem. C* **2016**, *4* (17), 3686–3698.

(17) Reus C., Baumgartner T. Stimuli-Responsive Chromism in Organophosphorus Chemistry. *Dalt. Trans.* **2016**, *45* (5), 1850–1855.

(18) Shameem M. A., Orthaber A. Organophosphorus Compounds in Organic Electronics. *Chem. - A Eur. J.* **2016**, *22* (31), 10718–10735.

(19) Duffy M. P., Delaunay W., Bouit P.-A., Hissler M. π-Conjugated Phospholes and Their Incorporation into Devices: Components with a Great Deal of Potential. *Chem. Soc. Rev.* **2016**, *45* (19), 5296–5310.

(20) Jeon S. O., Lee J. Y. Phosphine Oxide Derivatives for Organic Light Emitting Diodes. *J. Mater. Chem.* **2012**, *22* (10), 4233–4243.

(21) Thomas Baumgartner* † and, Régis Réau* ‡. Organophosphorus π-Conjugated Materials. **2006**.

(22) Duffy M. P., Delaunay W., Bouit P.-A., Hissler M. π-Conjugated Phospholes and Their Incorporation into Devices: Components with a Great Deal of Potential. *Chem. Soc. Rev.* **2016**, *45* (19), 5296–5310.

(23) Stępień M., Gońka E., Żyła M., Sprutta N. Heterocyclic Nanographenes and Other Polycyclic Heteroaromatic Compounds: Synthetic Routes, Properties, and Applications. *Chem. Rev.* **2017**, *117* (4), 3479–3716.

(24) Fu C., Luo S., Li Z., Ai X., Pang Z., Li C., Chen K., Zhou L., Li F., Huang Y., Lu Z. Highly

Efficient Deep-Blue OLEDs Based on Hybridized Local and Charge-Transfer Emitters Bearing Pyrene as the Structural Unit. *Chem. Commun.* **2019**, *55* (44), 6317–6320.

(25) Du C., Ye S., Liu Y., Guo Y., Wu T., Liu H., Zheng J., Cheng C., Zhu M., Yu G. Fused-Seven-Ring Anthracene Derivative with Two Sulfur Bridges for High Performance Red Organic Light-Emitting Diodes. *Chem. Commun.* **2010**, *46* (45), 8573.

(26) Christensen P. R., Nagle J. K., Bhatti A., Wolf M. O. Enhanced Photoluminescence of Sulfur-Bridged Organic Chromophores. *J. Am. Chem. Soc.* **2013**, *135* (22), 8109–8112.

(27) Nagahora N., Kushida T., Shioji K., Okuma K. Dicationic Heteroacenes Containing Thio- or Selenopyrylium Moieties. *Organometallics* **2019**, *38* (8), 1800–1808.

(28) Panda S., Panda A., Zade S. S. Organoselenium Compounds as Fluorescent Probes. *Coord. Chem. Rev.* **2015**, *300*, 86–100.

(29) Hirai M., Tanaka N., Sakai M., Yamaguchi S. Structurally Constrained Boron-, Nitrogen-, Silicon-, and Phosphorus-Centered Polycyclic π-Conjugated Systems. *Chem. Rev.* **2019**, 119 (14), 8291-8331.

(30) Fukazawa A., Yamada H., Yamaguchi S. Phosphonium- and Borate-Bridged Zwitterionic Ladder Stilbene and Its Extended Analogues. *Angew. Chemie Int. Ed.* **2008**, *47* (30), 5582–5585.

(31) Zhang Z., Edkins R. M., Nitsch J., Fucke K., Eichhorn A., Steffen A., Wang Y., Marder T. B. D-π-A Triarylboron Compounds with Tunable Push-Pull Character Achieved by Modification of Both the Donor and Acceptor Moieties. *Chem. - A Eur. J.* **2015**, *21* (1), 177–190.

(32) Mellerup S. K., Wang S. Boron-Based Stimuli Responsive Materials. *Chem. Soc. Rev.* **2019**, 48, 3537-3549.

(33) Hu Z., Tian R., Zhao K., Liu Y., Duan Z., Mathey F. Generation and Trapping of a 1-Phosphafulvene: An Illustration of the P═C/C═C Analogy. *Org. Lett.* **2017**, *19* (18), 5004–5006.

(34) Washington M. P., Gudimetla V. B., Laughlin F. L., Deligonul N., He S., Payton J. L., Simpson M. C., Protasiewicz J. D. Phosphorus Can Also Be a "Photocopy." *J. Am. Chem. Soc.* **2010**, *132* (13), 4566–4567.

(35) Mathey F. Phospha-Organic Chemistry: Panorama and Perspectives. *Angew. Chemie Int. Ed.* **2003**, *42* (14), 1578–1604.

(36) Vasiuta R., Plenio H. Observing Initial Steps in Gold-Catalyzed Alkyne Transformations by Utilizing Bodipy-Tagged Phosphine-Gold Complexes. *Chem. - A Eur. J.* **2016**, *22* (18), 6353–6360.

(37) Yip J. H. K., Prabhavathy J. A Luminescent Gold Ring That Flips Like Cyclohexane. *Angew. Chemie Int. Ed.* **2001**, *40* (11), 2159–2162.

(38) Yamaguchi S., Akiyama S., Tamao K. The Coordination Number–Photophysical Properties Relationship of Trianthrylphosphorus Compounds: Doubly Locked Fluorescence of Anthryl Groups. *J. Organomet. Chem.* **2002**, *646* (1–2), 277–281.

(39) Sanji T., Fuchigami A., Tanaka M. Synthesis and Photophysical Properties of Phenyleneethynylenes Containing a Combination of Two Main Group Element Moieties of B, Si, or P on the Side Chain. *Organometallics* **2018**, *37* (3), 350–358.

(40) Shritz R., Shapira R., Borzin E., Tumanskii B., Reichstein W., Meichner C., Schwaiger F., Reichstein P. M., Kreyenschmidt J., Haarer D., Kador L., Eichen Y. Measuring Cumulative Exposure to Oxygen with a Diphenylphosphine-Alkyl Naphthaleneimide Luminescence Turn-On Dyad. *Chem. - A Eur. J.* **2015**, *21* (32), 11531–11537.

(41) Bouit P.-A., Escande A., Szűcs R., Szieberth D., Lescop C., Nyulászi L., Hissler M., Réau R. Dibenzophosphapentaphenes: Exploiting P Chemistry for Gap Fine-Tuning and Coordination-Driven Assembly of Planar Polycyclic Aromatic Hydrocarbons. *J. Am. Chem. Soc.* **2012**, *134* (15), 6524–6527.

(42) Koyanagi Y., Kimura Y., Matano Y. Effects of Boryl, Phosphino, and Phosphonio Substituents on Optical, Electrochemical, and Photophysical Properties of 2,5-Dithienylphospholes and 2-Phenyl-5-Thienylphospholes. *Dalt. Trans.* **2016**, *45* (5), 2190–2200.

(43) Christianson A. M., Gabbaï F. P. Synthesis and Coordination Chemistry of a Phosphine-Decorated Fluorescein: "Double Turn-On" Sensing of Gold(III) Ions in Water. *Inorg. Chem.* **2016**, *55* (12), 5828–5835.

(44) Lee Y. H., Jana S., Lee H., Lee S. U., Lee M. H. Rational Design of Time-Resolved Turn-on

Fluorescence Sensors: Exploiting Delayed Fluorescence for Hydrogen Peroxide Sensing. *Chem. Commun.* **2018**, *54* (85), 12069–12072.

(45) Shamsieva A. V., Musina E. I., Gerasimova T. P., Fayzullin R. R., Kolesnikov I. E., Samigullina A. I., Katsyuba S. A., Karasik A. A., Sinyashin O. G. Intriguing Near-Infrared Solid-State Luminescence of Binuclear Silver(I) Complexes Based on Pyridylphospholane Scaffolds. *Inorg Chem.* **2019**, 58 (12), 7698-7704.

(46) Yam V. W.-W., Au V. K.-M., Leung S. Y.-L. Light-Emitting Self-Assembled Materials Based on d^8 and d^{10} Transition Metal Complexes. *Chem. Rev.* **2015**, *115* (15), 7589–7728.

(47) Uoyama H., Goushi K., Shizu K., Nomura H., Adachi C. Highly Efficient Organic Light-Emitting Diodes from Delayed Fluorescence. *Nature* **2012**, *492* (7428), 234–238.

(48) Kondrasenko I., Chung K., Chen Y.-T., Koivistoinen J., Grachova E. V., Karttunen A. J., Chou P.-T., Koshevoy I. O. Harnessing Fluorescence versus Phosphorescence Ratio via Ancillary Ligand Fine-Tuned MLCT Contribution. *J. Phys. Chem. C* **2016**, *120* (22), 12196–12206.

(49) Chang Y.-C., Tang K.-C., Pan H.-A., Liu S.-H., Koshevoy I. O., Karttunen A. J., Hung W.-Y., Cheng M.-H., Chou P.-T. Harnessing Fluorescence versus Phosphorescence Branching Ratio in (Phenyl) n -Bridged (n = 0–5) Bimetallic Au(I) Complexes. *J. Phys. Chem. C* **2013**, *117* (19), 9623–9632.

(50) Yoshihara T., Yamaguchi Y., Hosaka M., Takeuchi T., Tobita S. Ratiometric Molecular Sensor for Monitoring Oxygen Levels in Living Cells. *Angew. Chemie Int. Ed.* **2012**, *51* (17), 4148–4151.

(51) Pan M., Liao W.-M., Yin S.-Y., Sun S.-S., Su C.-Y. Single-Phase White-Light-Emitting and Photoluminescent Color-Tuning Coordination Assemblies. *Chem. Rev.* **2018**, *118* (18), 8889–8935.

(52) Wauters I., Debrouwer W., Stevens C. V. Preparation of Phosphines through C–P Bond Formation. *Beilstein J. Org. Chem.* **2014**, *10* (1), 1064–1096.

(53) Mallesham G., Swetha C., Niveditha S., Mohanty M. E., Babu N. J., Kumar A., Bhanuprakash K., Rao V. J. Phosphine Oxide Functionalized Pyrenes as Efficient Blue Light Emitting Multifunctional Materials for Organic Light Emitting Diodes. *J. Mater. Chem. C* **2015**, *3* (6), 1208–1224.

(54) Qiu L., Hu W., Wu D., Duan Z., Mathey F. Regioselective Synthesis of 2- or 2,7-Functionalized Pyrenes via Migration. *Org. Lett.* **2018**, *20* (24), 7821–7824.

(55) Fang Q., Li J., Li S., Duan R., Wang S., Yi Y., Guo X., Qian Y., Huang W., Yang G. Thermally Populated "Bright" States for Wide-Range and High Temperature Sensing in Air. *Chem. Commun.* **2017**, *53* (42), 5702–5705.

(56) Fei Z., Kocher N., Mohrschladt C. J., Ihmels H., Stalke D. Single Crystals of the Disubstituted Anthracene 9,10-(Ph2P⊚S)2C14H8 Selectively and Reversibly Detect Toluene by Solid-State Fluorescence Emission. *Angew. Chemie Int. Ed.* **2003**, *42* (7), 783–787.

(57) Butkevich A. N., Sednev M. V., Shojaei H., Belov V. N., Hell S. W. PONy Dyes: Direct Addition of P(III) Nucleophiles to Organic Fluorophores. *Org. Lett.* **2018**, *20* (4), 1261–1264.

(58) Wu Z.-G., Zhou J., Yu L., Karotsis G., Wang Y., Zheng Y.-X., Pan Y. Novel Phosphine Oxide-Based Electron-Transporting Materials for Efficient Phosphorescent Organic Light-Emitting Diodes. *J. Mater. Chem. C* **2017**, *5* (33), 8579–8585.

(59) Stolar M., Baumgartner T. Phosphorus-Containing Materials for Organic Electronics. *Chem. - An Asian J.* **2014**, *9* (5), 1212–1225.

(60) Han C., Xie G., Xu H., Zhang Z., Xie L., Zhao Y., Liu S., Huang W. A Single Phosphine Oxide Host for High-Efficiency White Organic Light-Emitting Diodes with Extremely Low Operating Voltages and Reduced Efficiency Roll-Off. *Adv. Mater.* **2011**, *23* (21), 2491–2496.

(61) Misra R., Bhattacharyya S. P. John Wiley & Sons. Intramolecular Charge Transfer : Theory and Applications; Viley-VCH, **2018**.

(62) Li W., Li J., Liu D., Li D., Zhang D. Dual N-Type Units Including Pyridine and Diphenylphosphine Oxide: Effective Design Strategy of Host Materials for High-Performance Organic Light-Emitting Diodes. *Chem. Sci.* **2016**, *7* (11), 6706–6714.

(63) Jeon S. O., Yook K. S., Joo C. W., Lee J. Y. High-Efficiency Deep-Blue-Phosphorescent Organic Light-Emitting Diodes Using a Phosphine Oxide and a Phosphine Sulfide High-Triplet-Energy Host Material with Bipolar Charge-Transport Properties. *Adv. Mater.* **2010**, *22* (16), 1872–1876.

(64) Liu X.-Y., Tian Q.-S., Zhao D., Fan J., Liao L.-S. Novel O-D-π-A Arylamine/Arylphosphine Oxide Hybrid Hosts for Efficient Phosphorescent Organic Light-Emitting Diodes. *Org. Electron.* **2018**, *56*, 186–191.

(65) Yu D., Zhao F., Han C., Xu H., Li J., Zhang Z., Deng Z., Ma D., Yan P. Ternary Ambipolar Phosphine Oxide Hosts Based on Indirect Linkage for Highly Efficient Blue Electrophosphorescence: Towards High Triplet Energy, Low Driving Voltage and Stable Efficiencies. *Adv. Mater.* **2012**, *24* (4), 509–514.

(66) Zhang Z., Zhang Z., Chen R., Jia J., Han C., Zheng C., Xu H., Yu D., Zhao Y., Yan P., Liu S., Huang W. Modulating the Optoelectronic Properties of Large, Conjugated, High-Energy Gap, Quaternary Phosphine Oxide Hosts: Impact of the Triplet-Excited-State Location. *Chem. - A Eur. J.* **2013**, *19* (29), 9549–9561.

(67) Li J., Ding D., Wei Y., Zhang J., Xu H. A "Si-Locked" Phosphine Oxide Host with Suppressed Structural Relaxation for Highly Efficient Deep-Blue TADF Diodes. *Adv. Opt. Mater.* **2016**, *4* (4), 522–528.

(68) Liang Q., Han C., Duan C., Xu H. Blue Thermally Activated Delayed Fluorescence-Emitting Phosphine Oxide Hosts for Ultrasimple and Highly Efficient White Organic Light-Emitting Diodes. *Adv. Opt. Mater.* **2018**, *6* (12), 1800020.

(69) Tsujimura T. OLED Display Fundamentals and Applications **2017**.

(70) Yang X., Zhou G., Wong W.-Y. Functionalization of Phosphorescent Emitters and Their Host Materials by Main-Group Elements for Phosphorescent Organic Light-Emitting Devices. *Chem. Soc. Rev.* **2015**, *44* (23), 8484–8575.

(71) Tao Y., Xiao J., Zheng C., Zhang Z., Yan M., Chen R., Zhou X., Li H., An Z., Wang Z., Xu H., Huang W. Dynamically Adaptive Characteristics of Resonance Variation for Selectively Enhancing Electrical Performance of Organic Semiconductors. *Angew. Chemie Int. Ed.* **2013**, *52* (40), 10491–10495.

(72) Tao Y., Xu L., Zhang Z., Chen R., Li H., Xu H., Zheng C., Huang W. Achieving Optimal Self-Adaptivity for Dynamic Tuning of Organic Semiconductors through Resonance Engineering. *J. Am. Chem. Soc.* **2016**, *138* (30), 9655–9662.

(73) Liu X.-K., Zheng C.-J., Lo M.-F., Xiao J., Lee C.-S., Fung M.-K., Zhang X.-H. A Multifunctional Phosphine Oxide–Diphenylamine Hybrid Compound as a High Performance Deep-Blue Fluorescent Emitter and Green Phosphorescent Host. *Chem. Commun.* **2014**, *50* (16), 2027.

(74) Wang S., Qiao M., Ye Z., Dou D., Chen M., Peng Y., Shi Y., Yang X., Cui L., Li J., Li C., Wei B., Wong W.-Y. Efficient Deep-Blue Electrofluorescence with an External Quantum Efficiency Beyond 10%. *iScience* **2018**, *9*, 532–541.

(75) Chen W.-C., Yuan Y., Ni S.-F., Tong Q.-X., Wong F.-L., Lee C.-S. Achieving Efficient Violet-Blue Electroluminescence with CIE 0.06 and EQE 6% from Naphthyl-Linked Phenanthroimidazole–Carbazole Hybrid Fluorophores. *Chem. Sci.* **2017**, *8* (5), 3599–3608.

(76) Li C., Duan C., Han C., Xu H. Secondary Acceptor Optimization for Full-Exciton Radiation: Toward Sky-Blue Thermally Activated Delayed Fluorescence Diodes with External Quantum Efficiency of ≈ 30%. *Adv. Mater.* **2018**, *30* (50), 1804228.

(77) Gao F., Du R., Han C., Zhang J., Wei Y., Lu G., Xu H. High-Efficiency Blue Thermally Activated Delayed Fluorescence from Donor–Acceptor–Donor Systems *via* the through-Space Conjugation Effect. *Chem. Sci.* **2019**, *10* (21), 5556–5567.

(78) Duan C., Li J., Han C., Ding D., Yang H., Wei Y., Xu H. Multi-Dipolar Chromophores Featuring Phosphine Oxide as Joint Acceptor: A New Strategy toward High-Efficiency Blue Thermally Activated Delayed Fluorescence Dyes. *Chem. Mater.* **2016**, *28* (16), 5667–5679.

(79) Li Y., Liu J.-Y., Zhao Y.-D., Cao Y.-C. Recent Advancements of High Efficient Donor–Acceptor Type Blue Small Molecule Applied for OLEDs. *Mater. Today* **2017**, *20* (5), 258–266.

(80) Kondrasenko I., Tsai Z.-H., Chung K., Chen Y.-T., Ershova Y. Y., Doménech-Carbó A., Hung W.-Y., Chou P.-T., Karttunen A. J., Koshevoy I. O. Ambipolar Phosphine Derivatives to Attain True Blue OLEDs with 6.5% EQE. *ACS Appl. Mater. Interfaces* **2016**, *8* (17), 10968–10976.

(81) Lee C.-H., Tang M.-C., Cheung W.-L., Lai S.-L., Chan M.-Y., Yam V. W.-W. Highly Luminescent Phosphine Oxide-Containing Bipolar Alkynylgold(Iii) Complexes for Solution-Processable

Organic Light-Emitting Devices with Small Efficiency Roll-Offs. *Chem. Sci.* **2018**, *9* (29), 6228–6232.

(82) Wang L., Wu Y., Shan G.-G., Geng Y., Zhang J.-Z., Wang D.-M., Yang G.-C., Su Z.-M. The Influence of the Diphenylphosphoryl Moiety on the Phosphorescent Properties of Heteroleptic Iridium(Iii) Complexes and the OLED Performance: A Theoretical Study. *J. Mater. Chem. C* **2014**, *2* (16), 2859.

(83) Deng L., Zhang T., Wang R., Li J. Diphenylphosphorylpyridine-Functionalized Iridium Complexes for High-Efficiency Monochromic and White Organic Light-Emitting Diodes. *J. Mater. Chem.* **2012**, *22* (31), 15910.

(84) Zhou G., Wang Q., Ho C.-L., Wong W.-Y., Ma D., Wang L., Lin Z. Robust Tris-Cyclometalated Iridium(III) Phosphors with Ligands for Effective Charge Carrier Injection/Transport: Synthesis, Redox, Photophysical, and Electrophosphorescent Behavior. *Chem. - An Asian J.* **2008**, *3* (10), 1830–1841.

(85) Zhou G., Ho C.-L., Wong W.-Y., Wang Q., Ma D., Wang L., Lin Z., Marder T. B., Beeby A. Manipulating Charge-Transfer Character with Electron-Withdrawing Main-Group Moieties for the Color Tuning of Iridium Electrophosphors. *Adv. Funct. Mater.* **2008**, *18* (3), 499–511.

(86) Yu H., Liu C., Yu Z., Zhang L., Xiu J. Effect of Ancillary Ligands on the Properties of Diphenylphosphoryl-Substituted Cationic Ir(III) Complexes. *J. Mater. Chem. C* **2017**, *5* (14), 3519–3527.

(87) Platt A. W. G. Lanthanide Phosphine Oxide Complexes. *Coord. Chem. Rev.* **2017**, *340*, 62–78.

(88) Qin Y., Tao P., Gao L., She P., Liu S., Li X., Li F., Wang H., Zhao Q., Miao Y., Huang W. Designing Highly Efficient Phosphorescent Neutral Tetrahedral Manganese(II) Complexes for Organic Light-Emitting Diodes. *Adv. Opt. Mater.* **2019**, *7* (2), 1801160.

(89) Chen J., Zhang Q., Zheng F.-K., Liu Z.-F., Wang S.-H., Wu A.-Q., Guo G.-C. Intense Photo- and Tribo-Luminescence of Three Tetrahedral Manganese(Ii) Dihalides with Chelating Bidentate Phosphine Oxide Ligand. *Dalt. Trans.* **2015**, *44* (7), 3289–3294.

(90) Berezin A. S., Samsonenko D. G., Brel V. K., Artem'ev A. V. "Two-in-One" Organic–Inorganic Hybrid Mn^{II} Complexes Exhibiting Dual-Emissive Phosphorescence. *Dalt. Trans.* **2018**, *47* (21), 7306–7315.

(91) Wu Y., Zhang X., Xu L.-J., Yang M., Chen Z.-N. Luminescent Vapochromism Due to a Change of the Ligand Field in a One-Dimensional Manganese(II) Coordination Polymer. *Inorg. Chem.* **2018**, *57* (15), 9175–9181.

(92) Wu Z.-G., Jing Y.-M., Lu G.-Z., Zhou J., Zheng Y.-X., Zhou L., Wang Y., Pan Y. Novel Design of Iridium Phosphors with Pyridinylphosphinate Ligands for High-Efficiency Blue Organic Light-Emitting Diodes. *Sci. Rep.* **2016**, *6* (1), 38478.

(93) Jing Y.-M., Wang F.-Z., Zheng Y.-X., Zuo J.-L. Efficient Deep Red Electroluminescence of Iridium(III) Complexes with 2,3-Diphenylquinoxaline Derivatives and Tetraphenylimidodiphosphinate. *J. Mater. Chem. C* **2017**, *5* (15), 3714–3724.

(94) Xu H.-B., Jiao P.-C., Kang B., Deng J.-G., Zhang Y. Walkable Dual Emissions. *Sci. Rep.* **2013**, *3* (1), 2199.

(95) Yam V. W.-W., Au V. K.-M., Leung S. Y.-L. Light-Emitting Self-Assembled Materials Based on d^{8} and d^{10} Transition Metal Complexes. *Chem. Rev.* **2015**, *115* (15), 7589–7728.

(96) James S. L. Phosphines as Building Blocks in Coordination-Based Self-Assembly. *Chem. Soc. Rev.* **2009**, *38* (6), 1744.

(97) Gil-Rubio J., Vicente J. The Coordination and Supramolecular Chemistry of Gold Metalloligands. *Chem. - A Eur. J.* **2018**, *24* (1), 32–46.

(98) Koshevoy I., Koskinen L., Haukka M., Tunik S., Serdobintsev P., Melnikov A., Pakkanen T. Self-Assembly of Supramolecular Luminescent Au ^{I}Cu ^{I} Complexes: Wrapping an Au_6Cu_6 Cluster in a $[Au_3(Diphosphine)_3]^{3+}$ Belt. *Angew. Chemie Int. Ed.* **2008**, *47* (21), 3942–3945.

(99) Shu H.-X., Wang J.-Y., Zhang Q.-C., Chen Z.-N. Photophysical and Electroluminescent Properties of $PtAg_2$ Acetylide Complexes Supported with *Meso* - and *Rac* -Tetraphosphine. *Inorg. Chem.* **2017**, *56* (16), 9461–9473.

(100) Shakirova J. R., Grachova E. V., Gurzhiy V. V., Thangaraj S. K., Jänis J., Melnikov A. S.,

Karttunen A. J., Tunik S. P., Koshevoy I. O. Heterometallic Cluster-Capped Tetrahedral Assemblies with Postsynthetic Modification of the Metal Cores. *Angew. Chemie Int. Ed.* **2018**, *57* (43), 14154–14158.

(101) Wang Q. M., Lee Y-A., †, Crespo O., Deaton J., Tang C., Gysling H. J., Gimeno M.C., Larraz C., Villacampa M. D., Laguna A., Eisenberg R. Intensely Luminescent Gold(I)−Silver(I) Cluster Complexes with Tunable Structural Features. *J Am Chem Soc.* **2004**, 126 (31), 9488-9489.

(102) Liu Y., Yiu S.-C., Ho C.-L., Wong W.-Y. Recent Advances in Copper Complexes for Electrical/Light Energy Conversion. *Coord. Chem. Rev.* **2018**, *375*, 514–557.

(103) Bizzarri C., Spuling E., Knoll D. M., Volz D., Bräse S. Sustainable Metal Complexes for Organic Light-Emitting Diodes (OLEDs). *Coord. Chem. Rev.* **2018**, *373*, 49–82.

(104) Czerwieniec R., Leitl M. J., Homeier H. H. H., Yersin H. Cu(I) Complexes – Thermally Activated Delayed Fluorescence. Photophysical Approach and Material Design. *Coord. Chem. Rev.* **2016**, *325*, 2–28.

(105) Smith J. N., Hook J. M., Lucas N. T. Superphenylphosphines: Nanographene-Based Ligands That Control Coordination Geometry and Drive Supramolecular Assembly. *J. Am. Chem. Soc.* **2018**, *140* (3), 1131–1141.

(106) Davies L. H., Harrington R. W., Clegg W., Higham L. J. $^{B}R_2$BodPR$_2$: Highly Fluorescent Alternatives to PPh_3 and $PhPCy_2$. *Dalt. Trans.* **2014**, *43* (36), 13485–13499.

(107) Davies L. H., Stewart B., Harrington R. W., Clegg W., Higham L. J. Air-Stable, Highly Fluorescent Primary Phosphanes. *Angew. Chemie Int. Ed.* **2012**, *51* (20), 4921–4924.

(108) Davies L. H., Kasten B. B., Benny P. D., Arrowsmith R. L., Ge H., Pascu S. I., Botchway S. W., Clegg W., Harrington R. W., Higham L. J. Re and ^{99m}Tc Complexes of $BodP_3$ – Multi-Modality Imaging Probes. *Chem. Commun.* **2014**, *50* (98), 15503–15505.

(109) Ziegler C. B., Heck R. F. Palladium-Catalyzed Vinylic Substitution with Highly Activated Aryl Halides. *J. Org. Chem.* **1978**, *43* (15), 2941–2946.

(110) Marcoux D., Charette A. B. Nickel-Catalyzed Synthesis of Phosphonium Salts from Aryl Halides and Triphenylphosphine. *Adv. Synth. Catal.* **2008**, *350* (18), 2967–2974.

(111) Marcoux D., Charette A. B. Palladium-Catalyzed Synthesis of Functionalized Tetraarylphosphonium Salts. *J Org Chem.* **2008,** 73 (2), 590-593.

(112) Huang W., Zhong C.-H. Metal-Free Synthesis of Aryltriphenylphosphonium Bromides by the Reaction of Triphenylphosphine with Aryl Bromides in Refluxing Phenol. *ACS Omega* **2019**, *4* (4), 6690–6696.

(113) Li G., Xu Y., Zhuang W., Wang Y. Preparation of Organic Mechanochromic Fluorophores with Simple Structures and Promising Mechanochromic Luminescence Properties. *RSC Adv.* **2016**, *6* (88), 84787–84793.

(114) Li G., Xu Y., Kong Q., Zhuang W., Wang Y. Cation–Anion Interaction Directed Dual-Mode Switchable Mechanochromic Luminescence. *J. Mater. Chem. C* **2017**, *5* (33), 8527–8534.

(115) Rémond E., Tessier A., Leroux F. R., Bayardon J., Jugé S. Efficient Synthesis of Quaternary and P-Stereogenic Phosphonium Triflates. *Org. Lett.* **2010**, *12* (7), 1568–1571.

(116) Hilton M. C., Dolewski R. D., McNally A. Selective Functionalization of Pyridines via Heterocyclic Phosphonium Salts. *J. Am. Chem. Soc.* **2016**, *138* (42), 13806–13809.

(117) Fearnley A. F., An J., Jackson M., Lindovska P., Denton R. M. Synthesis of Quaternary Aryl Phosphonium Salts: Photoredox-Mediated Phosphine Arylation. *Chem. Commun.* **2016**, *52* (28), 4987–4990.

(118) Bugaenko D. I., Volkov A. A., Livantsov M. V., Yurovskaya M. A., Karchava A. Catalyst-Free Arylation of Tertiary Phosphines with Diarylodonium Salts Enabled by Visible Light. *Chem – A Eur J.* **2019,** 25 (54), 12502-12506.

(119) Nigam S., Burke B. P., Davies L. H., Domarkas J., Wallis J. F., Waddell P. G., Waby J. S., Benoit D. M., Seymour A.-M., Cawthorne C., Higham L. J., Archibald S. J. Structurally Optimised BODIPY Derivatives for Imaging of Mitochondrial Dysfunction in Cancer and Heart Cells. *Chem. Commun.* **2016**, *52* (44), 7114–7117.

(120) Ali M., Dondaine L., Adolle A., Sampaio C., Chotard F., Richard P., Denat F., Bettaieb A., Le Gendre P., Laurens V., Goze C., Paul C., Bodio E. Anticancer Agents: Does a Phosphonium

Behave Like a Gold(I) Phosphine Complex? Let a "Smart" Probe Answer! *J. Med. Chem.* **2015**, *58* (11), 4521–4528.

(121) Zielonka J., Joseph J., Sikora A., Hardy M., Ouari O., Vasquez-Vivar J., Cheng G., Lopez M., Kalyanaraman B. Mitochondria-Targeted Triphenylphosphonium-Based Compounds: Syntheses, Mechanisms of Action, and Therapeutic and Diagnostic Applications. *Chem. Rev.* **2017**, *117* (15), 10043–10120.

(122) Lambert C., Schmälzlin E., Meerholz K., Bräuchle C. Synthesis and Nonlinear Optical Properties of Three-Dimensional Phosphonium Ion Chromophores. *Chem. - A Eur. J.* **1998**, *4* (3), 512–521.

(123) Allen D. W., Li X. Solvatochromic and Halochromic Properties of Some Phosphonioarylimino- and Phosphonioarylazo-Phenolate Betaine Dyes. *J. Chem. Soc. Perkin Trans. 2* **1997**, No. 6, 1099–1104.

(124) Allen D. W., Mifflin J. P., Skabara P. J. Synthesis and Solvatochromism of Some Dipolar Aryl-Phosphonium and -Phosphine Oxide Systems. *J. Organomet. Chem.* **2000**, *601* (2), 293–298.

(125) Song K. C., Lee K. M., Nghia N. Van, Sung W. Y., Do Y., Lee M. H. Synthesis and Anion Binding Properties of Multi-Phosphonium Triarylboranes: Selective Sensing of Cyanide Ions in Buffered Water at PH 7. *Organometallics* **2013**, *32* (3), 817–823.

(126) Li Y., Kang Y., Lu J. S., Wyman I., Ko S. B., Wang S. A Dual-Emissive Phosphine-Borane Lewis Pair with a U-Shaped Linker: Impact of Methylation and Complexation on Fluoride Binding Affinity. *Organometallics* **2014**, *33* (4), 964–973.

(127) Lee M. H., Agou T., Kobayashi J., Kawashima T., Gabbai F. P. Fluoride Ion Complexation by a Cationic Borane in Aqueous Solution. *Chem. Commun.* **2007**, No. 11, 1133.

(128) Kim Y., Gabbaï F. P. Cationic Boranes for the Complexation of Fluoride Ions in Water below the 4 Ppm Maximum Contaminant Level. *J. Am. Chem. Soc.* **2009**, *131* (9), 3363–3369.

(129) Weber L., Kuhtz H., Böhling L., Brockhinke A., Chrostowska A., Dargelos A., Mazière A., Stammler H.-G., Neumann B. Syntheses of Rod-Shaped Fluorescent 1,3,2-Benzodiazaboroles with Phosphonium, and Phosphane Chalcogenide Acceptor Functions. *Dalt. Trans.* **2012**, *41* (34), 10440.

(130) Zhao Q., Wang J., Freeman J. L., Murphy-Jolly M., Wright A. M., Scardino D. J., Hammer N. I., Lawson C. M., Gray G. M. Syntheses, and Optical, Fluorescence, and Nonlinear Optical Characterization of Phosphine-Substituted Terthiophenes. *Inorg. Chem.* **2011**, *50* (5), 2015–2027.

(131) Shameem M. A., Orthaber A. Organophosphorus Compounds in Organic Electronics. *Chem. - A Eur. J.* **2016**, *22* (31), 10718–10735.

(132) Reus C., Baumgartner T. Stimuli-Responsive Chromism in Organophosphorus Chemistry. *Dalt. Trans.* **2016**, *45* (5), 1850–1855.

(133) Regulska E., Romero-Nieto C. Highlights on π-Systems Based on Six-Membered Phosphorus Heterocycles. *Dalt. Trans.* **2018**, *47* (31), 10344–10359.

(134) Szűcs R., Bouit P.-A., Nyulászi L., Hissler M. Phosphorus-Containing Polycyclic Aromatic Hydrocarbons. *ChemPhysChem* **2017**, *18* (19), 2618–2630.

(135) Matano Y., Imahori H. Design and Synthesis of Phosphole-Based π Systems for Novel Organic Materials. *Org. Biomol. Chem.* **2009**, *7* (7), 1258.

(136) Gershoni-Poranne R., Rahalkar A. P., Stanger A. The Predictive Power of Aromaticity: Quantitative Correlation between Aromaticity and Ionization Potentials and HOMO–LUMO Gaps in Oligomers of Benzene, Pyrrole, Furan, and Thiophene. *Phys. Chem. Chem. Phys.* **2018**, *20* (21), 14808–14817.

(137) Ren Y., Baumgartner T. Combining Form with Function – the Dawn of Phosphole-Based Functional Materials. *Dalt. Trans.* **2012**, *41* (26), 7792.

(138) Wittig G., Geissler G. Zur Reaktionsweise Des Pentaphenyl-Phosphors Und Einiger Derivate. *Justus Liebigs Ann. Chem.* **1953**, *580* (1), 44–57.

(139) Hibner-Kulicka P., Joule J. A., Skalik J., Bałczewski P. Recent Studies of the Synthesis, Functionalization, Optoelectronic Properties and Applications of Dibenzophospholes. *RSC Adv.* **2017**, *7* (15), 9194–9236.

(140) Su H-C., Fadhel O., Yang C.-J., Cho T.-Y., Fave C., Hissler M., Wu C.-C., Réau R. Toward

Functional π-Conjugated Organophosphorus Materials: Design of Phosphole-Based Oligomers for Electroluminescent Devices. *J. Am. Chem. Soc.* **2006**, 128 (3), 983-995.

(141) Matano Y., Saito A., Fukushima T., Tokudome Y., Suzuki F., Sakamaki D., Kaji H., Ito A., Tanaka K., Imahori H. Fusion of Phosphole and 1,1′-Biacenaphthene: Phosphorus(V)-Containing Extended π-Systems with High Electron Affinity and Electron Mobility. *Angew. Chemie Int. Ed.* **2011**, *50* (35), 8016–8020.

(142) Stolar M., Baumgartner T. Functional Conjugated Pyridines via Main-Group Element Tuning. *Chem. Commun.* **2018**, *54* (27), 3311–3322.

(143) Durben S., Baumgartner T. Azadibenzophospholes: Functional Building Blocks with Pronounced Electron-Acceptor Character. *Inorg. Chem.* **2011**, *50* (14), 6823–6836.

(144) Stolar M., Borau-Garcia J., Toonen M., Baumgartner T. Synthesis and Tunability of Highly Electron-Accepting, N-Benzylated "Phosphaviologens." *J. Am. Chem. Soc.* **2015**, *137* (9), 3366–3371.

(145) He X., Borau-Garcia J., Woo A. Y. Y., Trudel S., Baumgartner T. Dithieno[3,2-c:2′,3′-e]-2,7-Diketophosphepin: A Unique Building Block for Multifunctional π-Conjugated Materials. *J. Am. Chem. Soc.* **2013**, *135* (3), 1137–1147.

(146) Wang Z., Gelfand B. S., Baumgartner T. Dithienophosphole-Based Phosphinamides with Intriguing Self-Assembly Behavior. *Angew. Chemie Int. Ed.* **2016**, *55* (10), 3481–3485.

(147) Romero-Nieto C., Kamada K., Cramb D. T., Merino S., Rodríguez-López J., Baumgartner T. Synthesis and Photophysical Properties of Donor-Acceptor Dithienophospholes. *European J. Org. Chem.* **2010**, *2010* (27), 5225–5231.

(148) Higashino T., Yamada T., Sakurai T., Seki S., Imahori H. Fusing Porphyrins and Phospholes: Synthesis and Analysis of a Phosphorus-Containing Porphyrin. *Angew. Chemie Int. Ed.* **2016**, *55* (40), 12311–12315.

(149) Fadhel O., Gras M., Lemaitre N., Deborde V., Hissler M., Geffroy B., Réau R. Tunable Organophosphorus Dopants for Bright White Organic Light-Emitting Diodes with Simple Structures. *Adv. Mater.* **2009**, *21* (12), 1261–1265.

(150) Riobé F., Szűcs R., Bouit P.-A., Tondelier D., Geffroy B., Aparicio F., Buendía J., Sánchez L., Réau R., Nyulászi L., Hissler M. Synthesis, Electronic Properties and WOLED Devices of Planar Phosphorus-Containing Polycyclic Aromatic Hydrocarbons. *Chem. - A Eur. J.* **2015**, *21* (17), 6547–6556.

(151) Higashino T., Ishida K., Satoh T., Matano Y., Imahori H. Phosphole–Thiophene Hybrid: A Dual Role of Dithieno[3,4-B :3′,4′-d]Phosphole as Electron Acceptor and Electron Donor. *J. Org. Chem.* **2018**, *83* (6), 3397–3402.

(152) Wakatsuki A., Yukimoto M., Minoura M., Fujii K., Kimura Y., Matano Y. Regioselective Functionalization at the 7-Position of 1,2,3-Triphenylbenzo[b]Phosphole Oxide via P⊙O-Directed Lithiation. *Dalt. Trans.* **2018**, *47* (21), 7123–7127.

(153) Unoh Y., Hirano K., Satoh T., Miura M. An Approach to Benzophosphole Oxides through Silver- or Manganese-Mediated Dehydrogenative Annulation Involving C-C and C-P Bond Formation. *Angew. Chemie Int. Ed.* **2013**, *52* (49), 12975–12979.

(154) Chen Y.-R., Duan W.-L. Silver-Mediated Oxidative C–H/P–H Functionalization: An Efficient Route for the Synthesis of Benzo[*b*]Phosphole Oxides. *J. Am. Chem. Soc.* **2013**, *135* (45), 16754–16757.

(155) Liu L., Dong J., Yan Y., Yin S.-F., Han L.-B., Zhou Y. Photoredox-Catalyzed Decarboxylative Alkylation/Cyclization of Alkynylphosphine Oxides: A Metal- and Oxidant-Free Method for Accessing Benzo[b]Phosphole Oxides. *Chem. Commun.* **2019**, *55* (2), 233–236.

(156) Nishimura K., Unoh Y., Hirano K., Miura M. Phosphenium-Cation-Mediated Formal Cycloaddition Approach to Benzophospholes. *Chem. - A Eur. J.* **2018**, *24* (50), 13089–13092.

(157) Quint V., Morlet-Savary F., Lohier J.-F., Lalevée J., Gaumont A.-C., Lakhdar S. Metal-Free, Visible Light-Photocatalyzed Synthesis of Benzo[*b*]Phosphole Oxides: Synthetic and Mechanistic Investigations. *J. Am. Chem. Soc.* **2016**, *138* (23), 7436–7441.

(158) Yamaguchi E., Wang C., Fukazawa A., Taki M., Sato Y., Sasaki T., Ueda M., Sasaki N., Higashiyama T., Yamaguchi S. Environment-Sensitive Fluorescent Probe: A Benzophosphole

Oxide with an Electron-Donating Substituent. *Angew. Chemie Int. Ed.* **2015**, *54* (15), 4539–4543.

(159) Wang C., Fukazawa A., Taki M., Sato Y., Higashiyama T., Yamaguchi S. A Phosphole Oxide Based Fluorescent Dye with Exceptional Resistance to Photobleaching: A Practical Tool for Continuous Imaging in STED Microscopy. *Angew. Chemie Int. Ed.* **2015**, *54* (50), 15213–15217.

(160) Fukazawa A., Osaki H., Yamaguchi S. Hydroxyphenyl-Substituted Benzophosphole Oxides: Impact of the Intramolecular Hydrogen Bond on the Fluorescence Properties. *Asian J. Org. Chem.* **2014**, *3* (2), 122–127.

(161) Fukazawa A., Yamaguchi E., Ito E., Yamada H., Wang J., Irle S., Yamaguchi S. Zwitterionic Ladder Stilbenes with Phosphonium and Borate Bridges: Intramolecular Cascade Cyclization and Structure–Photophysical Properties Relationship. *Organometallics* **2011**, *30* (14), 3870–3879.

(162) Yavari K., Delaunay W., De Rycke N., Reynaldo T., Aillard P., Srebro-Hooper M., Chang V. Y., Muller G., Tondelier D., Geffroy B., Voituriez A., Marinetti A., Hissler M., Crassous J. Phosphahelicenes: From Chiroptical and Photophysical Properties to OLED Applications. *Chem. – A Eur. J.* **2019**, *25* (20), 5303–5310.

(163) Wu D., Zheng J., Xu C., Hong W., Mathey F. Phosphindole Fused Pyrrolo[3,2-b]Pyrroles: New Single-Molecule Junction for Charge Transport. *Dalt. Trans.* **2019**.

(164) Wu N. M.-W., Ng M., Yam V. W.-W. Photochromic Benzo[*b*]Phosphole Alkynylgold(I) Complexes with Mechanochromic Property to Serve as Multistimuli-Responsive Materials. *Angew. Chemie Int. Ed.* **2019**, *58* (10), 3027–3031.

(165) Hayashi M., Nishimura Y., Watanabe Y. Syntheses of 3-Oxo-λ 5 -Benzophospholes by an Intramolecular Cyclization of Phosphorus-Ylide. *Chem. Lett.* **2017**, *46* (12), 1732–1735.

(166) Suter R., Benkő Z., Bispinghoff M., Grützmacher H. Annulated 1,3,4-Azadiphospholides: Heterocycles with Widely Tunable Optical Properties. *Angew. Chemie Int. Ed.* **2017**, *56* (37), 11226–11231.

(167) Yoshikai N., Santra M., Wu B. Synthesis of Donor–Acceptor-Type Benzo[*b*]Phosphole and Naphtho[2,3-*b*]Phosphole Oxides and Their Solvatochromic Properties. *Organometallics* **2017**, *36* (14), 2637–2645.

(168) Yamaguchi E., Fukazawa A., Kosaka Y., Yokogawa D., Irle S., Yamaguchi S. A Benzophosphole *P* -Oxide with an Electron-Donating Group at 3-Position: Enhanced Fluorescence in Polar Solvents. *Bull. Chem. Soc. Jpn.* **2015**, *88* (11), 1545–1552.

(169) Adler R. A., Wang C., Fukazawa A., Yamaguchi S. Tuning the Photophysical Properties of Photostable Benzo[b]Phosphole P -Oxide-Based Fluorophores. *Inorg. Chem.* **2017**, *56* (15), 8718–8725.

(170) Greulich T. W., Suzuki N., Daniliuc C. G., Fukazawa A., Yamaguchi E., Studer A., Yamaguchi S. A Biphenyl Containing Two Electron-Donating and Two Electron-Accepting Moieties: A Rigid and Small Donor–Acceptor–Donor Ladder System. *Chem. Commun.* **2016**, *52* (11), 2374–2377.

(171) Higashino T., Ishida K., Sakurai T., Seki S., Konishi T., Kamada K., Kamada K., Imahori H. Pluripotent Features of Doubly Thiophene-Fused Benzodiphospholes as Organic Functional Materials. *Chem. – A Eur. J.* **2019**, *25* (25), 6425–6438.

(172) Wu S., Rheingold A. L., Golen J. A., Grimm A. B., Protasiewicz J. D. Synthesis of a Luminescent Azaphosphole. *Eur. J. Inorg. Chem.* **2016**, *2016* (5), 768–773.

(173) Laughlin F. L., Deligonul N., Rheingold A. L., Golen J. A., Laughlin B. J., Smith R. C., Protasiewicz J. D. Fluorescent Heteroacenes with Multiply-Bonded Phosphorus. *Organometallics* **2013**, *32* (23), 7116–7121.

(174) Romero-Nieto C., Durben S., Kormos I. M., Baumgartner T. Simple and Efficient Generation of White Light Emission From Organophosphorus Building Blocks. *Adv. Funct. Mater.* **2009**, *19* (22), 3625–3631.

(175) Wu N. M.-W., Ng M., Lam W. H., Wong H.-L., Yam V. W.-W. Photochromic Heterocycle-Fused Thieno[3,2- *b*]Phosphole Oxides as Visible Light Switches without Sacrificing Photoswitching Efficiency. *J. Am. Chem. Soc.* **2017**, *139* (42), 15142–15150.

(176) Chan J. C.-H., Lam W. H., Wong H.-L., Wong W.-T., Yam V. W.-W. Tunable Photochromism in Air-Stable, Robust Dithienylethene-Containing Phospholes through Modifications at the Phosphorus Center. *Angew. Chemie Int. Ed.* **2013**, *52* (44), 11504–11508.

(177) Koyanagi Y., Kawaguchi S., Fujii K., Kimura Y., Sasamori T., Tokitoh N., Matano Y. Effects of Counter Anions, P-Substituents, and Solvents on Optical and Photophysical Properties of 2-Phenylbenzo[b]Phospholium Salts. *Dalt. Trans.* **2017**, *46* (29), 9517–9527.

(178) Yavari K., Delaunay W., De Rycke N., Reynaldo T., Aillard P., Srebro-Hooper M., Chang V. Y., Muller G., Tondelier D., Geffroy B., Voituriez A., Marinetti A., Hissler M., Crassous J. Phosphahelicenes: From Chiroptical and Photophysical Properties to OLED Applications. *Chem. - A Eur. J.* **2019**.

(179) Romero-Nieto C., Marcos M., Merino S., Barberá J., Baumgartner T., Rodríguez-López J. Room Temperature Multifunctional Organophosphorus Gels and Liquid Crystals. *Adv. Funct. Mater.* **2011**, *21* (21), 4088–4099.

(180) Ren Y., Kan W. H., Thangadurai V., Baumgartner T. Bio-Inspired Phosphole-Lipids: From Highly Fluorescent Organogels to Mechanically Responsive FRET. *Angew. Chemie Int. Ed.* **2012**, *51* (16), 3964–3968.

(181) Ito S., Koshino K., Mikami K. CF 3 -Inspired Synthesis of Air-Tolerant 9-Phosphaanthracenes That Feature Fluorescence and Crystalline Polymorphs. *Chem. - An Asian J.* **2018**, *13* (7), 830–837.

(182) Lee J., Aizawa N., Yasuda T. Molecular Engineering of Phosphacycle-Based Thermally Activated Delayed Fluorescence Materials for Deep-Blue OLEDs. *J. Mater. Chem. C* **2018**, *6* (14), 3578–3583.

(183) Hindenberg P., Busch M., Paul A., Bernhardt M., Gemessy P., Rominger F., Romero-Nieto C. Diphosphahexaarenes as Highly Fluorescent and Stable Materials. *Angew. Chemie Int. Ed.* **2018**.

(184) Fukazawa A., Suda S., Taki M., Yamaguchi E., Grzybowski M., Sato Y., Higashiyama T., Yamaguchi S. Phospha-Fluorescein: A Red-Emissive Fluorescein Analogue with High Photobleaching Resistance. *Chem. Commun.* **2016**, *52* (6), 1120–1123.

(185) Zhou X., Lai R., Beck J. R., Li H., Stains C. I. Nebraska Red: A Phosphinate-Based near-Infrared Fluorophore Scaffold for Chemical Biology Applications. *Chem. Commun.* **2016**, *52* (83), 12290–12293.

(186) Baba K., Tobisu M., Chatani N. Palladium-Catalyzed Synthesis of Six-Membered Benzofuzed Phosphacycles via Carbon–Phosphorus Bond Cleavage. *Org. Lett.* **2015**, *17* (1), 70–73.

(187) Omori H., Hiroto S., Takeda Y., Fliegl H., Minakata S., Shinokubo H. Ni(II) 10-Phosphacorrole: A Porphyrin Analogue Containing Phosphorus at the Meso Position. *J. Am. Chem. Soc.* **2019**, *141* (12), 4800–4805.

(188) Chai X., Cui X., Wang B., Yang F., Cai Y., Wu Q., Wang T. Near-Infrared Phosphorus-Substituted Rhodamine with Emission Wavelength above 700 Nm for Bioimaging. *Chem. - A Eur. J.* **2015**, *21* (47), 16754–16758.

(189) Fukazawa A., Usuba J., Adler R. A., Yamaguchi S. Synthesis of Seminaphtho-Phospha-Fluorescein Dyes Based on the Consecutive Arylation of Aryldichlorophosphines. *Chem. Commun.* **2017**, *53* (61), 8565–8568.

(190) Fang Y., Good G. N., Zhou X., Stains C. I. Phosphinate-Containing Rhodol and Fluorescein Scaffolds for the Development of Bioprobes. *Chem. Commun.* **2019**, *55* (42), 5962–5965.

(191) Ge Q., Zong J., Li B., Wang B. Copper-Mediated Annulation of Phosphorus-Containing Arenes with Alkynes: An Approach to Phosphindolium Salts. *Org. Lett.* **2017**, *19* (24), 6670–6673.

(192) Nieto S., Metola P., Lynch V. M., Anslyn E. V. Synthesis of a Novel Bisphosphonium Salt Based on 2,2′-Bis(Diphenylphosphino)-1,1′-Binaphthyl (Binap). *Organometallics* **2008**, *27* (14), 3608–3610.

(193) Kawai H., Wolf W. J., DiPasquale A. G., Winston M. S., Toste F. D. Phosphonium Formation by Facile Carbon–Phosphorus Reductive Elimination from Gold(III). *J. Am. Chem. Soc.* **2016**, *138* (2), 587–593.

(194) Kuwabara T., Kato T., Takano K., Kodama S., Manabe Y., Tsuchida N., Takano K., Minami Y., Hiyama T., Ishii Y. P–C Reductive Elimination in Ru(Ii) Complexes to Convert Triarylphosphine Ligands into Five- or Six-Membered Phosphacycles. *Chem. Commun.* **2018**.

(195) Kato T., Kuwabara T., Minami Y., Hiyama T., Ishii Y. Synthesis of Phosphaphenalenium Salts via P–C Reductive Elimination at a Ru(II) Center and Their Fluorescence Properties. *Bull Chem Soc Jpn*. **2019**, 92 (7), 1131-1141.

(196) Romero-Nieto C., López-Andarias A., Egler-Lucas C., Gebert F., Neus J.-P., Pilgram O. Paving the Way to Novel Phosphorus-Based Architectures: A Noncatalyzed Protocol to Access Six-Membered Heterocycles. *Angew. Chemie Int. Ed.* **2015**, *54* (52), 15872–15875.

(197) Hindenberg P., López-Andarias A., Rominger F., de Cózar A., Romero-Nieto C. A Guide for the Design of Functional Polyaromatic Organophosphorus Materials. *Chem. - A Eur. J.* **2017**, *23* (56), 13919–13928.

(198) Romero-Nieto C., Rominger F., Hindenberg P. Phosphorus Post-Functionalization of Diphosphahexaarenes. *Chem – A Eur J*. **2019**, 25 (57), 13146-13151.

(199) Hatakeyama T., Hashimoto S., Nakamura M. Tandem Phospha-Friedel–Crafts Reaction toward Curved π-Conjugated Frameworks with a Phosphorus Ring Junction. *Org. Lett.* **2011**, *13* (8), 2130–2133.

(200) Nakatsuka S., Gotoh H., Kinoshita K., Yasuda N., Hatakeyama T. Divergent Synthesis of Heteroatom-Centered 4,8,12-Triazatriangulenes. *Angew. Chemie Int. Ed.* **2017**, *56* (18), 5087–5090.

(201) Nakatsuka S., Gotoh H., Kageyama A., Sasada Y., Ikuta T., Hatakeyama T. 5,9-Dioxa-13b-Oxophosphanaphtho[3,2,1- *de*]Anthracenes Prepared by Tandem Phospha-Friedel–Crafts Reaction as Hole-/Exciton-Blocking Materials for OLEDs. *Organometallics* **2017**, *36* (14), 2622–2631.

(202) Hashimoto S., Nakatsuka S., Nakamura M., Hatakeyama T. Construction of a Highly Distorted Benzene Ring in a Double Helicene. *Angew. Chemie Int. Ed.* **2014**, *53* (51), 14074–14076.

(203) Müller C., Wasserberg D., Weemers J. J. M., Pidko E. A., Hoffmann S., Lutz M., Spek A. L., Meskers S. C. J., Janssen R. A. J., van Santen R. A., Vogt D. Donor-Functionalized Polydentate Pyrylium Salts and Phosphinines: Synthesis, Structural Characterization, and Photophysical Properties. *Chem. - A Eur. J.* **2007**, *13* (16), 4548–4559.

(204) Loibl A., de Krom I., Pidko E. A., Weber M., Wiecko J., Müller C. Tuning the Electronic Effects of Aromatic Phosphorus Heterocycles: An Unprecedented Phosphinine with Significant P(π)-Donor Properties. *Chem. Commun.* **2014**, *50* (64), 8842–8844.

(205) Li Y., Li Z., Hou Y., Fan Y.-N., Su C.-Y. Photoluminescent Phosphinine Cu(I) Halide Complexes: Temperature Dependence of the Photophysical Properties and Applications as a Molecular Thermometer. *Inorg. Chem.* **2018**, *57* (21), 13235–13245.

(206) Habicht M. H., Wossidlo F., Bens T., Pidko E. A., Müller C. 2-(Trimethylsilyl)-λ ^{3} -Phosphinine: Synthesis, Coordination Chemistry, and Reactivity. *Chem. - A Eur. J.* **2018**, *24* (4), 944–952.

(207) Hashimoto N., Umano R., Ochi Y., Shimahara K., Nakamura J., Mori S., Ohta H., Watanabe Y., Hayashi M. Synthesis and Photophysical Properties of λ 5 -Phosphinines as a Tunable Fluorophore. *J. Am. Chem. Soc.* **2018**, *140* (6), 2046–2049.

(208) Nagahora N., Goto S., Inatomi T., Tokumaru H., Matsubara K., Shioji K., Okuma K. Buchwald–Hartwig Amination of Phosphinines and the Effect of Amine Substituents on Optoelectronic Properties of the Resulting Coupling Products. *J. Org. Chem.* **2018**, *83* (12), 6373–6381.

(209) Huang J., Tarábek J., Kulkarni R., Wang C., Dračínský M., Smales G. J., Tian Y., Ren S., Pauw B. R., Resch-Genger U., Bojdys M. J. A Π-conjugated, Covalent Phosphinine Framework. *Chem – A Eur J*. **2019**, 25 (53), 12342-12348.

(210) Schaub T. A., Brülls S. M., Dral P. O., Hampel F., Maid H., Kivala M. Organic Electron Acceptors Comprising a Dicyanomethylene-Bridged Acridophosphine Scaffold: The Impact of the Heteroatom. *Chem. - A Eur. J.* **2017**, *23* (29), 6988–6992.

(211) Grzybowski M., Taki M., Senda K., Sato Y., Ariyoshi T., Okada Y., Kawakami R., Imamura T., Yamaguchi S. A Highly Photostable Near-Infrared Labeling Agent Based on a Phospha-Rhodamine for Long-Term and Deep Imaging. *Angew Chemie Int Ed*. **2018**, 57 (32), 10137-10141.

(212) Grzybowski M., Taki M., Yamaguchi S. Selective Conversion of P=O-Bridged Rhodamines into P=O-Rhodols: Solvatochromic Near-Infrared Fluorophores. *Chem. - A Eur. J.* **2017**, *23* (53), 13028–13032.

(213) Ogasawara H., Grzybowski M., Hosokawa R., Sato Y., Taki M., Yamaguchi S. A Far-Red Fluorescent Probe Based on a Phospha-Fluorescein Scaffold for Cytosolic Calcium Imaging. *Chem. Commun.* **2018**, *54* (3), 299–302.

(214) Jiang X.-D., Zhao J., Xi D., Yu H., Guan J., Li S., Sun C.-L., Xiao L.-J. A New Water-Soluble

Phosphorus-Dipyrromethene and Phosphorus-Azadipyrromethene Dye: PODIPY/Aza-PODIPY. *Chem. - A Eur. J.* **2015**, *21* (16), 6079–6082.

(215) Wan W., Silva M. S., McMillen C. D., Creager S. E., Smith R. C. Highly Luminescent Heavier Main Group Analogues of Boron-Dipyrromethene. *J Am Chem Soc*. **2019**, 141 (22), 8703-8707.

(216) Chai X., Xiao J., Li M., Wang C., An H., Li C., Li Y., Zhang D., Cui X., Wang T. Bridge-Caging Strategy in Phosphorus-Substituted Rhodamine for Modular Development of Near-Infrared Fluorescent Probes. *Chem. - A Eur. J.* **2018**, *24* (54), 14506–14512.

(217) Joly D., Bouit P.-A., Hissler M. Organophosphorus Derivatives for Electronic Devices. *J. Mater. Chem. C* **2016**, *4* (17), 3686–3698.

(218) Blons C., Duval M., Delcroix D., Olivier-Bourbigou H., Mallet-Ladeira S., Sosa Carrizo E. D., Miqueu K., Amgoune A., Bourissou D. Formation of a *Peri* -Bridged Phosphonio-Naphthalene by Cu-Mediated Phosphine–Aryl Coupling. *Chem. – A Eur. J.* **2018**, *24* (46), 11922–11925.

(219) Chen H., Pascal S., Wang Z., Bouit P.-A., Wang Z., Zhang Y., Tondelier D., Geffroy B., Réau R., Mathey F., Duan Z., Hissler M. 1,2-Dihydrophosphete: A Platform for the Molecular Engineering of Electroluminescent Phosphorus Materials for Light-Emitting Devices. *Chem. - A Eur. J.* **2014**, *20* (31), 9784–9793.

(220) Ren Y., Sezen M., Guo F., Jäkle F., Loo Y.-L. [*D*]-Carbon–Carbon Double Bond Engineering in Diazaphosphepines: A Pathway to Modulate the Chemical and Electronic Structures of Heteropines. *Chem. Sci.* **2016**, *7* (7), 4211–4219.

(221) Lyaskovskyy V., van Dijk-Moes R. J. A., Burck S., Dzik W. I., Lutz M., Ehlers A. W., Slootweg J. C., de Bruin B., Lammertsma K. Dibenzo[b , f]Phosphepines: Novel Phosphane–Olefin Ligands for Transition Metals. *Organometallics* **2013**, *32* (2), 363–373.

(222) Delouche T., Mocanu A., Roisnel T., Szűcs R., Jacques E., Benkő Z., Nyulászi L., Bouit P.-A., Hissler M. π-Extended Phosphepines: Redox and Optically Active P-Heterocycles with Nonplanar Framework. *Org. Lett.* **2019**, *21* (3), 802–806.

(223) Cao Y., Nagle J. K., Wolf M. O., Patrick B. O. Tunable Luminescence of Bithiophene-Based Flexible Lewis Pairs. *J. Am. Chem. Soc.* **2015**, *137* (15), 4888–4891.

(224) Cao Y., Arsenault N. E., Hean D., Wolf M. O. Fluorescence Switching of Intramolecular Lewis Acid–Base Pairs on a Flexible Backbone. *J. Org. Chem.* **2019**, *84* (9), 5394–5403.

(225) Bruker A. X. S. APEX2-Software Suite for Crystallographic Programs. *Bruker AXS Inc., Madison* **2009**.

(226) Sheldrick G. M., IUCr. Crystal Structure Refinement with *SHELXL*. *Acta Crystallogr. Sect. C Struct. Chem.* **2015**, *71* (1), 3–8.

(227) Farrugia L. J., IUCr. WinGX and ORTEP for Windows: An Update. **2012**, *45* (4), 849–854.

(228) G. M. Sheldrick. SADABS-2008/1 - Bruker AXS Area Detector Scaling and Absorption Correction. *Bruker AXS, Madison, Wisconsin, USA* **2008**.

(229) Brouwer A. M. Standards for Photoluminescence Quantum Yield Measurements in Solution (IUPAC Technical Report). *Pure Appl. Chem.* **2011**, *83* (12), 2213–2228.

(230) Hindenberg P., Busch M., Paul A., Bernhardt M., Gemessy P., Rominger F., Romero-Nieto C. Diphosphahexaarenes as Highly Fluorescent and Stable Materials. *Angew. Chemie Int. Ed.* **2018**, *57* (46), 15157–15161.

(231) Iida A., Yamaguchi S. Intense Solid-State Blue Emission with a Small Stokes' Shift: π-Stacking Protection of the Diphenylanthracene Skeleton. *Chem. Commun.* **2009**, No. 21, 3002.

(232) Ren T., Xu W., Jin F., Cheng D., Zhang L., Yuan L., Zhang X. Rational Engineering of Bioinspired Anthocyanidin Fluorophores with Excellent Two-Photon Properties for Sensing and Imaging. *Anal. Chem.* **2017**, *89* (21), 11427–11434.

(233) Liu J., Sun Y.-Q., Zhang H., Shi H., Shi Y., Guo W. Sulfone-Rhodamines: A New Class of Near-Infrared Fluorescent Dyes for Bioimaging. *ACS Appl. Mater. Interfaces* **2016**, *8* (35), 22953–22962.

(234) Makarov N. S., Drobizhev M., Rebane A. Two-Photon Absorption Standards in the 550-1600 Nm Excitation Wavelength Range. *Opt. Express* **2008**, *16* (6), 4029.

(235) Huang P.-H., Shen J.-Y., Pu S.-C., Wen Y.-S., Lin J. T., Chou P.-T., Yeh M.-C. P. Synthesis and Characterization of New Fluorescent Two-Photon Absorption Chromophores. *J. Mater. Chem.* **2006**, *16* (9), 850–857.

(236) Pawlicki M., Collins H. A., Denning R. G., Anderson H. L. Two-Photon Absorption and the Design of Two-Photon Dyes. *Angew. Chemie Int. Ed.* **2009**, *48* (18), 3244–3266.
(237) Kim H. M., Cho B. R. Small-Molecule Two-Photon Probes for Bioimaging Applications. *Chem. Rev.* **2015**, *115* (11), 5014–5055.
(238) Li Z. H., Wong M.-S., Tao Y., D'Iorio M. Synthesis and Functional Properties of Strongly Luminescent Diphenylamino End-Capped Oligophenylenes. *J Org Chem.* **2004**, 69 (3), 921-927.
(239) Yang X., Zhao Y., Zhang X., Li R., Dang J., Li Y., Zhou G., Wu Z., Ma D., Wong W.-Y., Zhao X., Ren A., Wang L., Hou X. Thiazole-Based Metallophosphors of Iridium with Balanced Carrier Injection/Transporting Features and Their Two-Colour WOLEDs Fabricated by Both Vacuum Deposition and Solution Processing-Vacuum Deposition Hybrid Strategy. *J. Mater. Chem.* **2012**, *22* (15), 7136.
(240) Kisel K. S., Eskelinen T., Zafar W., Solomatina A. I., Hirva P., Grachova E. V., Tunik S. P., Koshevoy I. O. Chromophore-Functionalized Phenanthro-Diimine Ligands and Their Re(I) Complexes. *Inorg Chem*. **2018**, 57 (11), 6349-6361.
(241) Migita T., Nagai T., Kiuchi K., Kosugi M. Convenient Preparation of Tetraarylphosphonium Halides. *Bull. Chem. Soc. Jpn.* **1983**, *56* (9), 2869–2870.
(242) Toda Y., Komiyama Y., Kikuchi A., Suga H. Tetraarylphosphonium Salt-Catalyzed Carbon Dioxide Fixation at Atmospheric Pressure for the Synthesis of Cyclic Carbonates. *ACS Catal.* **2016**, *6* (10), 6906–6910.
(243) Moritz R., Wagner M., Schollmeyer D., Baumgarten M., Müllen K. Hydrophobic Encapsulated Phosphonium Salts-Synthesis of Weakly Coordinating Cations and Their Application in Wittig Reactions. *Chem. - A Eur. J.* **2015**, *21* (25), 9119–9125.
(244) Carlotti B., Consiglio G., Elisei F., Fortuna C. G., Mazzucato U., Spalletti A. Intramolecular Charge Transfer of Push–Pull Pyridinium Salts in the Singlet Manifold. *J. Phys. Chem. A* **2014**, *118* (20), 3580–3592.
(245) Lakowicz J. R. Principles of Fluorescence Spectroscopy, Springer, **2006**.
(246) Englman R., Jortner J. The Energy Gap Law for Radiationless Transitions in Large Molecules. *Mol. Phys.* **1970**, *18* (2), 145–164.
(247) Simoes M. C., Hughes K. J., Ingham D. B., Ma L., Pourkashanian M. Estimation of the Thermochemical Radii and Ionic Volumes of Complex Ions. *Inorg. Chem.* **2017**, *56* (13), 7566–7573.
(248) Uchiyama S., Prasanna de Silva A., Iwai K. Luminescent Molecular Thermometers. *J. Chem. Educ.* **2006**, *83* (5), 720.
(249) Saha S., Stoddart J. F. Photo-Driven Molecular Devices. *Chem. Soc. Rev.* **2007**, *36* (1), 77–92.
(250) Belyaev A., Kolesnikov I., Melnikov A. S., Gurzhiy V. V., Tunik S. P., Koshevoy I. O. Solution *versus* Solid-State Dual Emission of the Au(i)-Alkynyl Diphosphine Complexes *via* Modification of Polyaromatic Spacers. *New J Chem*. **2019**, 43, 13741-13750.
(251) Rajamouli B., Sivakumar V. Effect of Carbazole Functionalization with a Spacer Moiety in the Phenanthroimidazole Bipolar Ligand in a Europium(III) Complex on Its Luminescence Properties: Combined Experimental and Theoretical Study. *New J. Chem.* **2017**, *41* (3), 1017–1027.
(252) Singh K., Boddula R., Vaidyanathan S. Versatile Luminescent Europium(III)−β-Diketonate-Imidazo-Bipyridyl Complexes Intended for White LEDs: A Detailed Photophysical and Theoretical Study. *Inorg. Chem.* **2017**, *56* (15), 9376–9390.
(253) Solovyev I. V., Kondinski A., Monakhov K. Y., Koshevoy I. O., Grachova E. V. Synthesis, Photophysical Properties and Cation-Binding Studies of Bipyridine-Functionalized Gold(i) Complexes. *Inorg. Chem. Front.* **2018**, *5* (1), 160–171.
(254) Rajamouli B., Dwaraka Viswanath C. S., Giri S., Jayasankar C. K., Sivakumar V. Carbazole Functionalized New Bipolar Ligand for Monochromatic Red Light-Emitting Europium(Iii) Complex: Combined Experimental and Theoretical Study. *New J. Chem.* **2017**, *41* (8), 3112–3123.
(255) Rajamouli B., Sood P., Giri S., Krishnan V., Sivakumar V. A Dual-Characteristic Bidentate Ligand for a Ternary Mononuclear Europium(III) Molecular Complex - Synthesis, Photophysical, Electrochemical, and Theoretical Study. *Eur. J. Inorg. Chem.* **2016**, *2016* (24), 3900–3911.

(256) Xu H., Sun Q., An Z., Wei Y., Liu X. Electroluminescence from Europium(III) Complexes. *Coord. Chem. Rev.* **2015**, *293–294*, 228–249.
(257) Xu H., Yin K., Huang W. Comparison of the Electrochemical and Luminescence Properties of Two Carbazole-Based Phosphine Oxide Eu^{III} Complexes: Effect of Different Bipolar Ligand Structures. *ChemPhysChem* **2008**, *9* (12), 1752–1760.
(258) Marini A., Muñoz-Losa A., Biancardi A., Mennucci B. What Is Solvatochromism? *J. Phys. Chem. B* **2010**, *114* (51), 17128–17135.
(259) Reichardt C. Solvatochromic Dyes as Solvent Polarity Indicators. *Chem. Rev.* **1994**, *94* (8), 2319–2358.

ANDREI BELIAEV

The research results presented in this work emphasize the great potential and importance of the electron-accepting phosphorus units in the rational design of (metal) organophosphorus chromophores of a "push–pull" donor–acceptor architecture. The novel luminophores demonstrate high efficiency, tunability and adaptivity of the optical characteristics, and are expected to provide rich opportunities for further development of the field of light-emissive molecular materials.

UNIVERSITY OF
EASTERN FINLAND

uef.fi

**PUBLICATIONS OF
THE UNIVERSITY OF EASTERN FINLAND**
Dissertations in Forestry and Natural Sciences

ISBN 978-952-61-3284-6
ISSN 1798-5668